HYDRODYNAMIC INTERACTION BETWEEN FLOATING BODIES

Susanne Rusnes

Master Thesis

Norwegian University of
Science and Technology

11.06.2010

NTNU
Norwegian University of Science and Technology
Department of Marine Technology

MASTER THESIS IN MARINE HYDRODYNAMICS

SPRING 2010

FOR

Stud.techn. Susanne Rusnes

HYDRODYNAMIC INTERACTION BETWEEN FLOATING BODIES

Interaction between two bodies floating in waves is going to be studied. The candidate shall use the Wadam software and in order to get familiar with the software, specify its assumptions and restrictions, and analyze the motion of one single circular cylinder. The natural extension is to analyze the motion of two cylinders of different size or in different configurations. Proper visualization of the results must be done.

This is the basis for doing more specific analysis of the Hywind wind turbine and Windflip barge. Different conditions in the launching operation, i.e. flipped positions, shall be investigated together with the planned operational conditions. Actual cases are discussed with the supervisor.
Available results from model experiments can be compared with numerical calculations. Any disagreement may be explained.

In the thesis the candidate shall present his personal contribution to the resolution of the problem within the scope of the thesis work. Theories and conclusions should be based on mathematical derivation and logic reasoning identifying the various steps in the deduction. The original contribution of the candidate and material taken from other sources shall be clearly defined. Work from other sources shall be properly referenced. The candidate should utilize the existing possibilities for obtaining relevant literature.

The thesis should be organized in a rational manner to give a clear exposition of results, assessments and conclusions. The text should be brief and to the point, with a clear language.

The thesis shall contain the following elements: A text defining the scope, preface, list of contents, summary, main body of thesis, conclusions with recommendations for further work, list of symbols and acronyms, references and appendices. All figures, tables and equations shall be numerated.
It is supposed that Department of Marine Technology, NTNU, can use the results freely in its research work by referring to the student's thesis.

The thesis shall be submitted June 14, 2010, in two copies.

Bjørnar Pettersen
Professor/supervisor

Preface

This master thesis is written as the final part of a Master of Science degree in Marine Technology at Norwegian University of Science and Technology. The thesis has a magnitude of 30 ECTS and has been written from January to June 2010. As a preparation for the master thesis a project thesis was written fall 2009 and the master thesis is a continuing of the work carried out in the projects thesis. Chapter 2 and 3 in this report is from the project thesis, and only minor changes have been performed in these two chapters.

The thesis is written in collaboration with WindFlip AS, and the study of interaction between two floating bodies was a suggested problem from their part. The WindFlip vessel is a newly designed concept for transportation and launching of offshore wind turbines.

The collaboration with the WindFlip team has been very valuable in the writing of the thesis, for several reasons. It has been a great motivation in knowing that my work is an important contribution to the development of WindFlip, and the WindFlip team has been very helpful and willing to discuss encountered problems during the writing process.

I'm very grateful for all the help the WindFlip team has given me, all the good advices and helping tips from my supervisor Bjørnar Pettersen and the library staff for being most helpful in the search for relevant literature. The Wadam software support also deserves a thank for their effort in finding the malfunctions in the Wadam analyses.

Susanne Rusnes
Trondheim, 11th June 2010

Summary

This thesis is written in collaboration with WindFlip AS in order to investigate the behavior of Hywind and WindFlip after the release of Hywind from the WindFlip vessel. Potential theory has been applied, and no viscosity has been taken into account in any part of the analysis.

The interaction between two floating bodies in waves has been the major topic in this thesis. A literature study has been performed on the effects of interaction in steady flow and waves. The findings from the study indicate an increase in motions for the structure placed against the weather, and a reduction in motions for the lee-side structure. This results in a suggested configuration for the release operation, where WindFlip is placed up against the waves and Hywind in the sheltered area behind WindFlip.

The motions of a basic single circular cylinder in regular waves are also looked into. By performing simplified analyses in Matlab and Wadam, the fundamental behavior of buoy-like structures such as Hywind and WindFlip was looked into in order to obtain an understanding of how the structures respond to incident waves.

The WindFlip barge is to transport the wind turbine lying horizontally on top of WindFlip. Ballasting the barge at location will cause the structures to rotate to vertical position. The flipping procedure is estimated to last about six hours, and within this timeframe the structures will go through many different positions which again will lead to different responses to the waves. Three different positions have been looked into for the coupled WindFlip/Hywind structure, and the results are compared to results from model testing of these configurations. The numerical results compare well to the model test, which implies that the numerical analyses can be trusted and used for further evaluation of the process.

Two identical circular cylinders freely floating in waves are looked into by a multibody analysis in the potential theory solver Wadam. The effects of the multibody analyses show the same trends as the literature study – an increase in motions for the weather side cylinder, and a decrease for the lee-side cylinder. The interaction effects do not give large alterations in the motions compared to single body analyses. The reason for this may be the viscous effects in the interaction, which is not accounted for in Wadam.

By introducing an offbody point grid showing the free surface around the cylinders we observe lower waves in the wake behind the weather side cylinder. This also corresponds to the sheltering effects found in the literature study, and the reduction in response for the lee side-cylinder found in the multibody analyses.

Multibody analyses have been performed for the specific case of WindFlip and Hywind by the use of Wadam. The release configuration suggested from the literature study is applied in the analyses, and regular waves between 5 and 23 seconds are used. Also in this case the responses for the weather side structure (WindFlip) are increased when the spacing between the structures is reduced, and the responses for the lee-side cylinder (Hywind) show a decrease with reduced spacing. The effects from interaction on the response amplitudes are not prominent in this case either, and the viscous effects will most probably have a greater influence on the interaction between the structures.

A Matlab script has been made to visualize the motions of the two structures including the interaction effects on the phase angles and response amplitudes. From the visualizations we are able to detect combinations of wave periods and spacing that might be critical for the operation and hence should be looked into more closely.

A second Matlab script goes through all possible wave period and spacing combinations, and shows graphically which situations that will cause the structures to collide in either the top or bottom point. The script always uses the response amplitude values for the motions, and by that we end up with an RAO for the horizontal distance between the structures. This RAO for the distance will be further applied by the WindFlip team in order to perform statistical studies on which situations are likely to give collisions between WindFlip and Hywind during the release process.

Table of content

1. Introduction

Over the last couple of years energy from offshore wind has been a target area for energy companies such as Statoil and Statkraft. By placing wind turbines offshore instead of on land we obtain advantages such as much more steady wind, and we have the possibility of larger wind turbines with less intrusion for people and their surroundings. Today there are several bottom fixed offshore wind farms planned to be built, and Norwegian companies such as the ones mentioned above, are involved in the planning of two wind farms outside the coast of Great Britain. For the time being no wind farms has been built with floating wind turbines, but a smaller demo version of the ballast stabilized floating wind turbine Hywind is installed outside the coast of Haugesund on the Norwegian west coast.

There is as of today no solution for transporting a fully assembled floating wind turbine to site if the depths do not allow for vertical towing. In many areas of the world floating wind parks are not feasible because of the shallow waters outside the shore, and hence new transport solutions are needed in order to make floating wind parks a reality.

WindFlip AS is a newly established company with the aim of delivering an efficient transportation and launching solution for floating offshore wind turbines. The turbines which are transportable by the use of the WindFlip barge are ballast stabilized turbines, such as Statoils Hywind turbine. A sketch of a typical ballast stabilized offshore wind turbine, here exemplified by Hywind, is shown in Figure 1 and Figure 2.

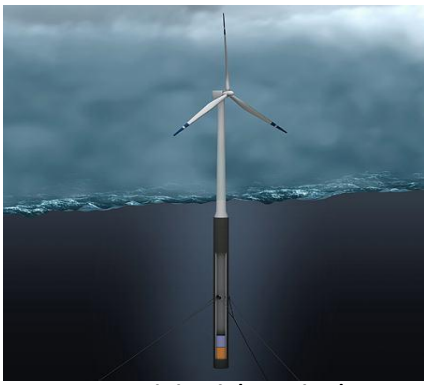

Figure 1 Hywind sketch (Statoil AS)

Figure 2 Towing of Hywind Demo (Statoil AS)

The concept of WindFlip is to transport the turbines horizontally lying on the WindFlip barge, ballast the WindFlip vessel until they reach upright position, and release the turbine with both turbine and WindFlip in vertical position, like shown in Figure 3.

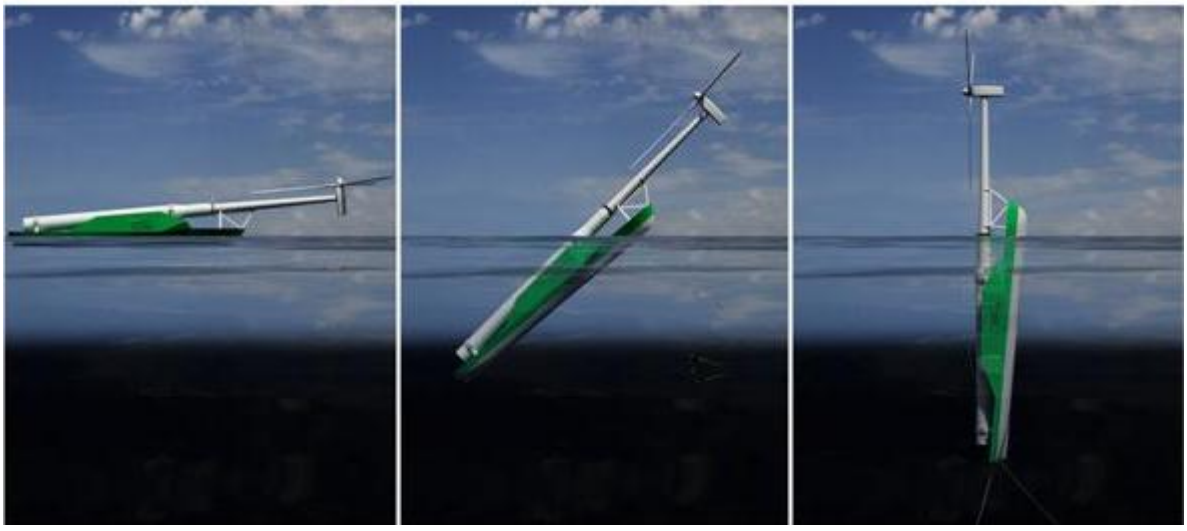

Figure 3 Flipping process of WindFlip (WindFlip AS)

The horizontal transit of the turbines open up for floating wind farms in areas that until now have been impossible due to shallow waters. By the use of WindFlip it is possible to launch the wind turbines fully assembled from coastal areas of limited water depths. The WindFlip barge has been developed continuously since the starting point in 2008. The share holders are all students at Norwegian University of Science and Technology, and they have put an enormous effort into the development of the concept. There are currently six master theses being written at the Institute of Marine Technology looking at different challenges regarding the WindFlip barge and its intended operation. As a part of the development a model test of a 1:45 scale model was performed at Marintek in Trondheim in February 2010. The results from the model testing act as a proof of concept, and are a large step towards a commercialising of the concept. Since then WindFlip has won Venture cup 2010, been 1st runner up in European Hopefuls for Innovation 2010 and been awarded The Norwegian Clean Tech award 2010. Two of the share holders will continue working on the concept full time, and the future for WindFlip AS is very exciting.

However, together with a lot of new possibilities, new challenges also arise. An issue for the launching of the turbine is how the WindFlip vessel and turbine will behave after the release, when they are floating in close proximity of each other. Many effects will in this case affect the motions of the floating bodies. Current, wind and waves will induce motions on both structures. Due to difference in size and geometry of the turbine and barge, their responses to the environmental loads will be different, and their motions will not be corresponding. This leads to a relative motion between the two bodies, which could possibly lead to collisions of the structures.

The motions of the bodies themselves also induce a motion of the two structures. These motions are caused by the diffraction from the structures, and the radiated waves from both bodies. These interaction effects are not so easy to predict, and numerical or/and experimental analyses has to be performed in order to see how the motions of the bodies will be affected by the interaction.

In August 2009 the WindFlip team asked me if I would like to spend my project and master thesis looking into how the structures will behave freely floating close to each other. How the interaction effects between the two structures will affect their motions after the release is one of the challenges in the operation, and needed to be looked into.

To be able to figure out what effects we can expect from the interaction between the structures, a literature study looking into structures interacting in current and waves is to be conducted. Several analyses looking into the basics behind how structures such as Hywind and WindFlip behave will be conducted, and the thesis is meant to give some insight into how interaction effects will influence the release operation of Hywind from the WindFlip barge.

2. Literature study

2.1. Single cylinder

In all cases when we have an incident flow around a structure, the flow will be disturbed by the presence of the body. Depending on the shape of the body we get different flow fields, and bluff bodies will affect the incident flow to a greater extent than more streamlined bodies. The cross-sectional shape of bluff bodies can vary a lot, from squares and triangles, to flat plates and ellipses. However, for many practical applications a circular cross section is applied, and hence the behaviour of circular cylinders is more widely studied than other bluff bodies.

The extent of the disturbance around a cylinder is highly dependent on the shape, size and orientation of the structure, and the velocity and viscosity of the flow (Zdravkovich, Flow around cirkular cylinders volume 1: Fundamentals 1997). The Reynolds number is a non dimensionalized parameter that can tell us something about the flow behaviour of a flow around a body. At low Reynolds numbers we have a laminar flow without flow separation, which can be modelled quite accurately by potential theory. When the Reynolds number increases we get a separation point at the body surface followed by a wake region behind the body. This real fluid[1] is not well described by potential theory, because the viscous effects are important (Faltinsen 1990). Steady flow around a circular cylinder for different Reynolds numbers is sketched by Sumer and Fredsøe (Sumer and Fredsøe 1997).

The disturbance of the flow can be divided into different regions, and these regions are given according to Zdravkovich (Zdravkovich, Flow around cirkular cylinders volume 1: Fundamentals 1997) as shown in Figure 4.

[1] Real fluid takes viscosity into account, and is the opposite of an ideal fluid, where the fluid is assumed inviscid

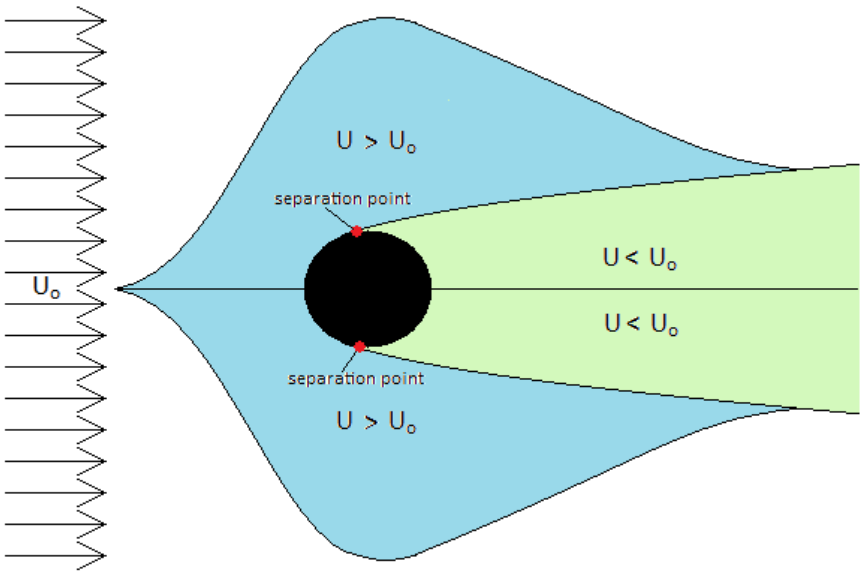

Figure 4 Disturbance regions around single cylinder, based on figure from Zdravkovich (1997)

We see that we have two main types of disturbance; an increase in velocity in front and around the cylinder and a wake with lower velocity behind the cylinder. This is due to the viscous effects which cause a no-slip condition on the body boundary (Faltinsen 1990). A consequence of the boundary layer is vortex shedding behind the cylinder, which again may lead to vortex induced vibrations, which can be a large problem for offshore structures.

Cylindrically shaped bodies, such as risers and spars are often long and have a small cross sectional area, both compared to the length of the buoy and to the wave length. When this is the case we may simplify the problem by using slender body theory[2]. The definition of a slender body is not concise. According to Newman (Newman 1977) a cylinder may be considered slender when the wavelength and length of the body is one order of magnitude larger than the diameter. Pettersen (Pettersen 2007) defines a body as slender when the wavelength is five times larger than the diameter of the structure. Faltinsen (Faltinsen 1990) uses the same slender body criterion as Pettersen (Pettersen 2007), and this report will follow the same definition as Pettersen and Faltinsen. By assuming slender body theory we only take drag and mass forces into account, and neglect the radiation and diffraction of the body (Pettersen 2007) (Agarwal and Jain 2003). When the wave height is smaller than $4\pi * diameter\ of\ cylinder$ the mass forces dominates the total force, and when the wave height exceeds this value the drag forces will dominate. By looking mathematically at the expressions for the mass and drag forces we see that the drag force decays like $e^{4\pi z/\lambda}$, and the mass force decays like $e^{2\pi z/\lambda}$. From this we see that the drag force decays very rapidly as we move away from the free surface, and hence the waves have to be of a certain size to have an impact on the total force (Pettersen 2007).

So far we have been looking at a fixed cylinder. We will experience the same effects for a floating cylinder, but when the body is freely floating many other effects arise as well. When regarding the body as stiff, hence without taking any hydroelastic effects into account, we have 6 degrees of

[2] Also referred to as long wave theory

freedom. A body can move in x-, y- and z- direction, and is also free to rotate around the same axes. We denote the 6 degrees of freedom as shown in Figure 5.

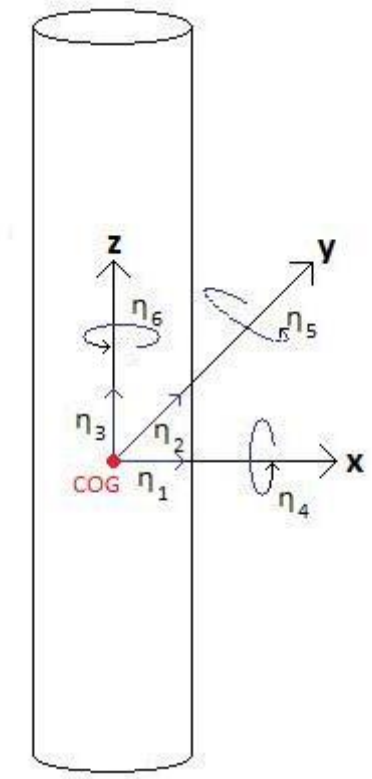

Notation of the 6 degrees of freedom	
η_1	Surge
η_2	Sway
η_3	Heave
η_4	Roll
η_5	Pitch
η_6	Yaw

Table 1 Degrees of freedom, cylinder

Figure 5 Degrees of freedom for vertical cylinder

When we have a flow around such a cylinder the forces from the stream will exert forces on the structure, which again induce motions in our 6 degrees of freedom. We can divide the force contributions into hydrostatic and dynamic forces. The hydrostatic effects will not contribute to movements of the structure, except from the restoring force, and will not be further discussed. The dynamic pressure, however, will induce motions in our 6 degrees of freedom.

Waves will create a dynamic pressure varying along the body. By using the slender body assumption we consider the dynamic pressure to be constant over the cross-section of the cylinder, i.e. in x- and y- direction, and that the force is acting at the midpoint of the cross section. In the vertical direction the dynamic pressure, and hence the dynamic force acting on the structure, vary to a great extent from the surface to the bottom of the cylinder. The orbits of the water particles in the waves decrease exponentially as we move away from the free surface, which means that the horizontal forces from the waves acting on the structure will decrease exponentially as well (Pettersen 2007).

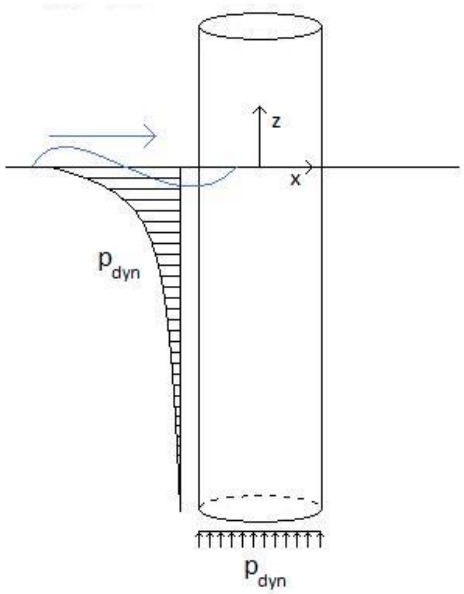

Figure 6 Dynamic pressure on cylinder from wave action

By finding the total force components in vertical and horizontal direction we can find the motions of the buoy. If we look at unidirectional waves arriving from the x-direction, as shown in Figure 6, the forces from the waves will not have a component in y-direction. We also find that since the buoy is axis symmetric there will be no yaw moment exerted (Jonkman 2009). By assuming a 2 dimensional sea state we can eliminate three out of our six degrees of freedom in the buoy, and by that make our calculations easier (Agarwal and Jain 2003) and (Ali 2005). Assuming that there are no motions in y-direction does not account for VIV, which often is a problem for bluff bodies, such as cylinders. This report will not address the issue of VIV, but if this is believed to be an important problem in the launching operations it should be investigated further.

We have now reduced our problem to three degrees of freedom, which are decided by the direction of the incoming waves. By assuming waves from head sea, along the x-axis, we will experience motions in the surge, pitch and heave directions. In waves from beam sea the degrees of freedom exerted are heave, sway and roll. In chapter 3, the latter wave direction has been applied.

2.2. Two cylinders

When we have two cylinders placed close to each other the flow field becomes much more complex. The interaction between the cylinders is dependent on many parameters, such as spacing, orientation and size. Zdravkovich (Zdravkovich, Flow Around Circular Cylinders volume 2: Applications 2003) has looked into two closely mounted cylinders in a steady flow, and investigated the interaction between them. According to Zdravkovich (Zdravkovich, Flow Around Circular Cylinders volume 2: Applications 2003) one of the most governing parameters when considering two identical interacting cylinders is their orientation. By dividing the configuration of the two cylinders into three different categories Zdravkovich covered all possible orientations of the cylinders.

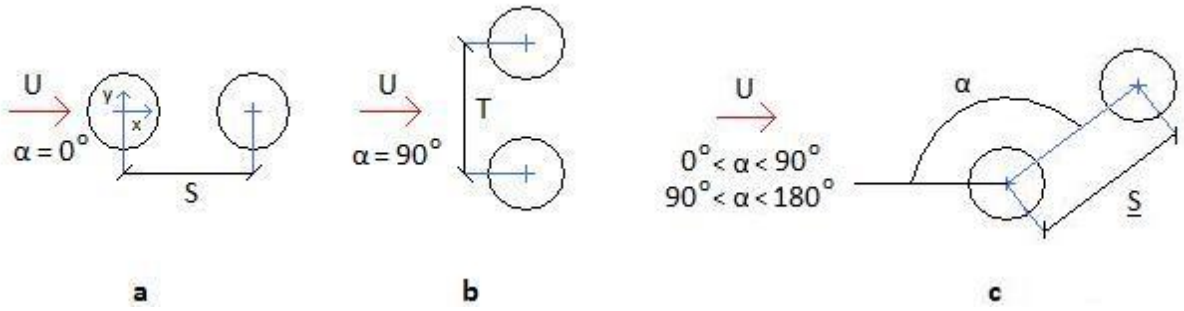

Figure 7 Cylinder arrangements, illustration based on Zdravkovich (2003)

In case **a** we have a tandem set of cylinders, case **b** is named side-by-side, and case **c** is staggered. When we have divided the configurations into these three categories, the most important parameter in each case is the distance between them. For case **c** the angle α is also an important parameter (Zdravkovich, Flow Around Circular Cylinders volume 2: Applications 2003).

Zhao et al. (Zhao, et al. 2007) have done an extensive numerical study of the forces acting on a pair of cylinders of different diameters. They varied the relative diameter of the cylinders (d/D), distance between them (G/D) and the configuration angle (α). The mentioned parameters are explained in Figure 8.

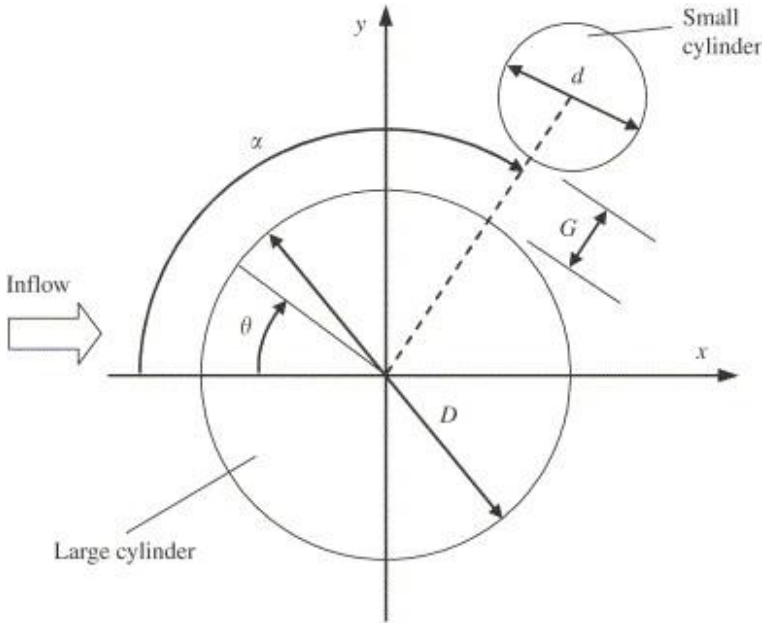

Figure 8 Two cylinder arrangement, illustration from Zhao et al. (2006)

For the side-by-side arrangement with low gap size we have a single eddy street behind the cylinders, and the cylinders acting as one large bluff body. As the distance (T)[3] increase we get a biased flow region, with one large and one small wake behind the cylinders. The large and small wake may easily trade place at any time. A further increase in T leads to coupled wake regimes behind the cylinders. For the coupled case the eddies are equal in size and shape, and mirrored around the midline between the cylinders. When the distance reach about four or five times the diameter ($T/D = 4 - 5$) the interaction is no longer of great importance. The flow around the side-by-side cases are also

[3] Distance between cylinder midpoints in side by side configuration

more widely discussed by Zdravkovich (Zdravkovich, Flow Around Circular Cylinders volume 2: Applications 2003).

The side-by-side arrangement is also associated with the highest drag forces on the cylinders. Zhao (Zhao, et al. 2007) concluded that the mean drag forces on the large cylinder attained its maximum when $\alpha \approx 90°$ (side-by-side configuration) for all values of G/D. The largest value of the drag coefficient occurs at $G/D \approx 0.05$, and in this case the drag coefficient is about 50% larger than if the large cylinder was alone. This is mainly due to increased pressure in front of the cylinders. The largest drag coefficient on the small cylinder is from the numerical analyses of Zhao (Zhao, et al. 2007) shown to appear at about $\alpha \approx 45°$ or $67.2°$. Different gap sizes gave slightly different values, and since the α increment is $22.5°$ the maximum value should be somewhere between these two values.

For the tandem configuration we have a wake regime around the cylinders. We can divide this regime into two main subcategories, with or without vortices forming in the middle. Whether formation of eddies in the mid region will appear or not is governed by the spacing and Reynolds number. When the spacing diameter ratio (G/D) is small we will not have eddy shedding behind the upstream cylinder, only a vortex street behind the downstream cylinder. When the distance between the two cylinders increases we will have a free stream separating from the upstream cylinder, and reattaching the downstream one. When the distances increase further two separate vortex streets behind the cylinders will form. The downstream cylinder may be affected by the upstream cylinder until the distance between them is as much as 60 times the diameter (based on findings for cylinders of equal diameter). However, the interference is weakened as we increase the distance between the cylinders. The sizes of the different sub regions are described to to greater detail by Zdravkovich (Zdravkovich, Flow Around Circular Cylinders volume 2: Applications 2003).

The drag forces reach their minimum in the near tandem arrangement, and according to Zhao (Zhao, et al. 2007) the drag force on the large cylinder in this arrangement is less than for a single cylinder on its own. By placing the smaller cylinder in front of the large one ($\alpha \approx 0°$) we create a sort of streamlined nose in front of the large cylinder, which decrease the stagnation pressure. We also obtain an increase in the base pressure, and these two pressure changes decrease the drag forces acting on the large cylinder. By placing the small cylinder behind the large cylinder ($\alpha \approx 180°$) we obtain similar reduction in the drag force on the large cylinder. In this arrangement we create a streamlined tail for the large cylinder and by that increase the base pressure, and hence decrease the drag force.

For the staggered cylinders case the interaction is affected by both wake and interference, and hence the effects are more difficult to predict. The common feature in all staggered arrangements for equally sized cylinders is that we observe a narrow wake behind the upstream cylinder, and a wide wake behind the downstream cylinder. The bigger the spacing is the less difference in wake size occurs. For equally sized cylinders the bias of the wake regions is bistable for $G/D < 0.1 - 0.15$, which means that the large and small wake regions may shift at any time (Zdravkovich, Flow Around Circular Cylinders volume 2: Applications 2003). Because of the asymmetry of the staggered arrangement, the lifting force will have its largest values in this arrangement. The lift force may act as either a repulsive or an attractive force on the cylinders, hence either try to pull them towards each other or push them away from each other. The lift force is negative when the cylinders are close to

each other in a side-by-side arrangement and positive in close tandem arrangement. This means that in a side-by-side arrangement we will have a lift force pulling the cylinders closer together (Zhao, et al. 2007). According to Zhao (Zhao, et al. 2007) the maximum absolute mean lift force on the large cylinder occurs when $\alpha \approx 112.5°$, hence in a staggered arrangement when the small cylinder has its origin a bit behind the large cylinder. The mean lift force coefficient on the small cylinder has its maximum for $\alpha \approx 45°$, when the small cylinder origin is placed in front of the large cylinder origin. (Zdravkovich, Flow Around Circular Cylinders volume 2: Applications 2003)

The absolute total force vector[4] attains its highest values when $\alpha \approx 90° \text{ and } 112.5°$ and the cylinders are placed very closely together. The magnitude of the force for the $90°$ case is 1.52 times the value for a single cylinder. For $112.5°$ the magnitude of total force is about 1.62 times that of a single cylinder. The maximum absolute mean total force on the small cylinder is 2.74 times the drag of a single cylinder, and appears when $\alpha \approx 45°$ and the gap size is very small. A summary of the maximum force for different configurations from Zhao (Zhao, et al. 2007) is given in Table 2.

	Large Cylinder		**Small Cylinder**	
	Drag	**Lift**	**Drag**	**Lift**
Angle, α	90°	112.5°	45 / 67.5°	45°
Arrangement	Side-by-side	Staggered	Staggered	Staggered
Gap size, G/D	0.05	0.05	0.1	0.05

Table 2 result summary from Zhao (Zhao, et al. 2007)

When we approach a tandem arrangement with the small cylinder upstream, the numerically calculated lift force from Zhao (Zhao, et al. 2007) approaches zero, as for a single cylinder. The minimum value of the drag force for both the large and small cylinder is also found in the tandem arrangement with the smaller cylinder further back, hence when $\alpha \approx 180°$. The drag coefficient for the small cylinder is in this case lower than the drag coefficient for the small cylinder alone.

As discussed, a tandem arrangement may lead to lift forces that are hard to predict accurately without performing an analysis on the specific case. Parameters such as gap size, diameter ratio and arrangement angle may lead to large variations from case to case. It has also been shown by the numerical analyses of Zhao (Zhao, et al. 2007) that the staggered arrangement may give the largest total mean force coefficients, and that combined with difficulties in predicting the behaviour accurately would lead us to believe that this is an arrangement in which one should try to avoid in a launching process.

Ali (Ali 2005) looked at the interaction between two and three freely cylinders floating when waves are present as well. The only heading addressed was the tandem arrangement as shown in Figure 9. He applied a 3D source-sink method[5] to determine the effects of the interaction, and compared the results to those of an equivalent single cylinder. As mentioned the wave heading is held constant, and so is the diameter of the bodies. The only thing varied is the gap size between the bodies.

[4] Mean force coefficient is defined as $\overline{C_F} = (\overline{C_D}, \overline{C_L})$, (Zhao, 2006)
[5] Also called panel method

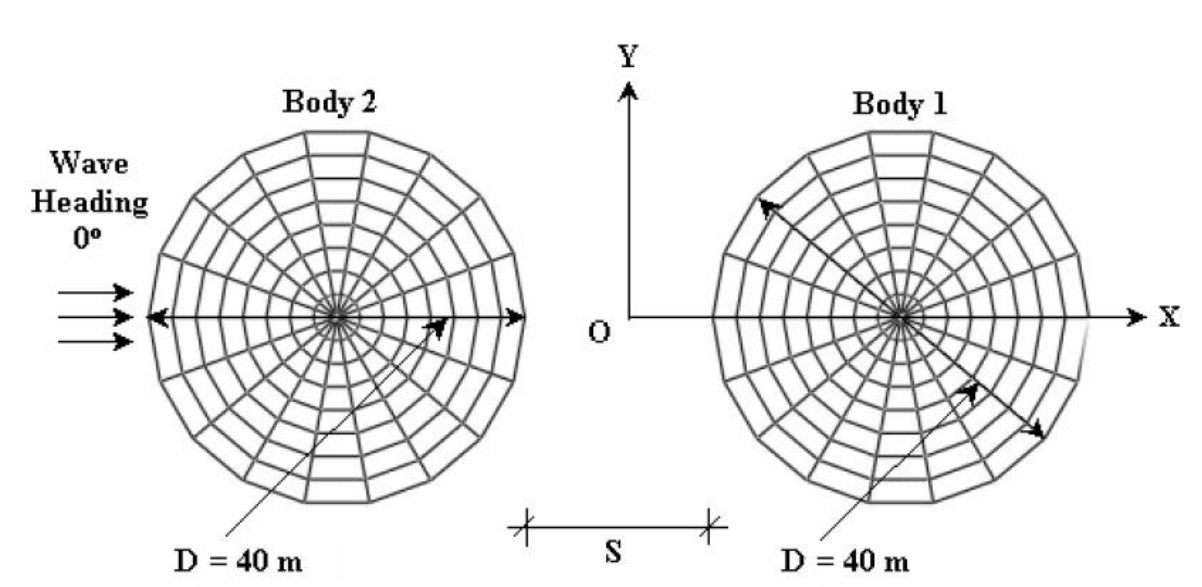

Figure 9 Cylinder configuration in analyses performed by Ali et al. (2005). Draft = 10m.

When we had multiple cylinders fixed in a fluid, it was sufficient to look at the incident waves together with the diffracted waves from the cylinders. In addressing multiple freely floating bodies, it's no longer enough to consider the diffraction effects. The diffraction from one body will, as before, affect the wave field, and hence have an impact on the motions of the closely situated body. However, when a body moves in a fluid its motions will generate waves radiating outwards. Radiating waves from a body will also affect the movements of the surrounding bodies. For the case of two cylinders placed closely together the radiations from the structures will affect each other. The incident waves will act together with the radiating and diffracting waves, and if any of these are in phase with each other the resulting wave loads on the structures will be amplified. (Ali 2005)

The actual importance of the interaction effects is dependent on the configuration of the multibody system, which includes the size and shape of the floating bodies and the separation distances between them (Ali 2005). The size difference is a very important parameter, as large size differences will give uneven interaction contributions. A large body will influence the smaller body to a much greater extent than the smaller body will influence the large one. This is shown in a numerical analysis by Kim (Kim 1972), where the interaction between two different bodies was tested. The shape of the analysed bodies is however not directly comparable to the cylinders in this thesis, and their analysis is only performed for heave motion. So the results should only be used as a qualitative indication on the interaction effects, and are not suitable to draw any general conclusions from.

The analyses executed by Ali (Ali 2005) focused on the force amplifications caused by the interaction effects between two freely floating cylinders. Also in the analysis by Ali (Ali 2005) the geometry is significantly different from the one addressed in this thesis. As shown in Figure 9 the diameter on both cylinders is 40m, and the draft is 10m. The analyses performed by Ali (Ali 2005) do hence not take size difference into account, and the large diameter compared to draft does not reflect the cylinders in analysed in this thesis, which are much more slender.

The results obtained by the earlier mentioned analysis from Ali (Ali 2005) show a large difference in the forces acting on body 1 and body 2. The lee-side cylinder (body 1) is subject to lower forces than the weather-side cylinder (body 2), and much higher interaction amplification is shown for surge

mode than for heave. For surge the weather-side cylinder has force peaks that exceed the single cylinder case quite significantly. The lee-side cylinder shows less variations in force when the wave number is changed, in addition to significantly lower force values over the entire tested wave number range. See Figure 10 and Figure 11. (Ali 2005)

These results coincide with the observations for fixed tandem cylinders by Zhao (Zhao, et al. 2007) discussed earlier, where the lowest forces were found in the tandem arrangement.

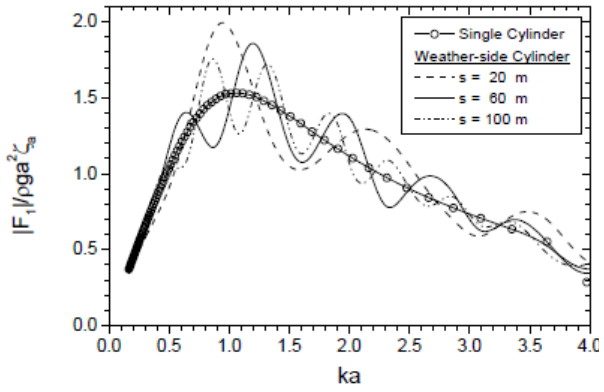

Figure 10 Surge force for weather-side cylinder, k = wave number, a = radius. (Ali 2005)

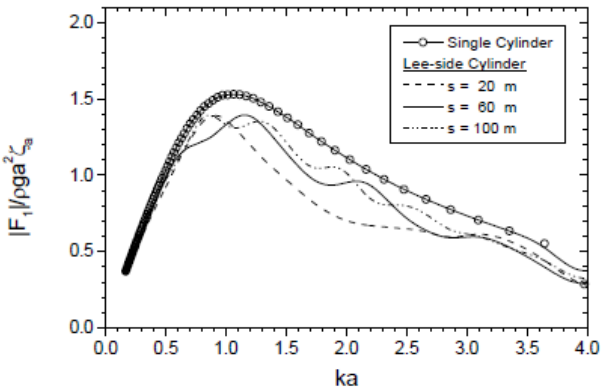

Figure 11 Surge force for lee-side cylinder, k = wave number, a = radius. (Ali2005)

None of the results presented in the mentioned analyses performed are directly applicable to the slender cylinders of different diameter we are looking at in this thesis. However, some of the main observations can be used as a guideline for what can be expected for the analyses that are to be performed on the WindFlip/Hywind interaction.

The diameters and cross sectional shapes, gap size and size difference are all parameters that cannot be altered during the launch and release process. The bodies will start off attached to each other, and will gradually move away until the interaction effects are negligible, and hence the entire range of gap sizes should be investigated. The results from both Ali (Ali 2005) and Zhao (Zhao, et al. 2007) indicate that the largest interaction effects occur when the bodies are situated close together, and gradually disappear as they move away from each other.

The displacement of the WindFlip barge is approximately four times larger than the displacement of Hywind, which according to the findings of Ali (Ali 2005) will give very different responses to the interaction effects. The size difference also gives different responses for the incident waves, which will be shown in chapter 3.

The parameter we can decide that will probably have the largest impact on the interaction effects is the arrangement of the bodies. From the analyses discussed earlier in the chapter staggered and side-by-side arrangements will give the largest interaction effects. The staggered arrangement also shows a bistability which is hard to predict. The tandem arrangement is by Zhao (Zhao, et al. 2007) pointed out as the arrangement which induces the lowest forces on the cylinders. This is also supported by other studies, such as Sumner et al. (Sumner, Richards and Akosile 2005).

The findings discussed above lead us to think a tandem arrangement will induce the least forces on the structures. The smaller body will be most influenced by the interaction effects, and the results from Ali (Ali 2005) indicate that the downstream cylinder will have the least force amplification

because of the interaction. From this a preliminary hypothesis regarding most favourable arrangement can be deduced. By placing the smaller body (turbine) downstream and the larger body (WindFlip barge) upstream in a tandem arrangement, the induced forces on the smallest body will be minimized as it is situated in the sheltered area of WindFlip.

This hypothesis is, as mentioned, only a preliminary statement based on the results from various analyses conducted for similar cases. No conclusions should be drawn from this, but it may serve as an indication on what can be expected from the analyses. In the subsequent chapters the tandem, configuration will be looked closely into, both for two identical cylinders and for the geometries of WindFlip and Hywind.

3. Numerical single-body analyses

3.1. Assumptions and course of action

Several simplifications have to be made in order to be able to carry out an analysis considering the interaction effects between the two floating bodies, such as Hywind and WindFlip. The analyses conducted in this chapter are simplified to a great extent, and their purpose is mainly to give an idea of the characteristics of a cylinders movement in waves. No interaction effects are considered, and this will be addressed in chapter 5 and chapter 6. In the literature study and the analyses in this chapter the main focus has been on trying to get an understanding of the principles behind a cylinder's motions in waves. Analyses in both Matlab and Wadam have been carried out on a small cylinder with main dimensions according to problem 3.4 in Faltinsen (Faltinsen 1990).

If we were to include higher order hydrodynamic effects and transient response due to for instance slamming loads, a time-domain analysis would be required. In neglecting these effects we are able to make use of a frequency domain solver, such as Wadam. Many other effects have also been neglected to be able to perform an analysis within the limited timeframe of this thesis. No hydroelasticity is accounted for, and both structures are regarded as infinitely stiff. Viscous effects are not considered, and by that the possibility of vortex induced vibrations is neglected. If viscous effects were to be considered in the analysis, a CFD program solving the Navier-Stokes equation[6] would have to be applied. This would be very time consuming and complex, and is normally not applied in problems like the one addressed in this thesis.

In both the Matlab and Wadam analyses airy wave theory is applied, and by this we assume horizontal sea bottom and a sea surface of infinite extent (Faltinsen 1990). Potential theory is used, and the basics of potential theory can be found in various books, such as White (White 2005) and Pettersen (Pettersen 2007). By adding the incident wave potential, diffraction potential and radiated wave potential we obtain a good picture of the wave action surrounding the structures. The incident wave potential does not sense the presence of the structure, and consequently we need a diffraction potential to take the effect of a structure into account. The radiating wave potential describes the waves radiating out from the body due to its motions, and we have radiation potential for each mode

[6] Often a Reynolds averaged Navier-Stokes equation (RANS) is used to make the problem solvable within a reasonable amount of time

of motion (i.e. our 6 degrees of freedom). For the interaction analyses that are to be performed in chapter 5 and chapter 6 all of these three mentioned potential will be a part of the solution, by performing a multibody analysis in Wadam. For the preliminary analysis in this chapter no interaction effects have been considered, and hence the effects of the motions induced by the radiation will not be taken into account.

The first analysis performed was by the use of Matlab, and the earlier mentioned problem 3.4 from Faltinsen (Faltinsen 1990) was solved and visualized by GLview Inova. The geometry for the cylinder analysed is shown in Figure 12, and by Table 3. The coordinate system is chosen such that the centre of gravity is in the origin, and hence will G be placed at $z = 0$.

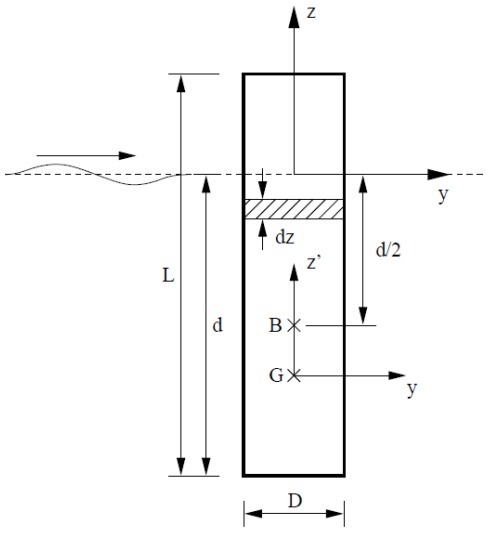

Symbol	Parameter	Value
L	Length	$14\ m$
d	Draft	$10\ m$
D	Diameter	$2\ m$
B	Centre of buoyancy	$1\ m$
G	Centre of gravity	$0\ m$

Table 3 Dimensions for buoy (Faltinsen 1990)

Figure 12 Buoy configuration (Faltinsen 1990)

The buoy is analysed with a wave length, λ, of 20 m. Since the diameter, d, of the buoy is 2 m, we can according to the discussion in chapter 2.1 treat the cylinder as a slender structure. By this assumption we assume the diffraction effects to be negligible, and only the incident waves are taken into account when the response of the buoy is found. The incident wave loads are assumed to act at the midpoint of the structure, and strip theory has been used to find the hydrodynamic coefficients. The problem is simplified to 2-dimensions, and only motions in the y-direction are looked into. The added mass coefficients are given as shown underneath (solution of problem 3.4, (Faltinsen 1990))

$$A_{22} = \rho A d \tag{3-1}$$

$$A_{44} = \rho A \left(\frac{d^3}{12} + d\overline{BG}^2\right) \tag{3-2}$$

$$A_{24} = A_{42} = -\rho A d \overline{BG} \tag{3-3}$$

$$F_2 = 2\rho g A \zeta_a \left(1 - e^{-kd}\right) \tag{3-4}$$

$$F_4 = -2\rho g A \zeta_a (C + De^{-kd}) \tag{3-5}$$

$$C = \left(\frac{d}{2} + \overline{BG}\right) - \frac{1}{k} \quad , \quad D = \left(\frac{d}{2} - \overline{BG}\right) + \frac{1}{k}$$

$$C_{44} = \rho g V \overline{GM} \quad \textbf{3-6}$$

We assume deep sea and may then use the following incident wave potential (Faltinsen 1990).

$$\varphi = \frac{g\zeta_a}{\omega} e^{kz} \cos(\omega t - ky) \quad \textbf{3-7}$$

The excitation forces on a small body can be expressed as(Faltinsen 1990)

$$F_i = -\iint_S \ pn_i dS + A_{i1}a_1 + A_{i2}a_2 + A_{i3}a_3 \quad \textbf{3-8}$$

where the first term is due to the Froude-Kriloff forces and the second is diffraction force. As mentioned earlier the forces are assumed to work at the centre point of the cross section. The coupled equations for sway and roll are given by Faltinsen (Faltinsen 1990)

$$(M + A_{22})\frac{d^2\eta_2}{dt^2} + A_{24}\frac{d^2\eta_4}{dt^2} = F_2 \cos \omega t \quad \textbf{3-9}$$

$$A_{24}\frac{d^2\eta_2}{dt^2} + (I_{44} + A_{44})\frac{d^2\eta_4}{dt^2} + C_{44}\eta_4 = F_4 \cos \omega t \quad \textbf{3-10}$$

The coupled equation can be solved by substituting the motions like shown in equation 3-11, (Faltinsen 1990)

$$\eta_k = \bar{\eta}_k \cos \omega t \qquad , \ k = 2, 4 \quad \textbf{3-11}$$

By solving these two differential equations by the use of 3-11 we get expressions for the amplitudes of motion $\bar{\eta}_2$ and $\bar{\eta}_4$.

In problem 3.4 from Faltinsen (Faltinsen 1990) no heave force is taken into account. Because the body has a low cross sectional area, and the draft is relatively large[7], the heave force will probably not induce large motions in the vertical direction. The pitch contribution to the heaving motion is not taken into account, because their contribution to the total heave motion are negligibly small. The heave force is found by looking at the dynamic pressure acting on the bottom of the cylinder. The dynamic pressure is found in the centre of the cross section, and multiplied with the cross-sectional area to find the force[8]. The expression for dynamic pressure is established by differentiating the potential, and according to Faltinsen (Faltinsen 1990) becomes

$$p_{dyn} = \rho g \zeta_a e^{kz} \sin(\omega t - ky) \quad \textbf{3-12}$$

The wave excitation force in heave is then found as

$$F_3 = -\frac{1}{4}\pi D^2 * p_{dyn}\Big|_{\substack{y=0 \\ z=-d}} \quad \textbf{3-13}$$

Added mass in heave for a surface piercing cylinder is approximated to be half of that of a heaving disk (Tao 2009). This gives us the following added mass according to Appendix 1 from Pettersen, (Pettersen 2007)

$$A_{33} = \frac{1}{2} * 0.637 \frac{\pi}{6} \rho D^3 = 0.05308 \pi \rho D^3 \quad \textbf{3-14}$$

[7] See discussion on decay of wave exciting force in chapter 6.1

[8] Ref. slender body theory

The restoring coefficient for a circular cylinder is, also according to Pettersen (Pettersen 2007), given as

$$C_{33} = \rho g A_w = \frac{1}{4}\pi\rho g D^2 \quad \textbf{3-15}$$

The standard equation of motion can be written on the following form according to Larsen (Larsen 2007)

$$(M + A_{33})\ddot{\eta}_3 + B_{33}\dot{\eta}_3 + C_{33}\eta_3 = F_3 \quad \textbf{3-16}$$

No damping is considered in the Matlab analysis, and hence the B_{33} term can be ignored, and we end up with

$$(M + A_{33})\ddot{\eta}_3 + C_{33}\eta_3 = F_3 \quad \textbf{3-17}$$

By using a similar relation as 3-11 for the motions we can solve the differential equation for $\bar{\eta}_3$, and we then obtain

$$\bar{\eta}_3 = \frac{\bar{F}_3}{-(M+A_{33})\omega^2+C_{33}} \quad \textbf{3-18}$$

It's important to remember that since the heave force oscillates as $\sin\omega t$, the heave motion will be given as

$$\eta_3 = \bar{\eta}_3 \sin\omega t \quad \textbf{3-19}$$

and not by a cosine function as for sway and roll. This implies a phase difference between the sway/roll motions, and the heave motion.

All the above equations are calculated by a Matlab script, and the buoy's movements are visualized by the use of Matlab. The main dimensions of the cylinder are easy to change, and the wave characteristics are as well. The program is also able to visualize two[9] buoys of different diameter at different separation gaps. The visualization of two buoys will only illustrate the relative motion between the buoys, and no diffraction or radiation effects are modelled.

The next approach consists of using Wadam to find the amplitudes of motion. Wadam is, as discussed earlier, a potential theory solver. 3D sink-source method is used to model the structure, and the resulting wave potential includes incident waves, diffracted waves and radiated waves. We are only analysing one buoy at the time in this thesis, and the interacting effects from the radiating and diffracting waves will not be modelled. However, by including these potentials we introduce a damping force, potential damping. This damping is due to the energy used to generate the outgoing waves, and will reduce the motions to some extent. Smaller bodies will have less potential damping, because the radiating waves are of little importance. Larger bodies will generate more waves, and thus will have a larger potential damping. To compare the motions for a slender body to those of a larger body, an analysis of an enlarged body has also been carried out. The geometry of this cylinder is similar to the small cylinder described in Figure 12 and Table 3, except all dimensions have been multiplied by three. The distance from keel to the centre of buoyancy has been multiplied by 2. This gives the following dimension table

[9] With minor changes in the code more than two buoys can easily be visualized at the same time.

Symbol	Parameter	Value
L	Length	$42\ m$
d	Draft	$30\ m$
D	Diameter	$6\ m$
B	Centre of buoyancy	$2\ m$
G	Centre of gravity	$0\ m$

Table 4 Dimensions for large cylinder

From the prior discussion on damping, it would make sense to expect the amplitudes of motion from Matlab to be less than the ones from Wadam. Also a more significant difference from Matlab to Wadam results can be expected for the larger cylinder due to the larger potential damping in this case. Wadam also includes 3 dimensional effects, and does not assume the cylinder to be infinitely long when calculating sway and roll motions. Matlab solves the problem with 2D strip theory, and hence no end effects are included. This difference between the two solution methods also introduces a deviance between the values from Wadam and Matlab.

The coordinate system used in Wadam is not the same as in Matlab. Wadam gives out the results in a coordinate system shifted to the mean free surface, and hence caution has to be shown in comparing the results from Matlab and Wadam.

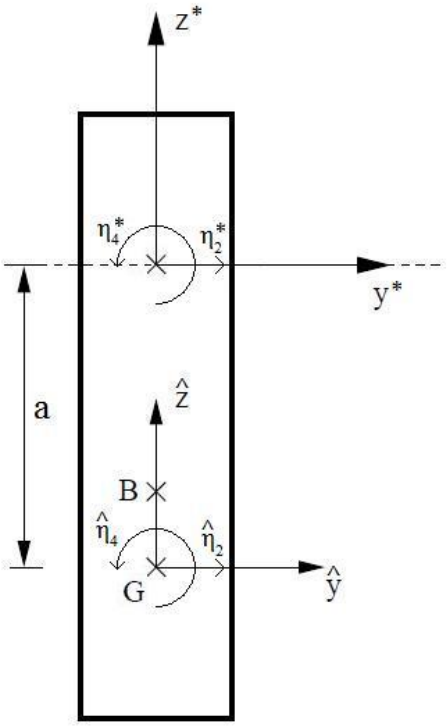

Figure 13 Coordinate systems for cylinder

$\hat{z}$ and $\hat{y}$ denotes the coordinate system used in the Matlab scripts, where the origin is in COG. In Wadam the origin is chosen at the mean surface and is denoted z^* and y^* in figure 13.

The results from Wadam are translated to the COG coordinate system used in Matlab before they are presented in chapter 3.2. The only degree of freedom that needs to be transformed is sway, and the expression for the transformation is given underneath.

$$\hat{\eta}_2 = \eta_2^* - a * \eta_4^* \qquad \textbf{3-20}$$

3.2. Results from numerical analyses

3.2.1. Single cylinder

Several analyses have been performed with different input. The size of the cylinder has been changed and compared to the original one, and a different set of cylinders has been used. GLview has been applied to make the simulations, and VTF files are produced when the Matlab programs run.

For simplicity the circular cylinders are modelled as squared boxes in GLview. The sides of the squares are equal to the diameter of the cylinder modelled, and the lengths have not been changed. This has no effect on the calculations, and is merely done to make the visualization process easier.

The first analysis was done with the geometry from problem 3.4 (Faltinsen 1990). A wave length of $20\,m$, and a wave height of $0.5\,m$ is used. The visualization is found in Appendix C as SmallCylinderHeave.vtf. The results from the analysis are amplitudes of motion in roll, sway and heave. These values will be presented in running the analysis, and are also given in Table 5. The same input has been used for an analysis in Wadam, and we have run the analysis for a single wave length. One great advantage by running a single frequency is that the results are very easy to interpret directly from the output file. By looking at the values of for instance GM, volume displacement and GB from the output file we can check to see if our hand calculations are performed accurately, or whether our input is correct or not.

GeniE has been used to model the cylinder, and HydroD as a pre-processor for the Wadam analysis. The motion output from Wadam are given in Table 5.

Motion Amplitude	Faltinsen (1990)	Matlab	Wadam	Difference[10]
$\bar{\eta}_2$ sway [m]	-0.07	-0.07011	-0.07041	0.4%
$\bar{\eta}_4$ roll [rad]	0.012	0.01206	0.01176	2.4%
$\bar{\eta}_3$ heave [m]		-0.004749	-0.003584	24.5%

Table 5 Results for small cylinders, compared with problem 3.4 in Faltinsen (1990)

We notice that the difference for the heave motion is much larger than the two other modes of motion. By comparing the added mass in heave calculated by Matlab from equation 3-14 to the added mass calculated by Wadam we see a quite large deviation. The added mass calculated by Wadam is almost 50% larger than the added mass from 3-14, and by noticing that the Matlab solution for $\bar{\eta}_3$ is larger than the $\bar{\eta}_3$ from Wadam, it's very reasonable to believe that the approximation for added mass is not very good and hence induce an error in the heave amplitude. The excitation force from Wadam is also found to differ from the excitation force calculated by equation 3-13. Matlab calculates an excitation force about 30% larger than the one from Wadam, which also contributes to the Matlab heave motion being significantly larger than the one found by Wadam. From this it seems that our simplifications in finding the heave force have been too inaccurate to capture the rolling motion well. Another reason for the large deviance from Matlab to Wadam might be a too coarse mesh on the cylinder bottom surface. The mesh used in the analysis is shown in Figure 14. The diameter of the cylinder is $2m$, and hence the panels are about $0.2m$ each. The wave length is $20\,m$, which gives us 100 elements per wave length. This should be sufficient for obtaining a reasonably accurate answer regarding the heave force, and I find it likely that the differences found is due to the approximations used for the Matlab calculations.

[10] Percentage of Matlab value

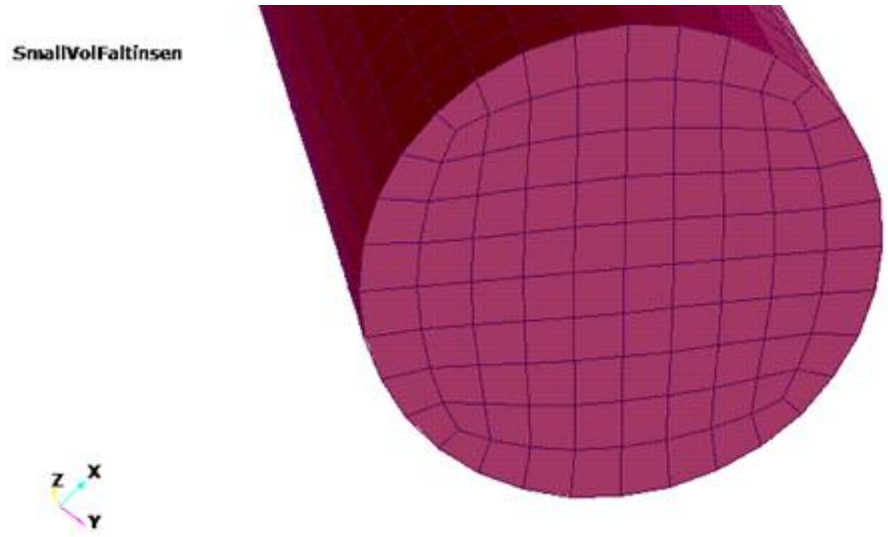

Figure 14 Grid bottom surface

3.2.2. Two cylinders of different size

As a next step in the analyses the size was changed to see how this alters its motions. By performing the analysis in chapter 3.2.1 we obtained a confirmation that the Matlab script gives out reasonably accurate values for motion in sway and roll. By obtaining quite similar results when running the analysis in Wadam it's reasonable to assume that the analysis is run in a correct manner. The geometry of the large cylinder is given in table 4. The results from the analysis are given in table 6.

Motion Amplitude	Matlab	Wadam	Difference[11]
$\bar{\eta}_2$ sway [m]	-0.02449	-0.01994	4.1%
$\bar{\eta}_4$ roll [rad]	0.002030	0.001446	28.8%
$\bar{\eta}_3$ heave [m]	$-2.286 * 10^{-6}$	$-1.432 * 10^{-6}$	37.4%

Table 6 Results for large cylinder

Again we notice that the difference for the heave motion is large. The calculations in Matlab are performed by the same script as above, so the error sources from inaccurate approximations for added mass and excitation force are still valid.

The values for sway and roll on the other hand are more comparable in Matlab and Wadam. However, a larger difference is expected due to the fact that the cylinder is enlarged, while the wave length is kept constant. When the diameter of the cylinder is $6\,m$ our assumption for a slender body from chapter 6.1 is no longer fulfilled, as $20/6 < 5$. When slender body theory is not longer valid the diffraction should have been taken into account, and hence the Matlab script becomes inaccurate as it doesn't include the diffraction potential. Wadam includes incident wave potential, diffraction potential and radiation potential. The latter potential will remove energy from the oscillating system, and hence act as a damping force on the motions. We see that the motions found by Wadam are lower than for what is found by Matlab. This is explained by the potential damping included in the Wadam analysis. The difference between Wadam and Matlab are more significant for the large cylinder, than for the smaller one. For the large cylinder, which is not considered slender, the

[11] Percentage of Matlab value

potential damping is too large to be left out of the analysis. For the smaller cylinder however, the potential damping is negligible and thus the Matlab script returns accurate results.

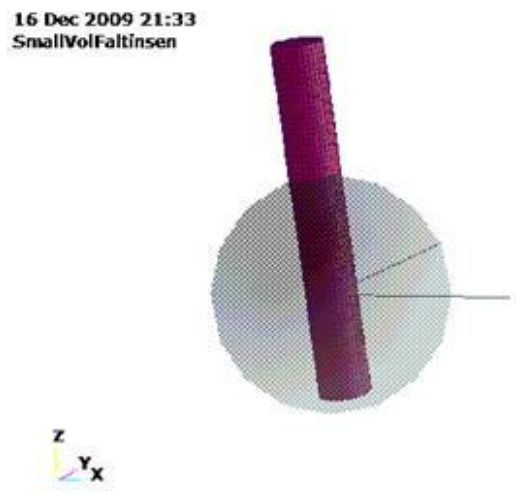

Figure 15 Small Cylinder from Wadam. Mass model coloured light.

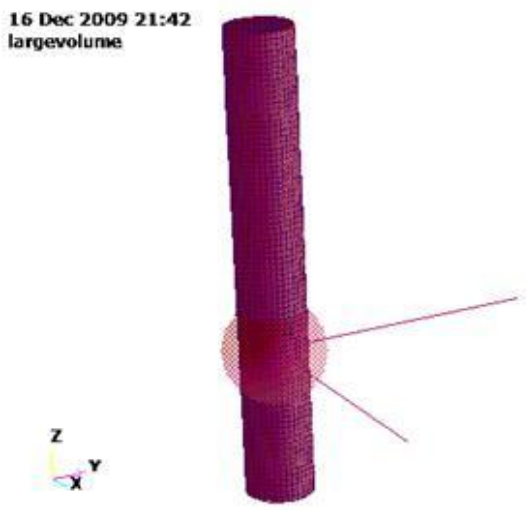

Figure 16 Large Cylinder from Wadam. Mass model coloured light .

The resulting simulation of both cylinders is named LargeSmallCylinders.vtf and found in Appendix C. The VTF file show the relative motion between the two cylinders, and uses the Matlab values for sway and roll motion. This induce a small mistake as we just discussed, and thus a corresponding simulation is included as well, which uses the Wadam values for the amplitudes of sway and roll motion of the large cylinder. The heave motion is corrected for both large and small cylinder, but the calculated values in sway and roll for small the cylinder are not corrected as the difference is negligible. This simulation is found as LargeSmallCorrected.vtf in Appendix C.

3.2.3. Simulation of Hywind and WindFlip

A simplified analysis in Matlab has also been done on cylinders with comparable characteristics to Hywind and WindFlip. For this analysis an equivalent diameter of the structures has been calculated based on draft and displacement. Parameters such as GM, radius of gyration and displaced volume are found from the dimension summary in Appendix B. Analyses for WindFlip and Hywind have not been carried out Wadam in this chapter, and this will be addressed in chapter 6.

From the previous chapter we have an indication that the Matlab script returns reasonably accurate values for slender body in long waves. Based on this the wavelength is chosen as $120\ m$, and the criterion for slender body is fulfilled. By making the case a slender body problem, the results from Matlab should be quite accurate. The potential damping is not assumed to be large, and if the analysis had been performed in Wadam similar results are to be expected. However, neither the Matlab script nor the panel model from Wadam takes any viscous damping into account. The viscous damping term might be quite significant in the case of a slender bluff body.

The chosen wave height of $5\ m$ is within what has to be expected if the launching is to be performed in a sea state with $H_s = 3\ m$.

Motion Amplitude	Hywind	WindFlip
$\overline{\eta}_2$ sway [m]	-0.2228	-0.3540
$\overline{\eta}_4$ roll [rad]	0.01876	0.01081
$\overline{\eta}_3$ heave [m]	-0.001706	-0.0008531

Table 7 Result summary for Hywind and WindFlip

By looking both at the printed results and the animation, HyFlip.vtf, we see that the wave induced motions for Hywind are much larger than the motions for WindFlip. This is easiest to see from the animation as the roll motions are very prominent for Hywind. Because of the large distance between the rotational point and the top of the structure the motions obtain very high values for the ends of the cylinder, particularly the top surface.

The surge/sway motion will not influence the relative motion between the two cylinders as much as the roll/pitch angle and the roll/pitch motion will probably be the most crucial parameter in the launching operation (Mannsåker, Private correspondence 2009). So the fact that the WindFlip vessel has a larger surge motion amplitude will most likely not affect the relative motion to a great extent.

For the heave motion the results for the two structures differ quite significantly. WindFlip weighs about 4.4 times more than Hywind, and A_{33} is about 7.6 times larger. This combined with the fact that the cross sectional area of the bottom where the heave force is acting is only about 3.8 times larger will contribute to the heave motion of WindFlip being significantly larger than the heave motion for Hywind. However, the heave motion will, as for the two cylinders in 3.2.2, not be very accurate, and should hence not be emphasized in analysing the results.

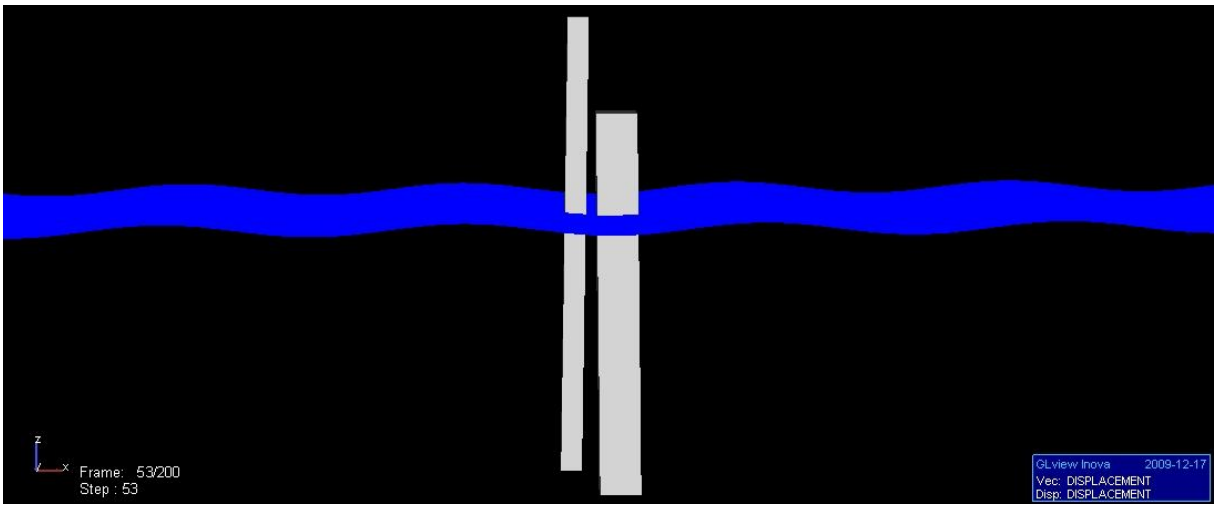

Table 8 Snapshot from Hywind + WindFlip in GLview

From the visualization we clearly see that the motions for the smaller cylinder (Hywind) are much larger than the motions of the large cylinder (WindFlip). This supports our preliminary hypothesis from chapter 2.2, where we suggested that the most favourable arrangement for launching is by placing Hywind downstream, and WindFlip upstream. By doing this Hywind is in the sheltered area in the wake of WindFlip, and the excitation forces will be reduced quite significantly and thus the motions of Hywind will be reduced. As discussed in chapter 2.2 this is merely a hypothesis and analyses need to be performed to investigate the effects of interaction in the specific case of WindFlip and Hywind.

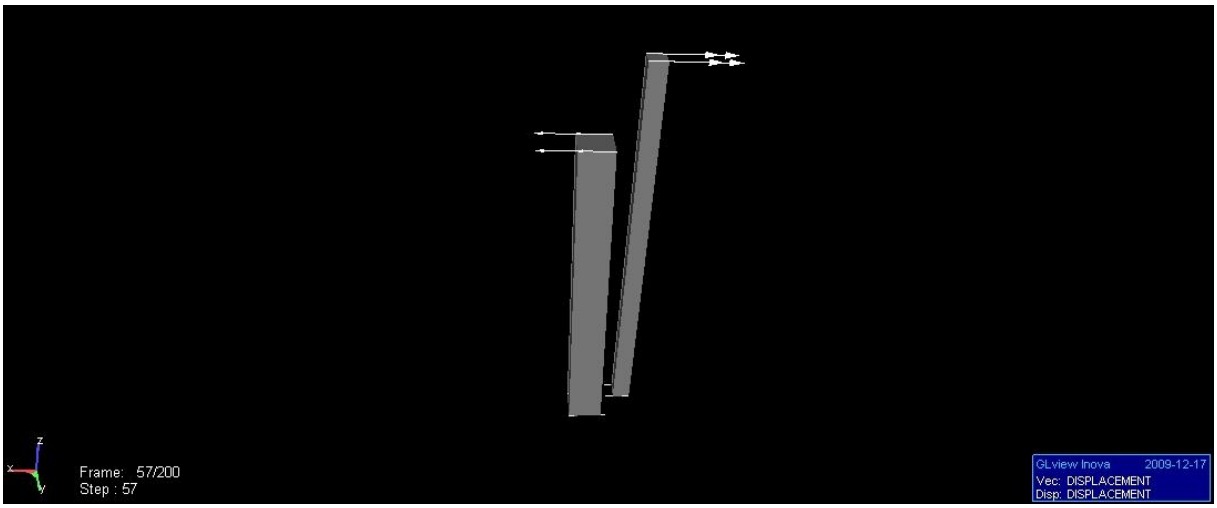

Figure 17 Motions of WindFlip and Hywind

Figure 17 shows the vector arrays of the motions. The waves are excluded from the animation to better be able to see the arrows.

3.2.4. Convergence

In chapter 3.2.1 we verified the accuracy of the Matlab script for slender bodies. Another way to get a confirmation that the analyses are performed correctly is by running the analyses with a very long wave length. When the wavelength goes towards infinity the structures should move as particles in the water, and hence follow the wave orbit. A general RAO for freely floating bodies will go towards 1 for heave and sway, and zero for roll when the wave length approaches infinity. The RAO is defined as $\left|\frac{motion\ amplitude}{wave\ amplitude}\right|$. For heave and surge the RAO is equal to one which means that the body simply follow the wave motions. This also leads to a roll RAO of 0 as there is no force tilting the body.

The convergence test in Wadam is performed to confirm that all the input values are correct. In the Matlab case the convergence test is to mainly validate that the script perform correct analyses with the given input. A test for infinitely long waves will not be numerically possible, but by using a wave length of $1\,000\,000\,m$, the results should show the expected RAOs for infinitely long waves. In Wadam, which does not assume deep sea as the Matlab script does, the depth also had to be change in order to avoid any sea bed effects. The results for the analyses performed with a wave amplitude of $0.25m$ and corresponding RAOs from the long wave tests in Matlab for the two cylinders from chapter 3.2.2 are shown in Table 9.

Mode of motion	**Small cylinder**		**Large cylinder**	
	Motion amplitude	**RAO**	**Motion amplitude**	**RAO**
$\bar{\eta}_2$ **sway [m]**	-0.24999	0.99996	-0.24998	0.99992
$\bar{\eta}_4$ **roll [rad]**	$-1.533 * 10^{-6}$	$6.1 * 10^{-6}$	$-1.5162 * 10^{-6}$	$6.1 * 10^{-6}$
$\bar{\eta}_3$ **heave [m]**	0.25	1	0.25	1

Table 9 Results for very long wavelengths, Faltinsen problem in Matlab

From the corresponding Wadam analyses the RAOs are given directly in the output file, and are presented in table 10.

Mode of motion	Small cylinder	Large cylinder
$\overline{\eta}_2$ sway [m]	$9.9939 * 10^{-1}$	1.0038
$\overline{\eta}_4$ roll [rad]	$1.2629 * 10^{-4}$	$5.3105 * 10^{-5}$
$\overline{\eta}_3$ heave [m]	1	1

Table 10 Results for very long wave lengths, Faltinsen problem in Wadam

Also for the simulation of the cylinders representing Hywind and WindFlip a convergence analysis has been performed, and the results are presented in table 11.

Mode of motion	Hywind		WindFlip	
	Motion amplitude	RAO	Motion amplitude	RAO
$\overline{\eta}_2$ sway [m]	-2.552	1.0208	-2.4995	0.9998
$\overline{\eta}_4$ roll [rad]	$-1.6054 * 10^{-5}$	$6.4 * 10^{-6}$	$-1.5417 * 10^{-5}$	$6.2 * 10^{-6}$
$\overline{\eta}_3$ heave [m]	2.5	1	2.5001	1.00004

Table 11 Results for very long wave lengths, Hywind + WindFlip

We see that all the RAOs are approaching 1 or 0 for sway/heave and roll respectively. This is as expected and implies that the Wadam input is correct, and is a good indication that the Matlab scripts are performing the analyses properly. There are larger deviation between the RAO at infinitely long wave and the wave length used in the convergence test for Hywind and WindFlip than for the cylinders in chapter 3.2.2. This is most likely due to the size difference, and by using even longer waves for the Hywind and WindFlip case this could have been avoided.

We also notice the signs for the sway motion to be the opposite of the wave. This is explained by the phase difference between the maximum sway motion of the cylinders, and the maximum wave elevation. We see that the heave has the same sign for both cylinder motion and wave motion, which implies that the cylinder is at its highest when the wave height is at its highest as well. This coincides with the fact that the cylinders follow the wave particle orbit.

4. Hydrodynamic response during flipping procedure

4.1. Flipping procedure

As mentioned in the introduction the concept behind WindFlip is to transport the wind turbine lying horizontally on top of WindFlip. When the final destination is reached, WindFlip will be ballasted until the structures achieve a vertical position, see Figure 18.

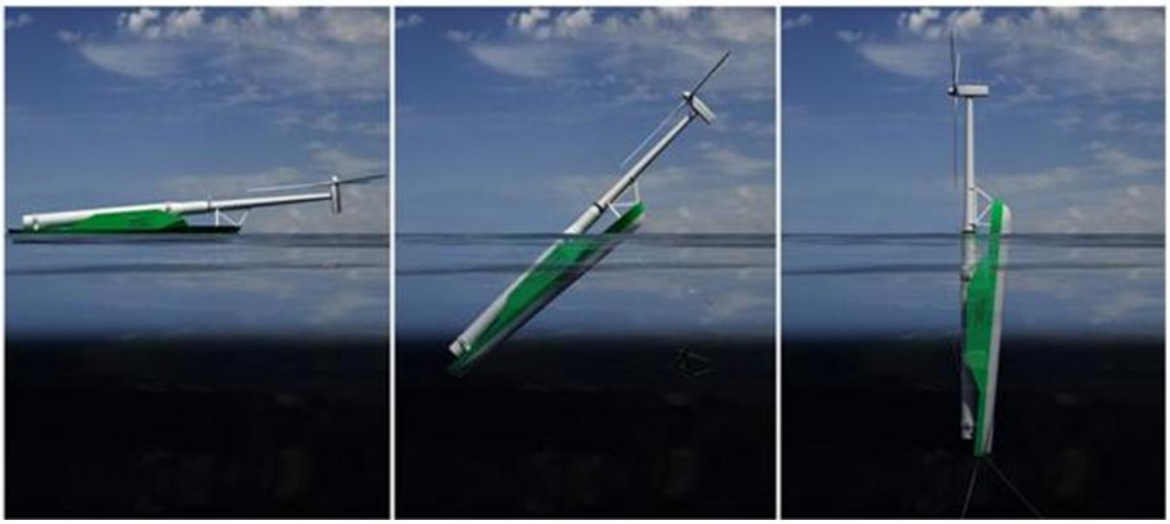

Figure 18 Flipping procedure

In the vertical position Hywind is released from WindFlip, and the turbine is ready to be moored and set into use. The flipping operation is performed by gradually filling the ballast tanks with sea water. During the filling dynamic stability is ensured in all positions, and reversing the operation is possible at all times. The flipping will most probably take about six hours from horizontal to vertical position (Mannsåker, Private correspondence 2010). During this time the hydrodynamic properties of the structures will change constantly, and hence the responses of the structures vary throughout the flipping operation.

In February WindFlip was tested at Marintek in Trondheim, and one of the addressed situations was the different stages of the flipping operation. The flipping operation is expected to last for several hours, which implies that the rotational velocity is very low. In the model tests and numerical analyses we have looked at different static flipping positions, and the rotational velocity of the

operation is not taken into account. This should give us a good impression of how the structures behave in the different stages of the flipping operation. The wave range for the analyses have been suggested by the WindFlip team as 5 to 23 seconds, and this range has been used for the analyses for all Hywind/WindFlip runs throughout this report.

The different stages looked into in the model test are 44 degrees, 60 degrees and 85 degrees, where the last one is the position where the release is to be carried out. The model test was performed by Torbjørn Mannsåker, Anders Hynne, Atle Alvheim and Espen Vårdal Kvalheim, and all model test results used in this thesis are taken from their measurements. The details behind the model test are found in the master theses of Mannsåker and Kvalheim.

In this thesis I have performed analyses at the same stages of the flipping operations. The panel model and mass models are made by the WindFlip team. The motion responses from the different analyses are presented in the subsequent chapters, and compared with results from the model tests. All results from the model test have been interpret and evaluated by Kvalheim, and the model test results in this thesis are used with his permission.

4.2. Responses in different flipped positions

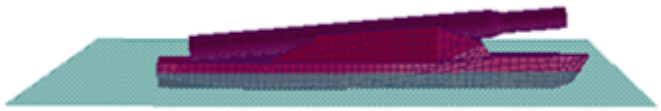

Figure 19 Panel model in transit condition

4.2.1. Comparing model test and numerical analyses

44 degrees

By using a mass model designed for the 44 degrees stage in the flipping operation we obtain a loading condition resulting in a trim angle of 44 degrees relative to the transit condition (ref. Figure 19), as shown in Figure 20.

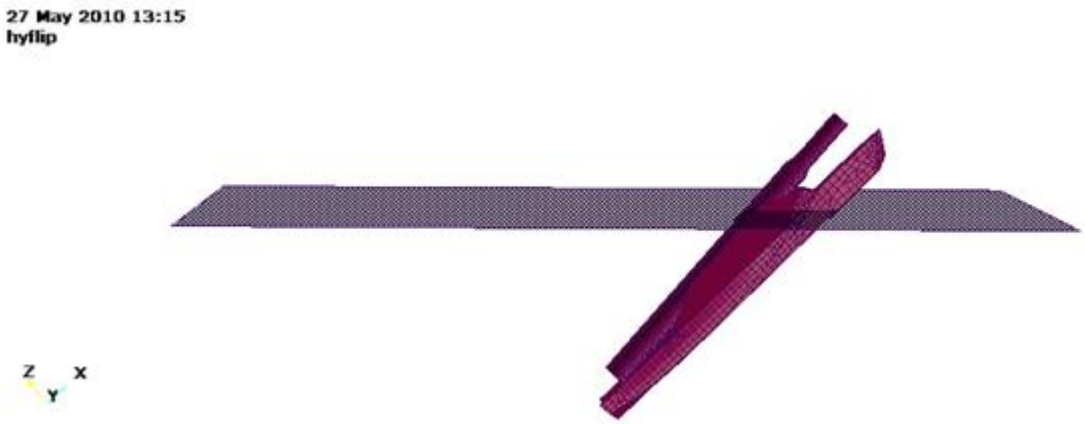

Figure 20 Model flipped 44 degrees

As suggested by the literature study and preliminary analyses in chapter 3 the preferred arrangement for release of the wind turbine is with the turbine sheltered behind WindFlip, like sketched in Figure 21. This is also the arrangements used during the model tests, and for the numerical analyses in this

chapter. Due to the symmetry of the bodies waves propagating along the x-axis will not induce any motion of significance in the y-direction, and the motions in the y-direction will not be looked into.

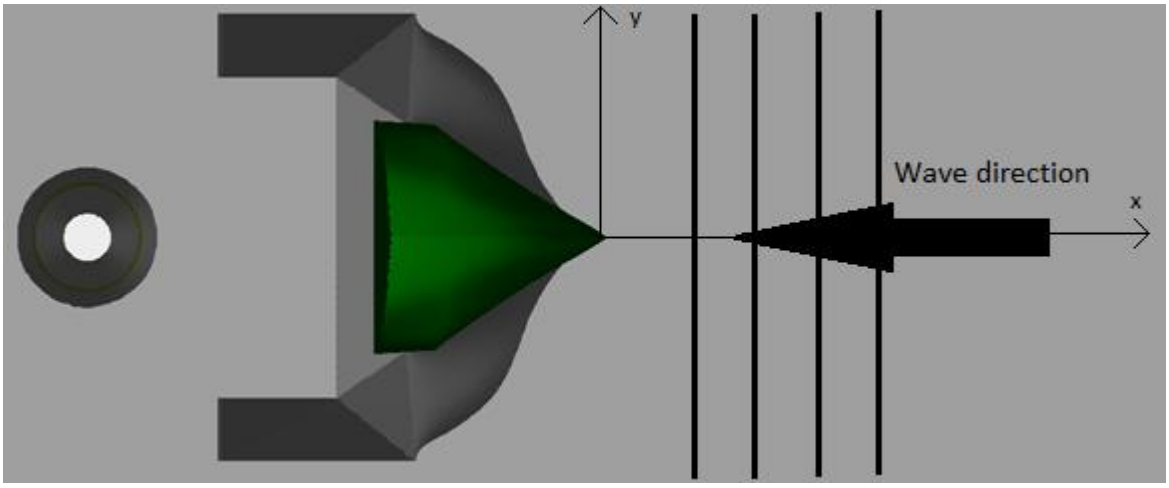

Figure 21 Wadam analysis setup

The results from Wadam have been exported to Postresp, where the response variables are given as response amplitude operators (RAOs). The three response variables evaluated are heave, pitch and surge, and the results from both numerical and experimental analyses are given beneath. The analyses are performed for a wave period of 5 to 23 seconds, and the response per meter wave amplitude is shown on the ordinate axis.

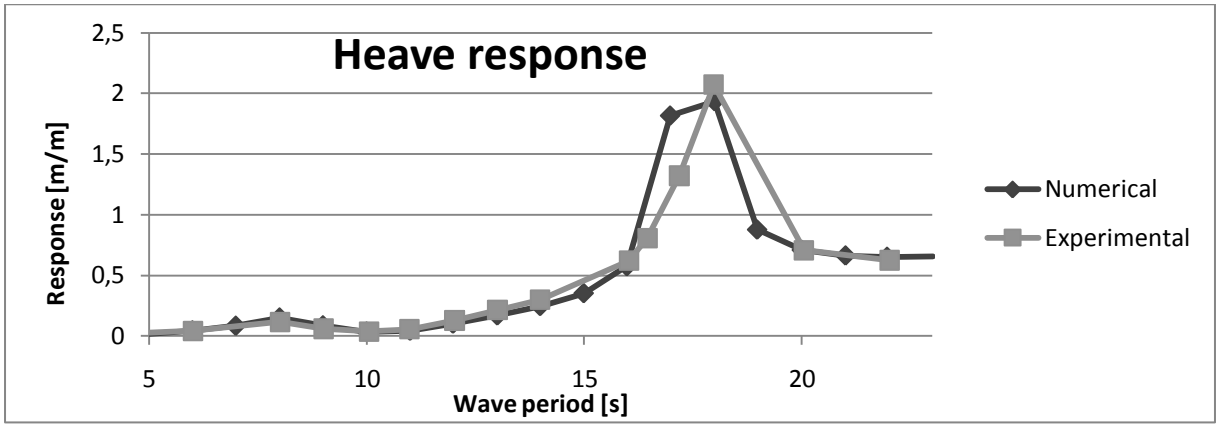

Graph 1 44 degrees trim, heave

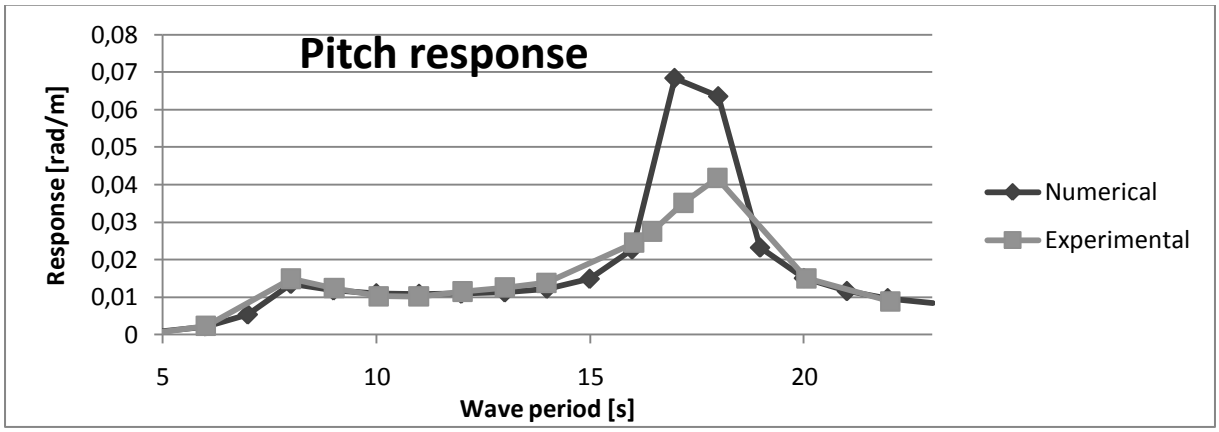

Graph 2 44 degrees trim, pitch

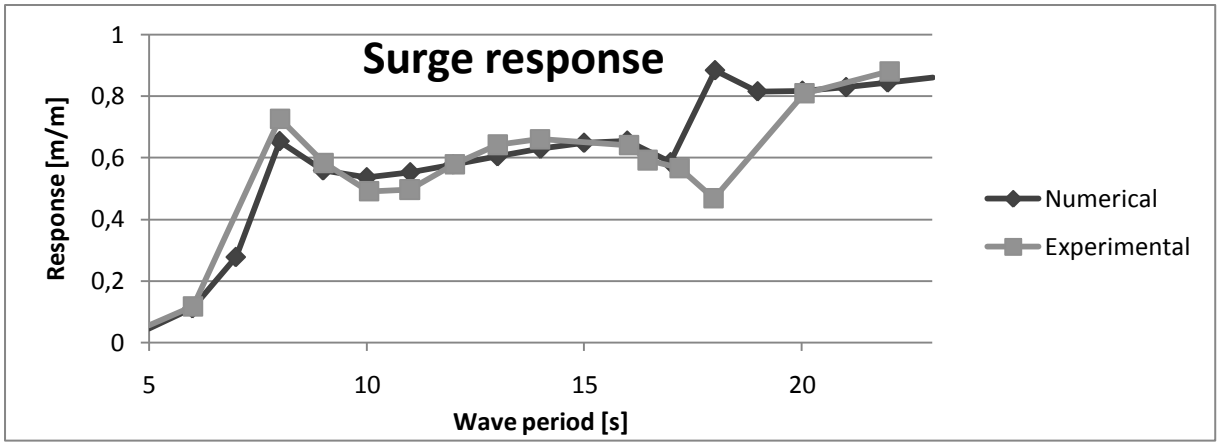

Graph 3 44 degrees trim, surge

In all modes of motion we see that the results from the numerical analyses compare well with the results obtained in the model tests. This is a good indication that both numerical and experimental analyses have been performed correctly. This knowledge is most valuable for the further development of WindFlip. It gives us good reason to assume that numerical analyses give sufficiently accurate results, and may be trusted for later analyses of the structures.

We notice that some of the parts of the graphs have larger deviations between experimental and numerical results. All the model test runs have only been run once for each wave period due to limited time frame during the testing. This means that each of the experimental points are very vulnerable to small errors in the testing, and the deviations in the graphs might be caused by disturbances in the model test run. By running two or more runs for each period this uncertainty in the measurements could have been greatly reduced, and we could have found a standard deviation for the uncertainties in the data points.

In the areas of the graphs where we find the deviations, there might be more going on than what is capture in our results. The time increment of the analyses is 1 second. By decreasing the increment in the areas where the deviations from the model test are significant, or in other areas where the graphs show a special behavior, we might get a better impression of what is going on in these areas.

There is a noticeable deviance in the responses around the resonance frequency. In potential theory, which is applied in Wadam, the damping is caused by waves generated by the body. The water plane area of WindFlip and Hywind is low, and this gives us a low damping and hence potentially a very high response around the resonance frequency. In the model test the viscous effects will also affect the motions, and by looking at the pitch motion we see that the motion amplitude around the resonance frequency is lower for the model test than for the numerical analyses. A reasonable explanation for this would be the increase in damping for the structure caused by the viscous effects for the flow passing around the structure. For the heave response the difference between the model test results and numerical results is not so significant. This could be explained by the viscous damping in heave being of less significance than the viscous damping in pitch.

60 degrees

When the mass model designed for the 60 degree stage in the flipping process is used to specify the mass of the structure we obtain a trim angle of 60 degrees. The orientation of the waves is the same

as for the analyses for 44 degrees, and the only parameter changed is the mass model altering the trim angle.

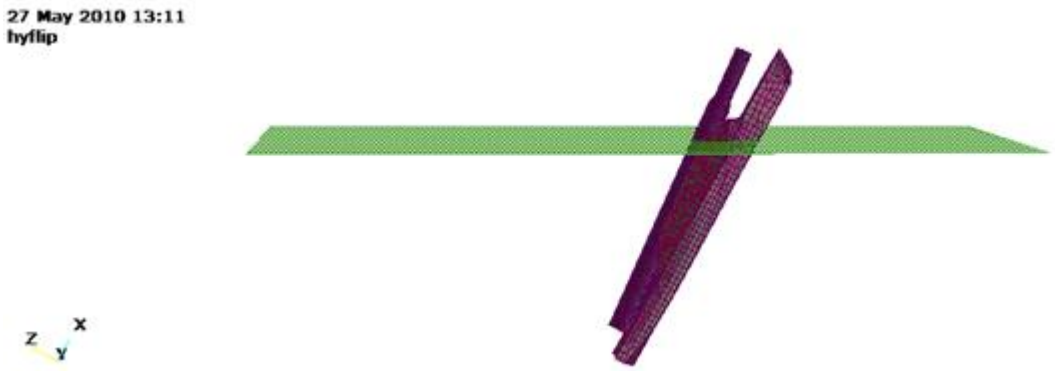

Figure 22 Model flipped 60 degrees

Also in this case the analyses are carried out with wave periods between 5 and 23 seconds, and the responses are given along the ordinate axes. Response in surge mode is shown underneath, whilst heave and pitch are given in Appendix D.

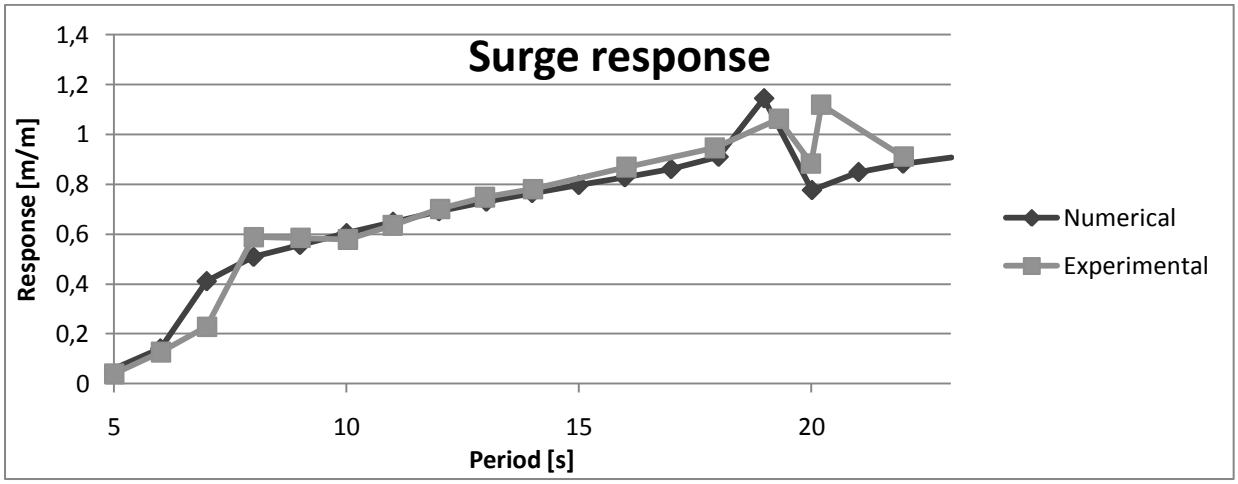

Graph 4 60 degrees trim, surge

We see the same trends for 60 degrees trim angle as for 44 degrees. The model test results and numerical results compare well. Also here we notice that the responses around the resonance frequency are lower for the model tests than for the numerical analyses in heave and pitch, and the viscous effects are most likely to be blamed here as well. As mentioned in the 44 degrees case, performing new numerical analyses with lower time increments in the areas with larger deviations and untypical behavior could give us more insight into why the graphs behave as they do. For the case in Graph 4 a suggestion for a new numerical analysis would be running from 17 to 23 seconds with 0.25 second increment to get a better picture of the responses in this area. The analyses could also have been extended to include higher wave periods. We notice in the graphs that we have no way of knowing how the graphs will look like in waves with higher period than 23 seconds. Since the behavior close in the area below 23 seconds is as unstable as shown in Graph 4, what happens to the responses at longer wave periods would be interesting to know.

85 degrees – release position

When WindFlip is positioned as shown in the figure below, at 85 degrees trim angle, Hywind is vertical. In this position there are no static forces between the bodies, and this is the position from which the release will be performed.

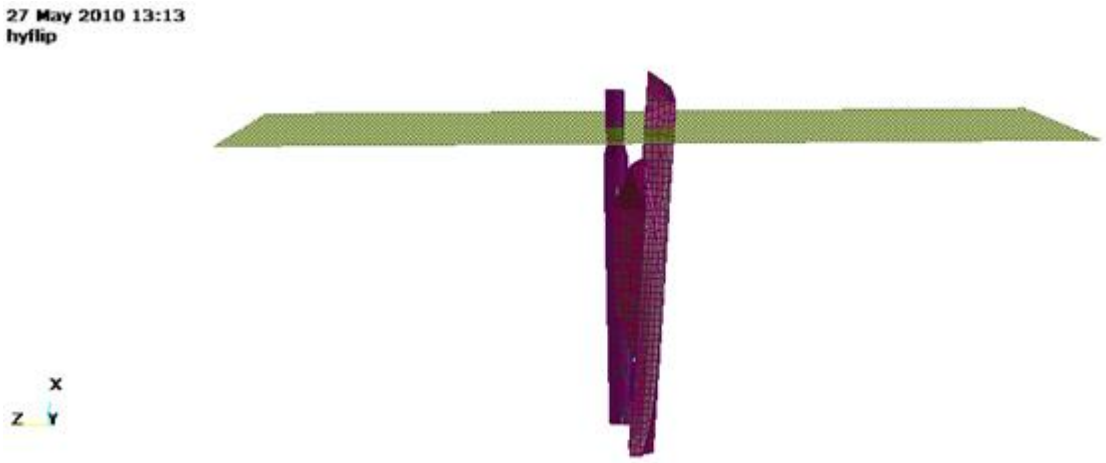

Figure 23 Model flipped 85 degrees

The results from these analyses are, together with the corresponding model test data, shown in the figure underneath and Appendix E.

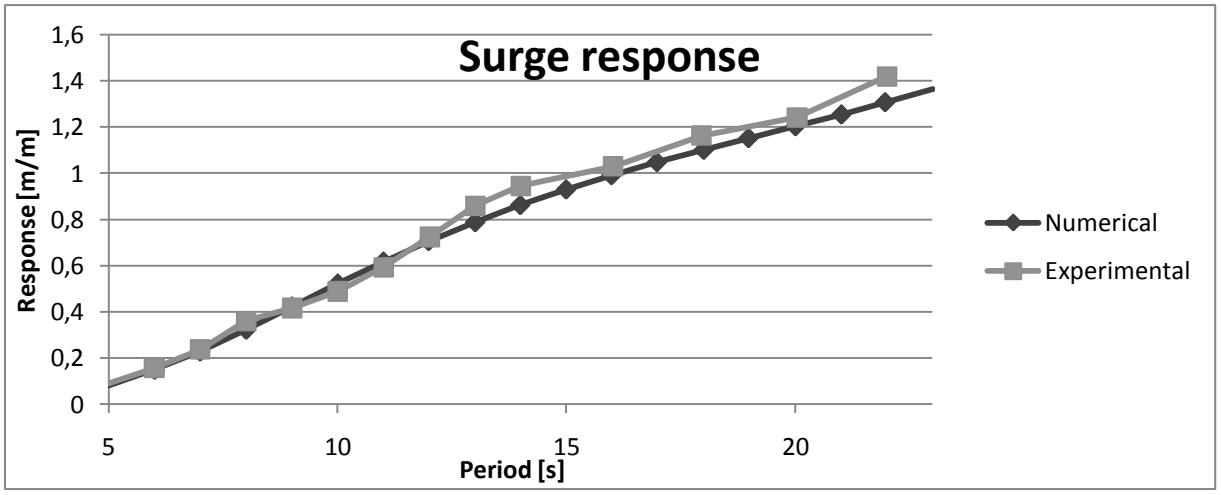

Graph 5 85 degrees trim, surge

Also for 85 degrees trim angle case the responses coincides well for pitch and heave mode. We see that the resonance frequency for the vertical WindFlip and Hywind is not within our period range, and hence the eigen periods of the three addressed motion modes must be higher than 23 seconds. Waves of 23 seconds are over 800 m long, and waves longer than this should not occur often in a normal sea state. In Appendix J the WindFlip eigen periods are found to be around 39 seconds for all three modes of motion. Due to the large volume of WindFlip compared to Hywind it should be safe to assume that the responses for WindFlip dominate the attached models response, leading to the attached structures eigen frequency being in this area as well.

4.2.2. Comparing the different flipped positions

For comparing the different flipped positions the numerical results have been plotted for the 44, 60 and 85 degree situation.

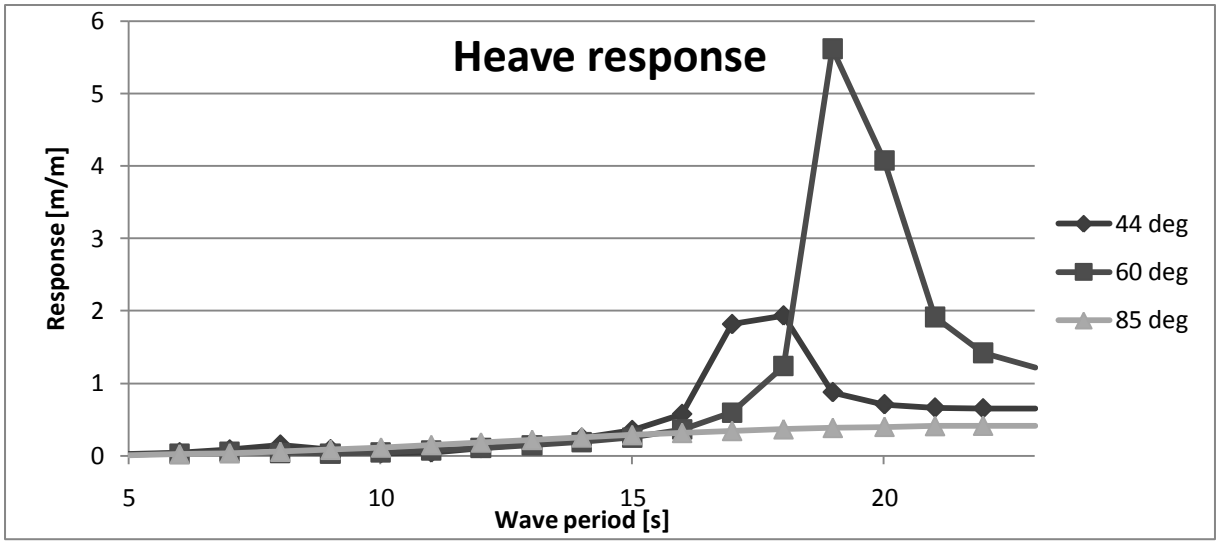

Graph 6 Comparing heave response

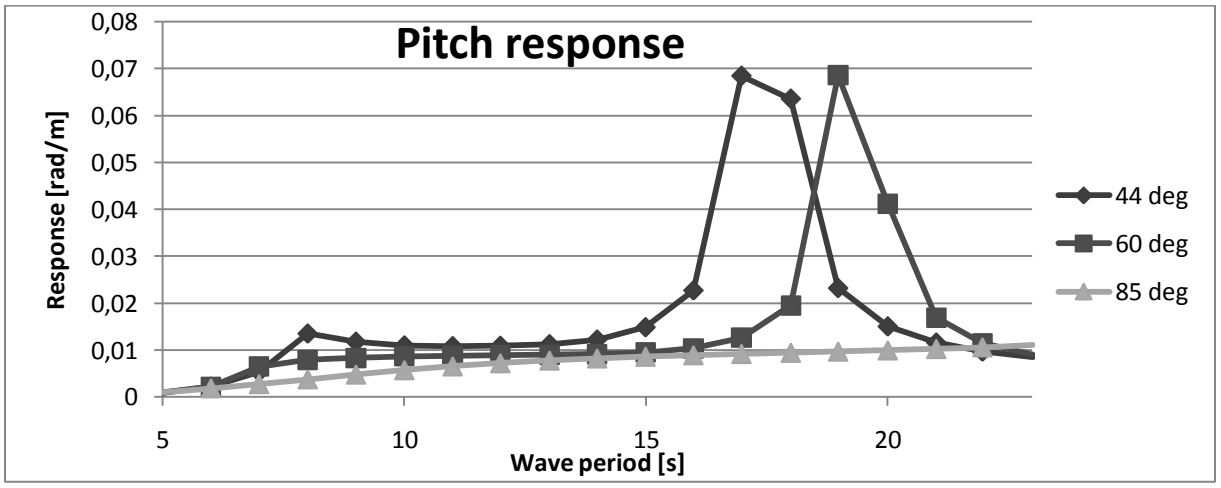

Graph 7 Comparing pitch response

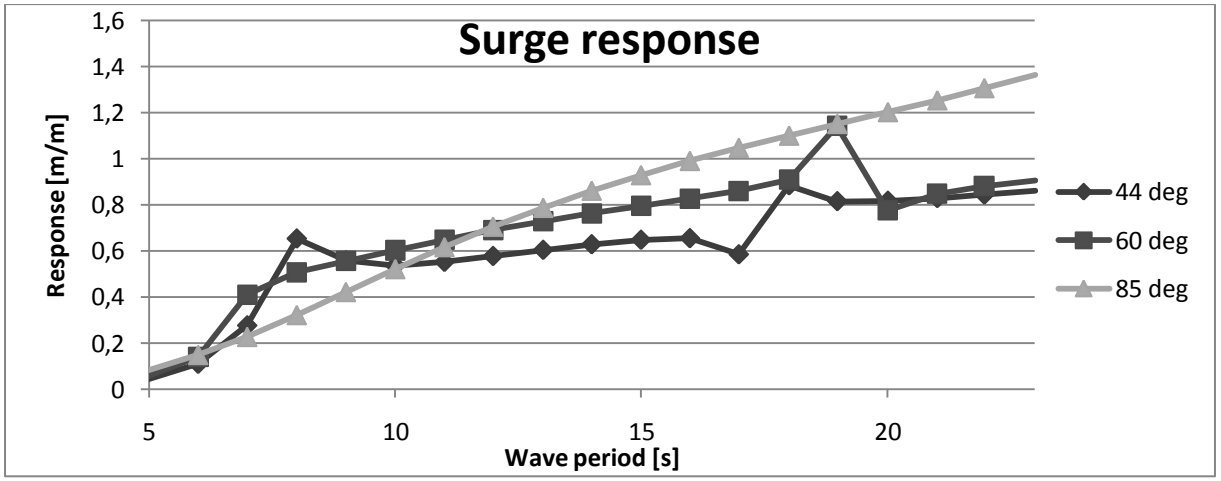

Graph 8 Comparing surge response

The heave and pitch responses are low for waves of high frequency, and increases as we approach the resonance frequency area for the structures. We notice that the resonance frequency increases when the flipping angle decrease. In 85 degrees trimmed position, which is the release position, the eigen period is at about 40 second. Waves of this period are about 2.5 kilometers long, and do not usually appear in normal sea states. The trimmed situations during the flipping operation are much

more sensitive for waves hitting the eigen frequency, which may cause resonance and needs to be avoided. The eigen period for the 44 degrees trimmed situation is around 17 seconds. This period corresponds to a wave length of 450 m, which is not uncommon in the oceans where the WindFlip barge might be be used.

The stability of the structure is also poorer when the trim angle is decreased.(Mannsåker, Private correspondence 2010) These two aspects indicate that the flipping procedure is a vulnerable operation, and should be carefully planned. Above we have confirmed that the numerical analyses can be used to calculate the responses in a sufficient manner, and can be trusted as tool to predict the behavior of the structures. By performing more numerical analyses on what is assumed to be challenging situations for the flipping it is possible to obtain an insight into the consequences of the worst case scenarios. By more extensive numerical analyzing it is also possible to define sea state limits for where the operation can be performed successfully and safely.

5. Multibody analyses on two identical cylinders

5.1. Hydrodynamic response

Earlier in the thesis the behavior of circular cylinders has been discussed. By using the same structures as in chapter 3.2.1 (Table 3 Dimensions for buoy Table 3) a multibody analysis is carried out to see how the interaction effects between the bodies affect the responses. In Figure 24 we see the multibody configurations used for the analyses. The diameter of the cylinder is two meters, and the spacing between the two analyzed bodies is given in Table 12.

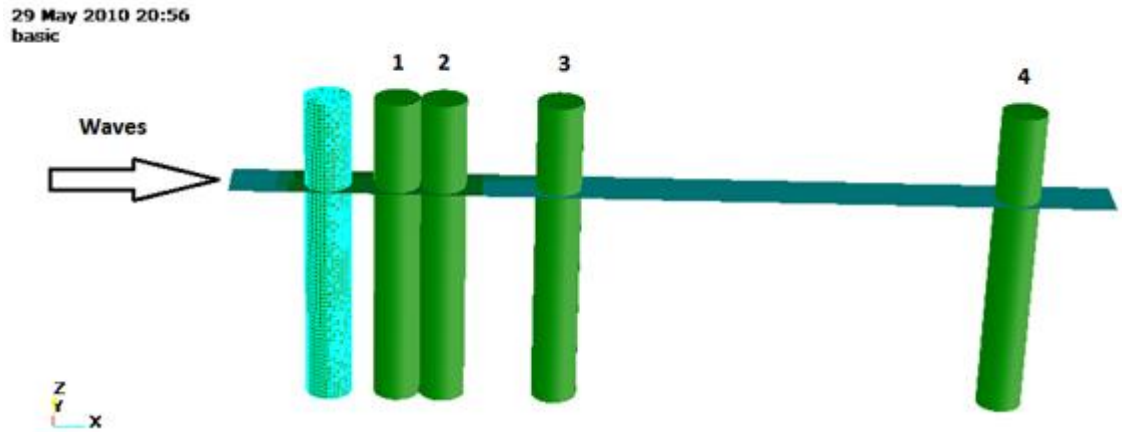

Figure 24 Multibody cylinder set up

Multibody model	Distance between the cylinder's origins [m]	Distance/Diameter [-]	Spacing/Diameter [-]
1	3	1.5	0.5
2	5	2.5	1.5
3	10	5	4
4	30	15	14

Table 12 Cylinder multibody set up

We have waves approaching from 0 degrees, which implies waves propagating along the positive x-axis. The highlighted cylinder in Figure 24 is body 1 in the analyses, and the four other cylinders represent the various multibody configurations, and will be body 2 in the analyses. The waves will hit

body 1 first, making it the weather side (upstream) cylinder, and body 2 will be in the wake area of body 1, hence the lee-side (downstream) cylinder.

To begin with the analyses were run with wave periods varying from 3 to 20 seconds. The responses from these analyses are given underneath for pitch, whilst heave and surge are given in Appendix F.

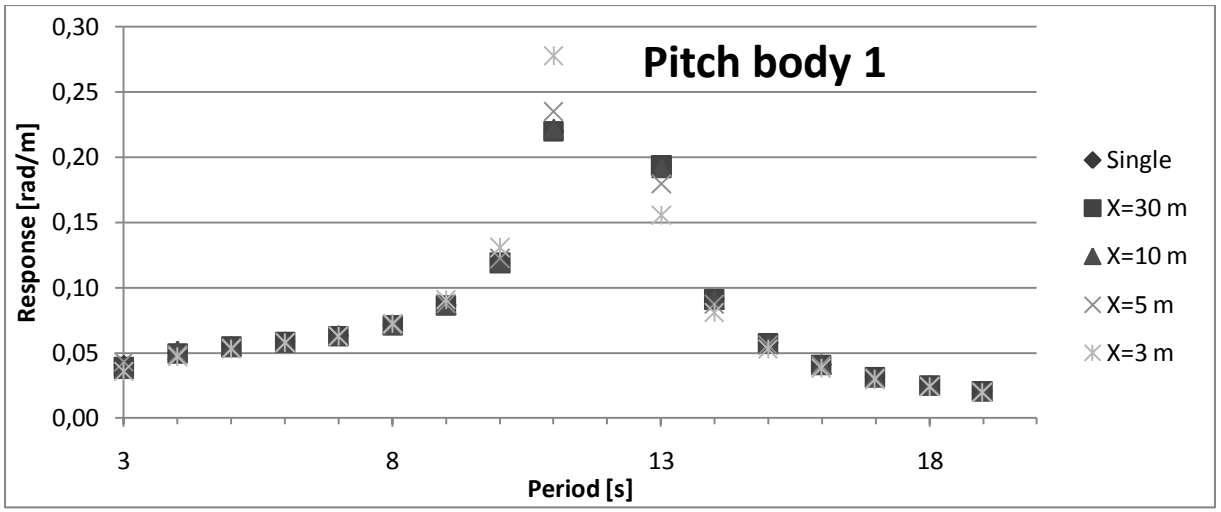

Graph 9 Pitch response weather side cylinder

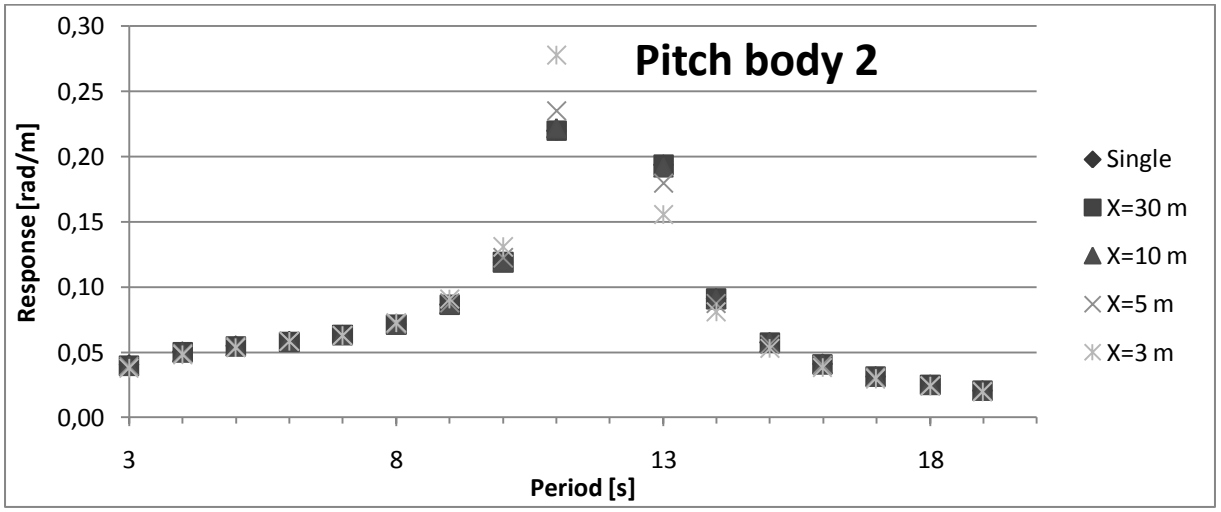

Graph 10 Pitch response lee side cylinder

We see from the two graphs above and the graphs in Appendix F that there are almost no difference in the responses for a single cylinder and the cylinders in the multi body analyses. When looking into the reason behind this the diameter of the cylinder has been compared to the wave lengths.

The smallest waves included in the analyses are 14 meters, which is seven times larger than the diameter of the cylinders, 2 meters. When the wave lengths exceed five times the characteristic length (the diameter for a cylinder), the body is characterized as a slender body (Faltinsen 1990)(Pettersen 2007), which is discussed in chapter 2.1. As our cylinder falls within this category it means that it will have close to no influence on the waves passing the structure. This means that the bodies will not alter the waves as they pass, and hence the downstream body will experience the same waves as the upstream body. Since we are working with a potential theory solver there are no viscous effects present. Hence, the only parameter of importance is the ratio between the size of the cylinders and the wave dimensions. We can scale all our parameters up and down, and 50 m long

waves will have the same effect on a cylinder with 20 m diameter, as 5 meter long waves will have on a 2 meter in diameter cylinder.

By using shorter waves in the analyses the slender body theory will no longer be valid, and the waves should affect the wave field and introduce a different response for the structures. New analyses with wave periods between 0.5 and 3 seconds are performed to see how shorter waves will affect the responses. Periods between 0.5 and 3 seconds correspond to wave lengths between 0.4 and 14 meters. Periods lower than about 2.5 meters gives us a situation where we no longer have a slender body, and radiation and interaction effects are expected to be present. The RAOs for the two bodies are given in the figures underneath for surge, whilst heave and pitch are given in Appendix G. The graphs have also been a bit modified so that they compare the weather side, lee-side and single cylinder for a given spacing.

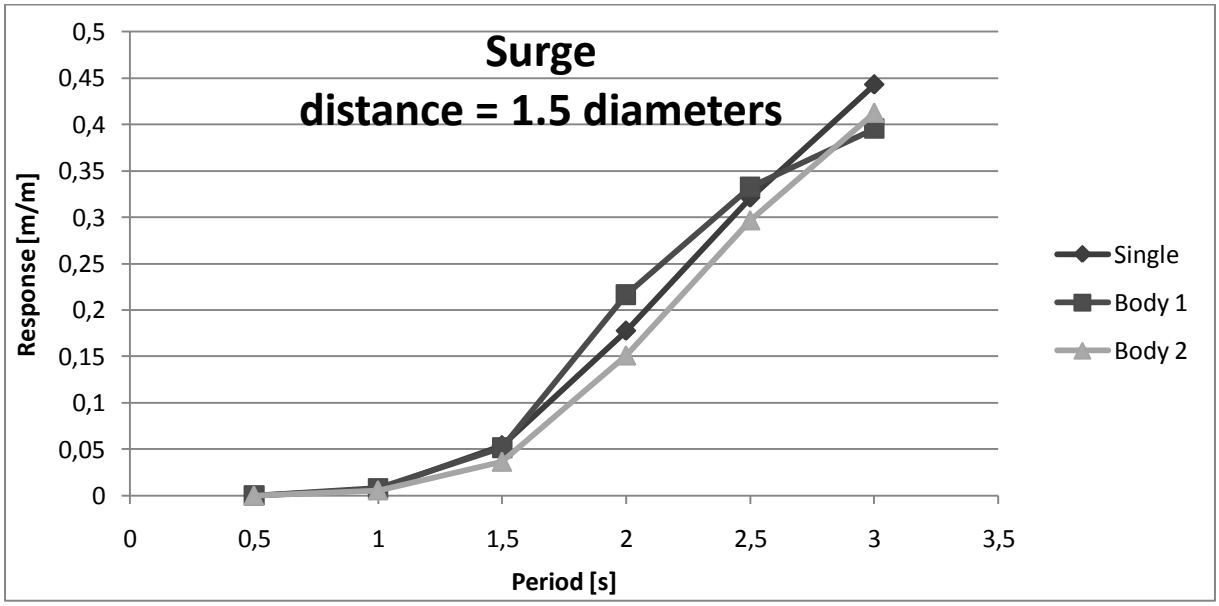

Graph 11 Surge response, multibody cylinders of distance 1.5 diameters

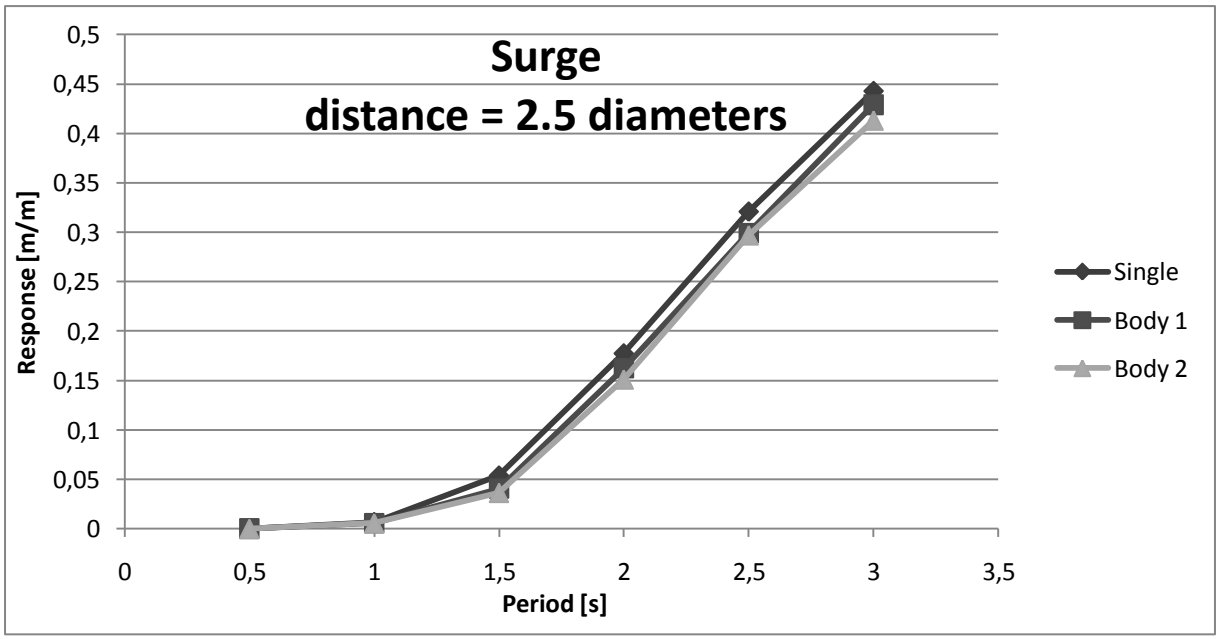

Graph 12 Surge response, multibody cylinders of distance 2.5 diameters

At the lower wave periods changes in the responses are noticeable. Firstly we see that the responses for the weather side cylinder (body 1/upstream) are higher than those for the lee side cylinder (body 2/downstream) in pitch and surge. The effect is larger at 1.5 diameters distance than for 2.5 diameters. This corresponds well to the sheltering effect looked into in chapter 2.2, and was an expected result for the analyses.

In confirming the assumptions regarding lower motions on the lee-side cylinder we also support the chosen release set up with Hywind situated downstream from WindFlip. This is to be investigated further in chapter 6 where the cylinders will be replaced by the correct geometries.

In heave mode the responses for body 1 and body 2 are almost identical, especially for 2.5 diameters distance. We notice that the magnitude of the heave responses is less than 1 percent of the surge responses. What will be looked into in chapter 7 is the horizontal spacing between the structures based on the Wadam output for the two interacting bodies. Due to the fact that the heave responses are significantly smaller than the motions in x-direction, neglecting the heave component of the response should not cause any large errors when looking into the horizontal spacing between the structures.

All the analyses in this thesis are carried out by the use of potential theory. This describes well how the waves affect the structures, but effects from current are not taken into account. The waves decrease exponentially from the surface as shown in Figure 6, and hence the wave action at the lower parts of our structures is very limited. However, the maximum pitch and surge motions of the structures at this point are high compared to the size of the structure. To exemplify this we will look only at the surge motion, and at 8 seconds wave period we have a response of about 1 m/m (ref. Appendix F). By using the relation (Faltinsen 1990)

$$\dot{\eta_2}\sin(\omega t) = \omega * \eta_2 \cos(\omega t) \qquad \textbf{5-1}$$

the maximum surge velocity then becomes 0.78 m/s in one meter waves. This gives us a Reynolds number of (White 2005)

$$Re = \frac{U*D}{\nu} = \frac{0.78m/s*2m}{1.462*10^{-5}m^2/s} = 107442[-] \qquad \textbf{5-2}$$

This Reynolds number gives, according to Sumer and Fredsøe(Sumer and Fredsøe 1997), a turbulent flow around the cylinder. This turbulence will not be taken into account in the Wadam analyses, where no viscous effects are included. The interaction effects found by potential theory do not have a large impact on the motions, and it is possible that the viscous effects would influence the motions characteristics to a greater extent.To be able to numerically find out how the viscous effects will affect the motions and interactions a CFD analysis would have to be run. Alternatively more extensive experimental testing can be performed.

5.2. Free surface between the cylinders

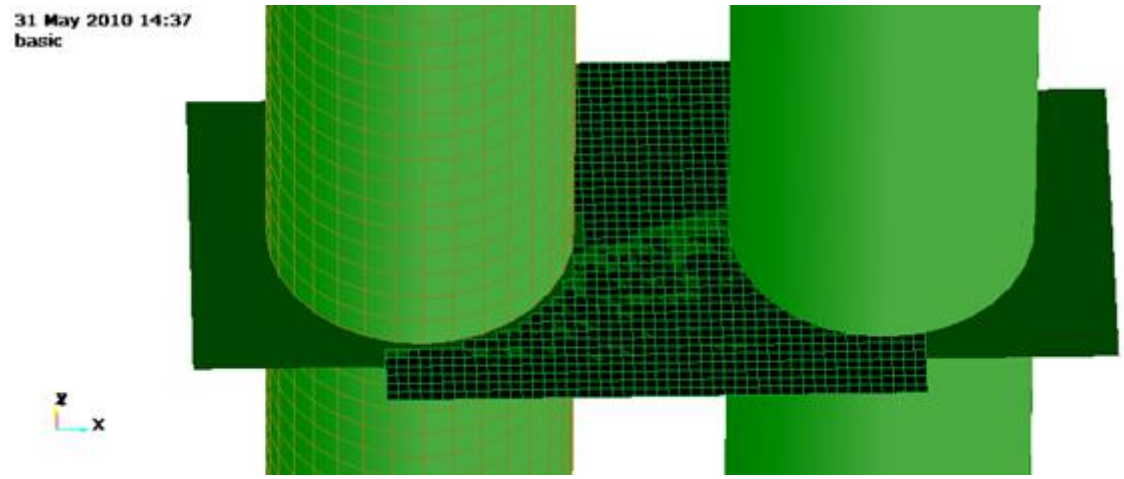

Figure 25 Offbody points to investigate wave disturbance

When a wave hits a body the wave field around it is changed due to the wave having to make its way around the body and due to the wave induced motions of the structure. These changes in the wave field cause the bodies to act differently as reviewed in the previous chapter. How the wave field is altered due to the two cylinders interacting is possible to investigate visually by the use of offbody points in Wadam. HydroD has a limitation of 2000 offbody points in a grid, which means we should be careful in deciding where and how to place our mesh. As discussed in chapter 5.1 the waves that will result in a noticeable altered wave field around the cylinders are small, and to be able to show the changes in an accurate matter we need a coarse mesh.

The waves are simulated by the postprocessor SESAM Xtract after the Wadam run. Xtract is a version of GLview specialized to present Wadam output. Xtract is today not able to simulate multibody motions, so the visualizations will only show the wave field between the structures, and not how the structures are affected. For the single cylinder and multibody 1.5 diameters case the meshes are as shown in Figure 26. For 2.5 diameters distance the mesh is as shown in Figure 27. To be able to compare the wave field between the cylinders to the incoming wave a reference analysis has been run as well. This with the mesh situated in front of the weather side cylinder, hence the first to be hit by the waves. See Figure 27.

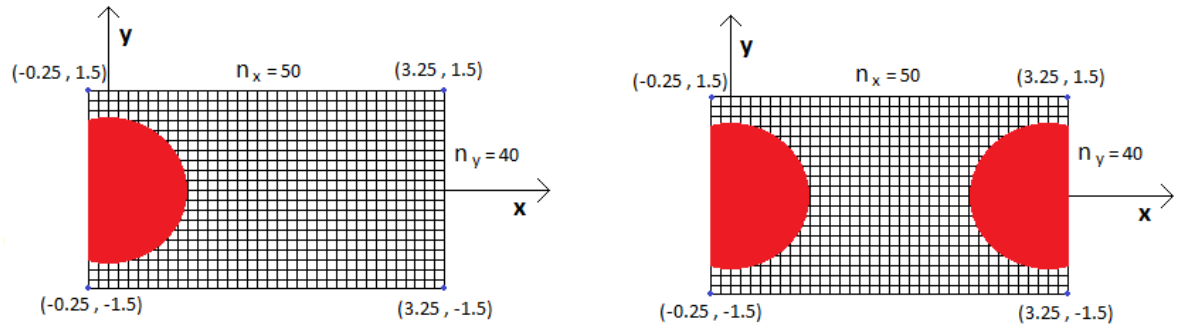

Figure 26 Offbody mesh, single (left) and 3 m distance (right)

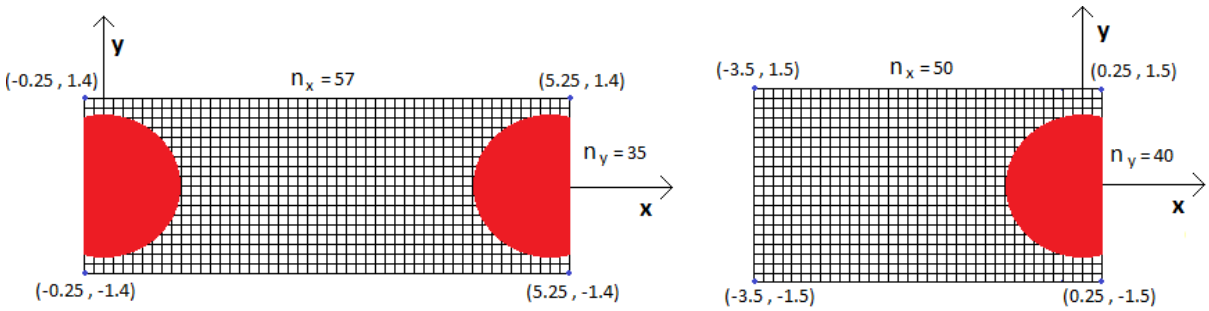

Figure 27 Offbody mesh 5 m distance (left) and reference run with mesh in front (right)

A range of wave frequencies has been evaluated, and the one that illustrates the wave action best is 1.42 Hz, which corresponds to wave a length of 0.76m i.e. about 40% of the diameter of the cylinders. Snapshots from analyses with this frequency are given below, and the animations are given as VTF files ready to run in GLview in Appendix C. The colors indicate the surface displacement from still water level, and indicate both troughs and crests. Yellow and red indicate the largest elevations, as specified in the contour bar far left in the figures.

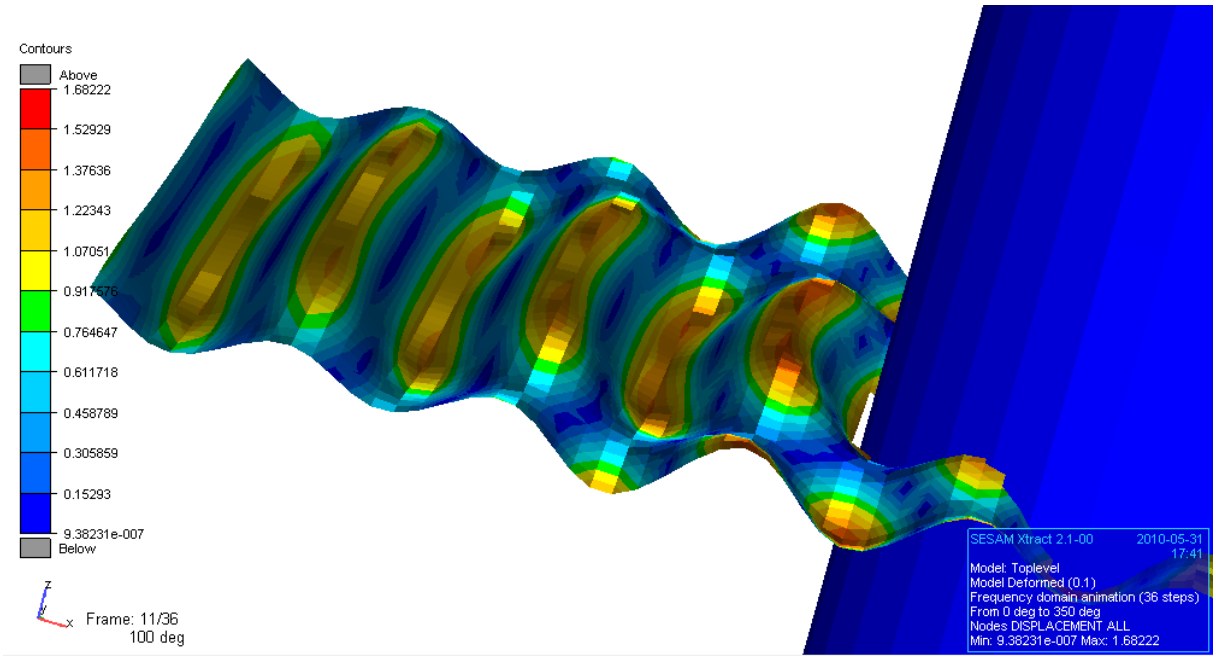

Figure 28 Visualization in front of single cylinder, 1.43 Hz

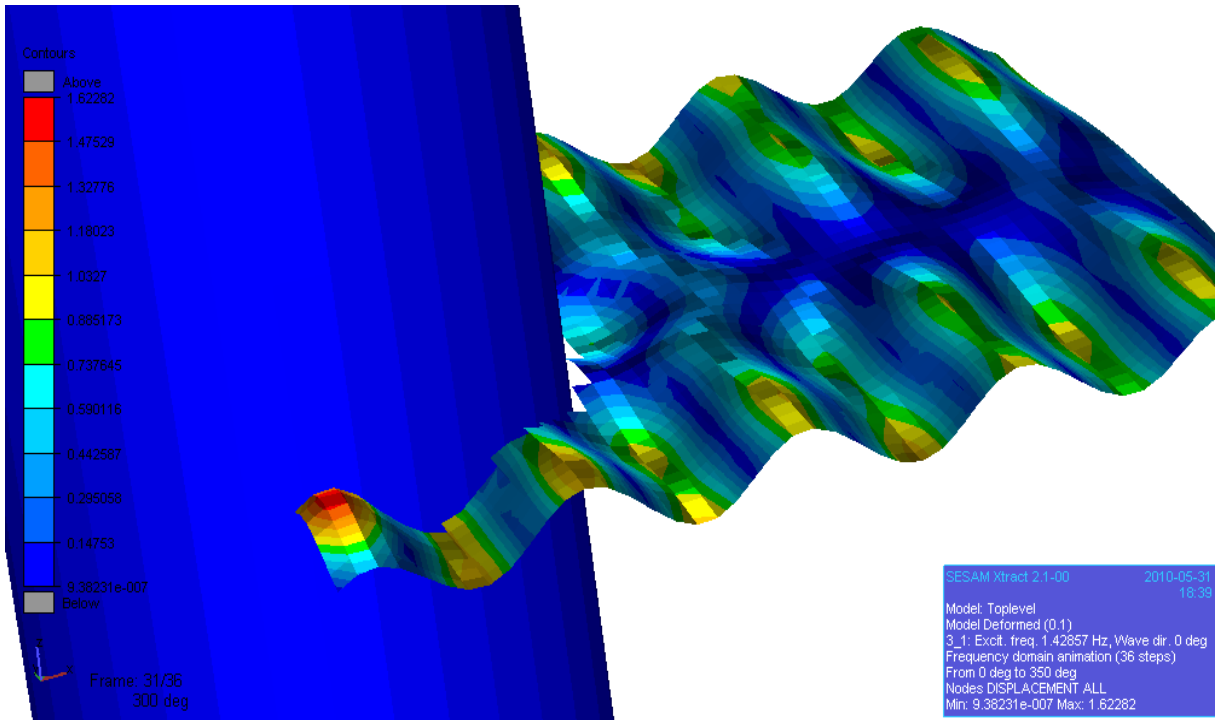

Figure 29 Waves behind single cylinder, 1.43 Hz

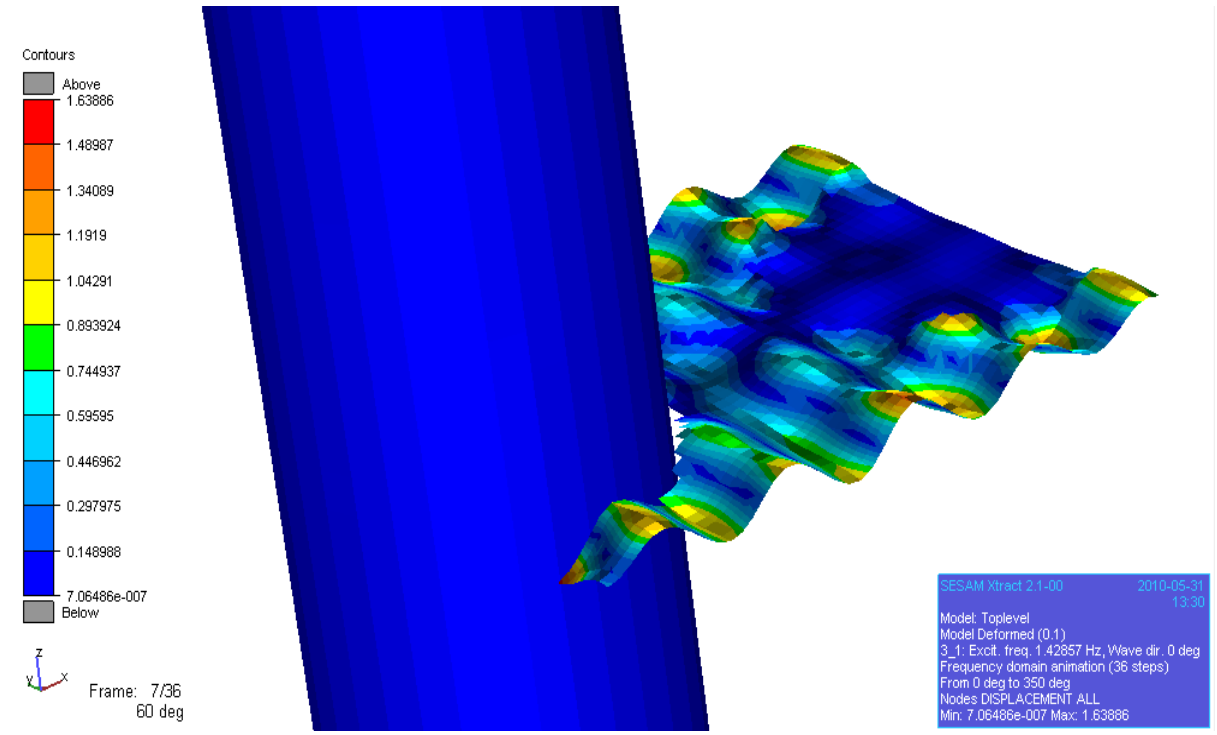

Figure 30 Waves between cylinders of 1.5 diameters distance, 1.43 Hz

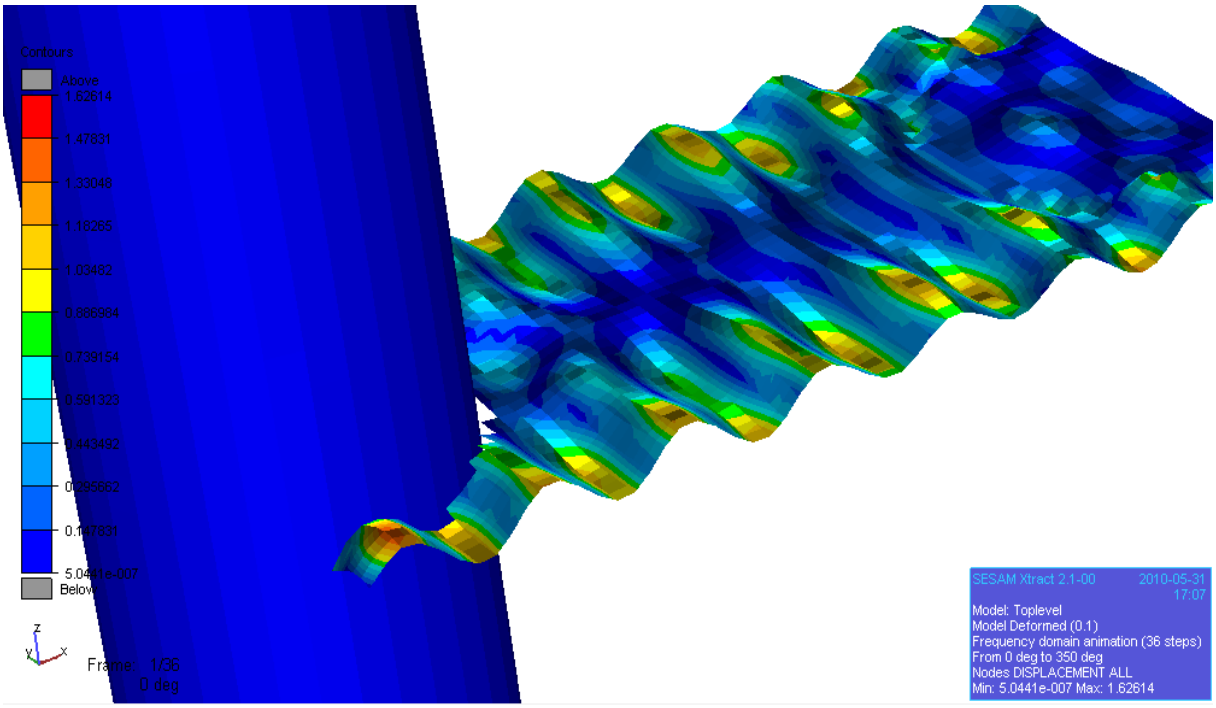

Figure 31 Waves around cylinders of 2.5 diameters distance

By comparing the wave field in front of the single cylinder (Figure 28) to the wave fields in the wake of the weather side cylinder (Figure 29, Figure 30 and Figure 31), we see a clear reduction in the wave heights behind the cylinder. In chapter 2 the wake region behind structures were looked into, and the effect we see above will hence be due to the first cylinder creating an area with less wave action behind itself. The reduced wave action behind the weather side cylinder corresponds to the lower responses of the lee-side cylinder, as discussed in the previous chapter.

6. Multibody analyses of WindFlip and Hywind

6.1. Preparing the analyses

The multi body analysis in chapter 5 was the first multibody analysis to be performed. Together with giving a better insight into interaction effects, it was meant to act as a confirmation that the multibody tool in Wadam is understood properly and works as intended. After finding reasonable results in the analyses of two identical cylinders, the next step was to use Hywind and WindFlip as input. Both structures have been modeled in GeniE, with corresponding mass models. This has been done by Andres Hynne, structural responsible on WindFlip. The coordinate system originally used is sketched in Figure 32, and both structures had this as their input coordinate system. After running test analyses several times without obtaining reasonable results, and discussing with both the WindFlip team and supervisor without any luck, DNV Support was contacted and made aware of the situation. After conferring with Jan Henrik Berg-Jensen in DNV, errors in the user manual and shortcomings in the software were discovered. This is further adressed in Appendix H.

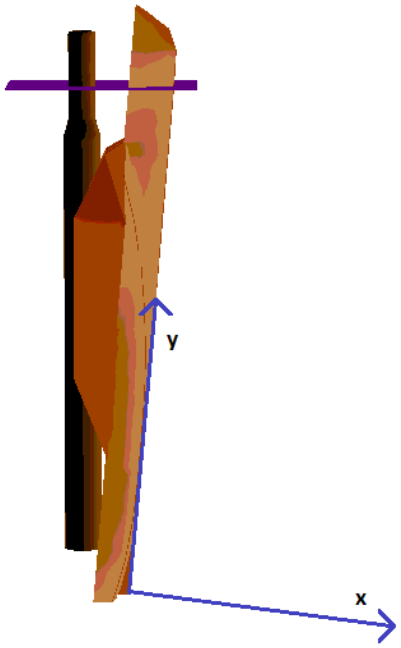

Figure 32 Original input coordinate system

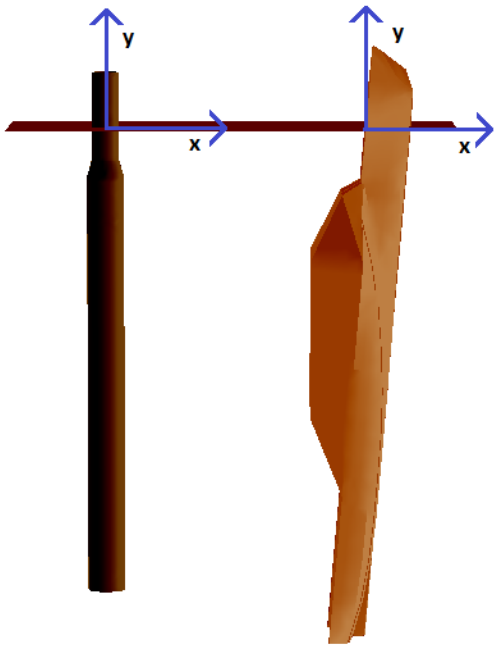

Figure 33 Final input coordinate systems

The two models were remodeled in GeniE, and the new input system is now placed with the origin in the still water line, and tilted so that no trim angle has to be defined in the preprocessor for HydroD. We also gave each structure an individual input system as sketched in Figure 33.

The analyses were first performed to validate the set-up, and single runs with both structures were run together with a side-by-side multi body analysis with a spacing of 800 m. See Figure 34. Waves are propagating along negative x-axis, and WindFlip is shifted 800 m along the positive y-axis.

Figure 34 Reference run, y-distance = 800m

Due to the earlier encountered problems with the coordinate system errors in the user manual, two different set-ups with 800 meters distance were run. By shifting WindFlip a small distance in the x-direction in one multibody model, and keeping them in line in x-direction in an otherwise similar model, we find the coordinate system for which the phase angle is given. We find the same results for the phase angle in the multibody run with no x-shift as the single body run for WindFlip. When WindFlip is moved a small distance in the x-direction the multibody phase angle differs from the single body phase angle. By subtracting the distance times the wave number, k, from the phase angle given by Wadam we obtain the single body results. This implies that the phase angles for both structures are given in the global coordinate system for all multibody runs. By only changing the

position for WindFlip in the analyses, we always keep Hywind's input coordinate system coinciding with the global system, and all phase angles for both structures are given relative to Hywind and the incident wave.

The RAOs for surge are shown in Graph 13 for both bodies to illustrate how the responses correspond. The equivalent graphs for heave and pitch are given in Appendix I.

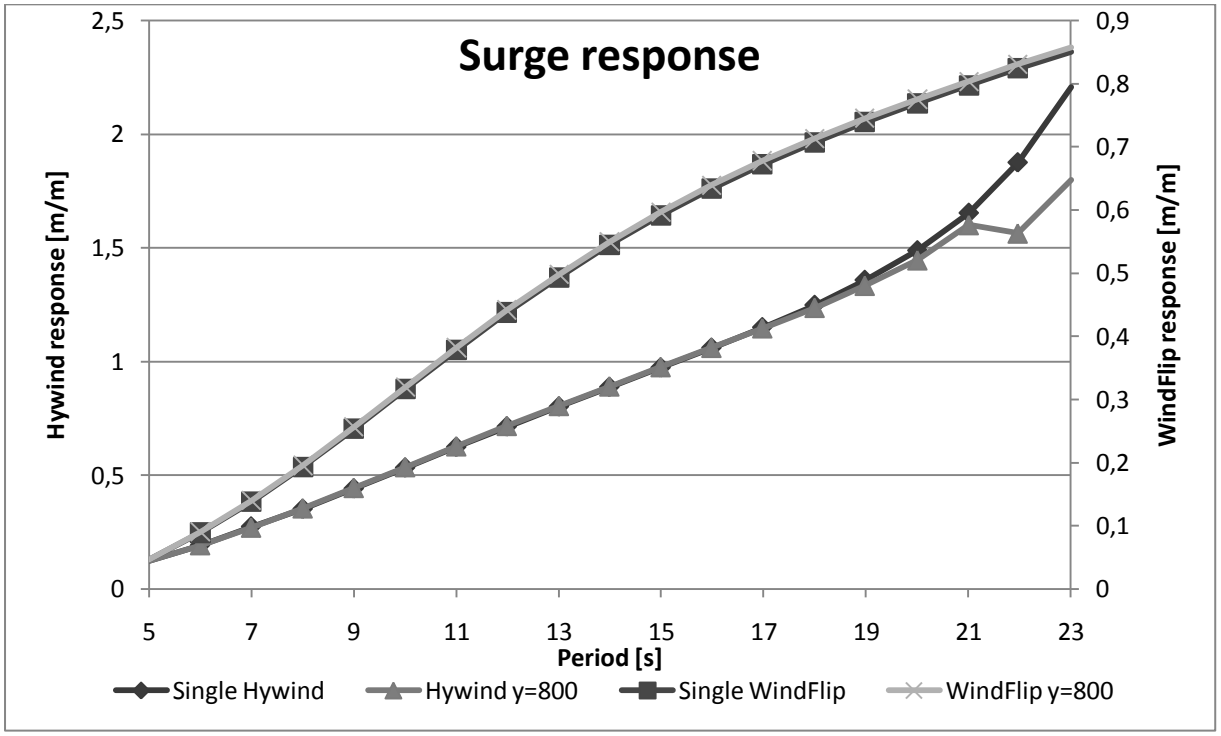

Graph 13 Surge response, reference run

We see from Graph 13 that the WindFlip reference run y = 800 meters corresponds well to the single body run. For Hywind we see the same trend for the lower wave periods, but around a wave period of 22 seconds we find a distinct abnormality between the two runs. Both reference runs with y-spacing of 800 meters show the same drop in surge and pitch response around 22 seconds. After running a new set-up with a 500 meters spacing in y-direction, the exact same values as in the 800 meters runs were found. At the same time a new single body run was executed to verify the results found from the original single body run, and the exact same results were found here as well. A run with higher wave periods were also executed to see whether we are close to the eigen frequency for Hywind at 22 seconds. However, the eigen periods are found to be around 27 seconds for surge and pitch, and 28 seconds for heave. This does not imply that the deviations are due to extreme values around the structures eigen frequency. Graphs for finding the eigen period are given in Appendix J.

The deviations seen above are insignificant to the ones discovered with the original coordinate system. After all the problems in setting up functioning Wadam runs with multibody configurations encountered earlier, and seeing as the analyses was sat up according to what was discussed with DNV and nothing appeared to be out of order, it was decided within the WindFlip team that the planned analyses were to be run regardless of the deviations found around 22 seconds. This is further discussed in chapter 6.3.2.

6.2. Configurations analyzed

After the flipping procedure has been executed successfully the two structures will be placed in the arrangement shown in Figure 35.

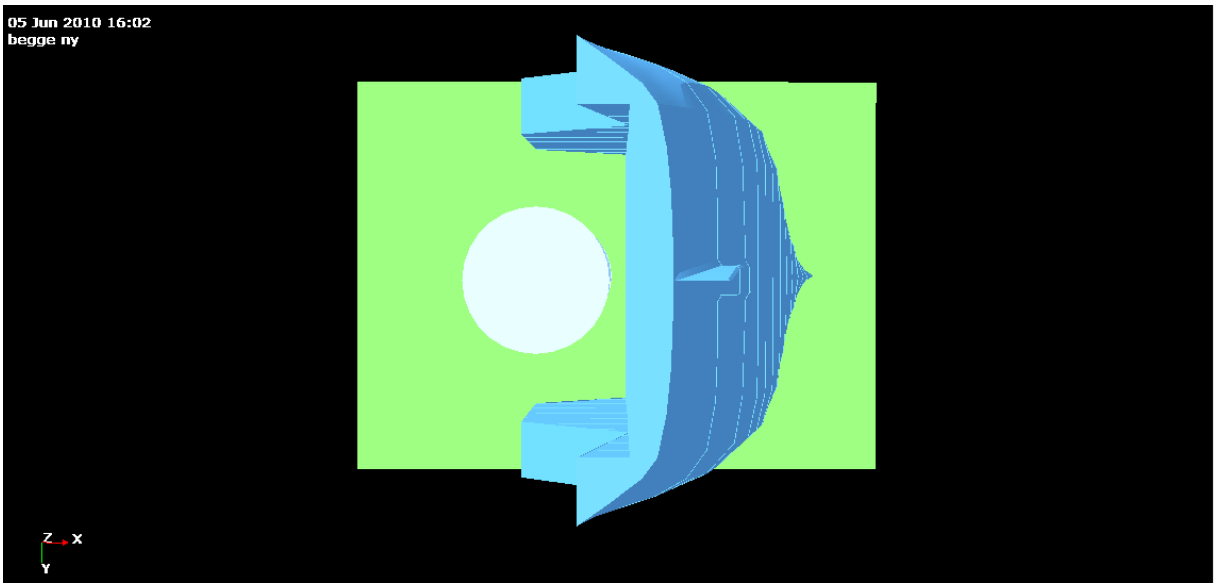

Figure 35 Initial release arrangement seen from the stern

This is how Hywind is situated on WindFlip during transit, and will be the starting point for the release. Fastening mechanisms to keep Hywind on WindFlip during transit are not shown in Figure 35, but a sketch of the mechanism is shown in Figure 36. The presence of these structures makes the configuration in Figure 35 our "zero spacing condition", and if any points of the structures are closer than this at any time, we have a collision.

Figure 36 Sketch of fastening mechanism during transit

All the other distances are given relative to the zero spacing condition in Figure 35. Nine different multibody runs are executed with different spacing between the structures in the x-direction. Regular waves with periods between 5 and 23 seconds are propagating in negative direction along the x-axis, as sketched in Figure 21. The wave range has been suggested by the WindFlip team, and has been used for all WindFlip/Hywind analyses in this thesis.

In Table 13 the test set up, including test runs, is given. The input to the multibody analyses is specified in HydroD, and by giving in each bodys input coordinate system relative to the global system we create multibody models with different spacing. As mentioned in chapter 6.1 we have placed the origin of Hywind's input system in the origin of the global system, and varied the position

of WindFlip's input coordinate system. Two examples of the multibody set-up are given in Figure 37 and Figure 38.

Run nr	Run name	Spacing x-dir [m]	x-distance origins [m]	y-distance origins [m]
1	SingleHy	N/A	N/A	N/A
2	SingleFlip	N/A	N/A	N/A
3	multi_y800_1	N/A	11.2076	800
4	multi_y800_2	N/A	0	800
5	multi_y500	N/A	0	500
6	multi_x0	0	11.2076	0
7	multi_x1	1	12.2076	0
8	multi_x2	2	13.2076	0
9	multi_x3	3	14.2076	0
10	multi_x5	5	16.2076	0
11	multi_x10	10	21.2076	0
12	multi_x15	15	26.2076	0
13	multi_x20	20	31.2076	0
14	multi_x30	30	41.2076	0

Table 13 Hywind/WindFlip test set-up

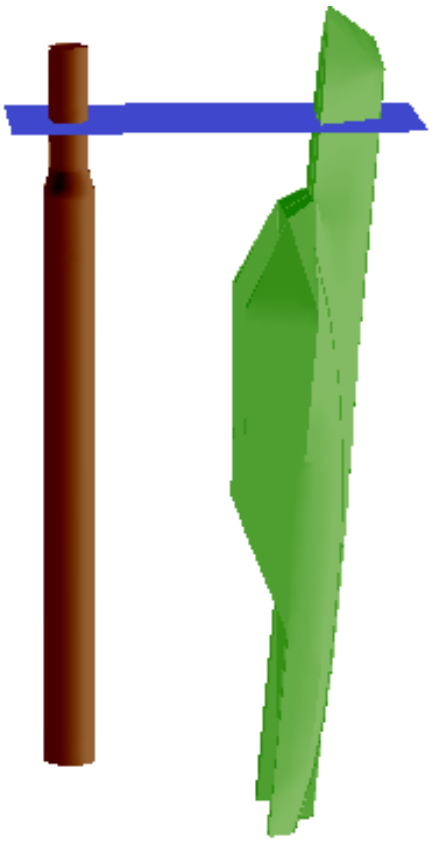

Figure 37 Multibody model, spacing 30 m

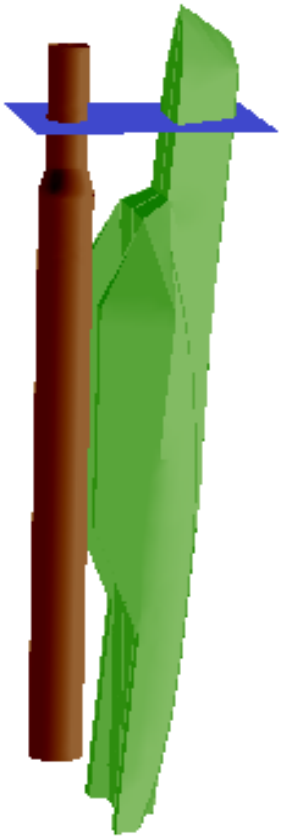

Figure 38 Multibody model, spacing 5 m

6.3. Results from the analyses

The analyses are post processed in Postresp, and the RAOs for the three different modes of motion are given for our frequency range. All the results are assembled in the spreadsheet Compare_HyFlip.xlsx that is attached in Appendix K, and is used as input to the Matlab scripts referred to in chapter 7.

There are several approaches possible for investigating in the results. By looking at changes in phase angles and amplitudes over the frequency range or over the different spacings, some of the effects caused by the interaction can be discovered.

6.3.1. Comparing RAOs for the multibody runs

By comparing the results from the single body runs with multibody runs with zero spacing we get an insight into how the interaction between the structures affects their motions. In Graph 14 the surge RAOs for Hywind and WindFlip are given, both with and without interaction. Corresponding graphs for heave and pitch are presented in Appendix L. The responses for the two Hywind cases are given on the primary axis, whilst the responses for the two WindFlip cases are given on the secondary axis.

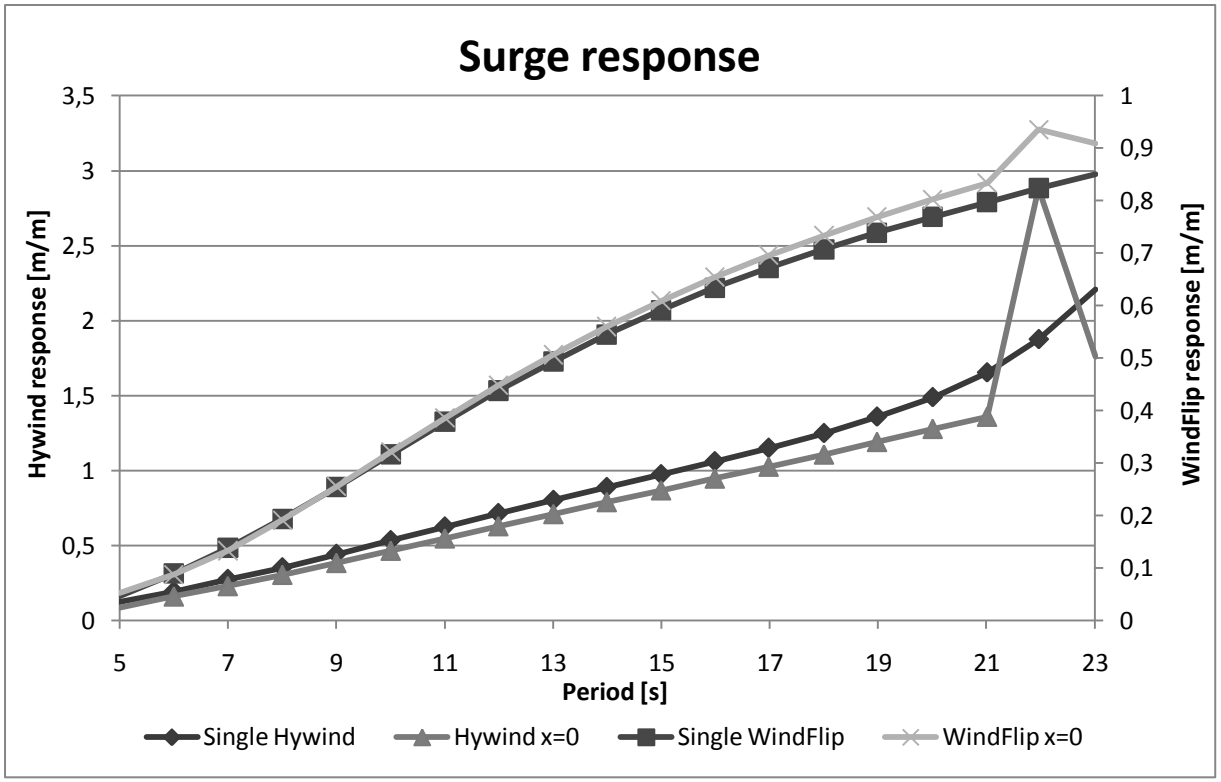

Graph 14 Surge, compare single body with close multi body

From Graph 14 we see that the multibody run for Hywind has lower response amplitude than the single body run. The multibody WindFlip run have slightly higher amplitude than the single body run. This coincides with the findings of Ali (Ali 2005) in Figure 10 and Figure 11 in chapter 2.2, which show a reduction in the horizontal forces for the lee-side cylinder, and an increase in the horizontal forces acting on the weather side cylinder. From the offbody points analyses in chapter 5.2 we noticed a reduction in waves behind the weather side cylinder, which also corresponds to the reduction in pitch response found in Graph 14.

By the end of chapter 2.2 a configuration for the release with WindFlip placed upstream, and Hywind in the sheltered area behind WindFlip was suggested. This is the planned configuration for the release operation, and the configuration used in the model tests discussed in chapter 4. No model tests were performed for the release operation, but the 85 degrees attached model is the starting point for the release and is placed with WindFlip as the weather side structure. The motion RAOs for WindFlip are lower than the corresponding RAOs for Hywind. This can be seen in the graphs in Appendix L and the graph above, and is also discussed in chapter 2.2 and illustrated by the simple single body analyses in chapter 3.2.2 and 3.2.3. By placing Hywind where the forces are lowest, we may avoid motion amplifications due to interaction on the structure most vulnerable to wave and interaction forces.

Again we notice a large jump in the Hywind response at 22 seconds. This irregularity is noticeable in all the multibody analyses around this period. The jump in the motion response is more evident when the bodies are close to each other, than when they have a larger spacing. When looking merely at Graph 14 and in Appendix L, it might look like we have hit some sort of interaction induced eigen period around 22 seconds for Hywind. This is looked more closely into in chapter 6.3.2.

6.3.2. Comparing the different multibody spacing configurations

By choosing one of the evaluated wave periods from the analyses and comparing the different spacing configurations we can see how the interaction effects change when the gap size decreases. In Graph 15 19 seconds wave period and surge motion is chosen as an example. Corresponding graphs for heave and pitch response are given in Appendix M.

Due to the fact that the response magnitude for the two structures is quite different the Hywind response is given on the primary axis, whilst the secondary axis shows the WindFlip response.

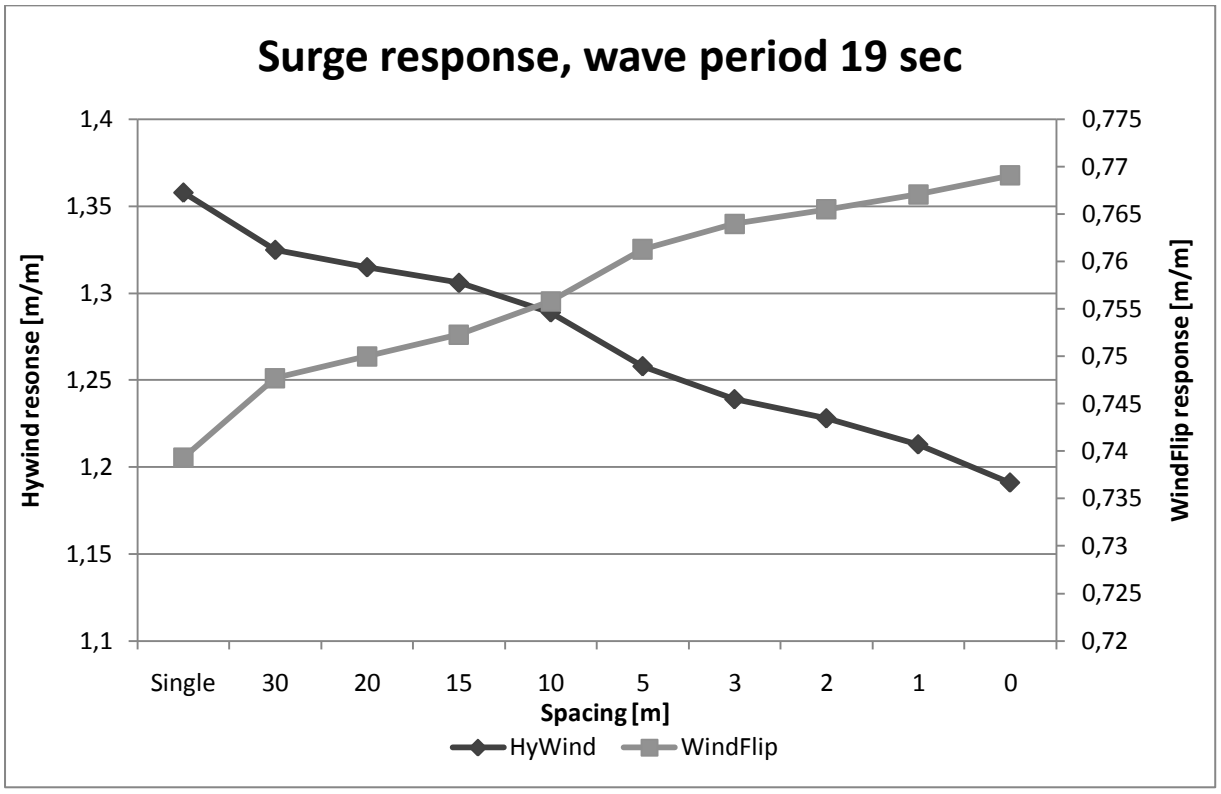

Graph 15 Surge response at 19 seconds wave period

From Graph 15 and the graphs in Appendix M we can clearly see that the responses for the weather side structure are increasing with decreased spacing. For Hywind the responses decrease with reduced spacing. This again supports the findings in chapter 2.2 and chapter 3, and the comparing of the RAOs in chapter 6.3.1.

By doing the same comparison as in Graph 15 for 22 seconds, we can look more closely into the abnormalities found for the response of Hywind at 22 seconds from Graph 14.

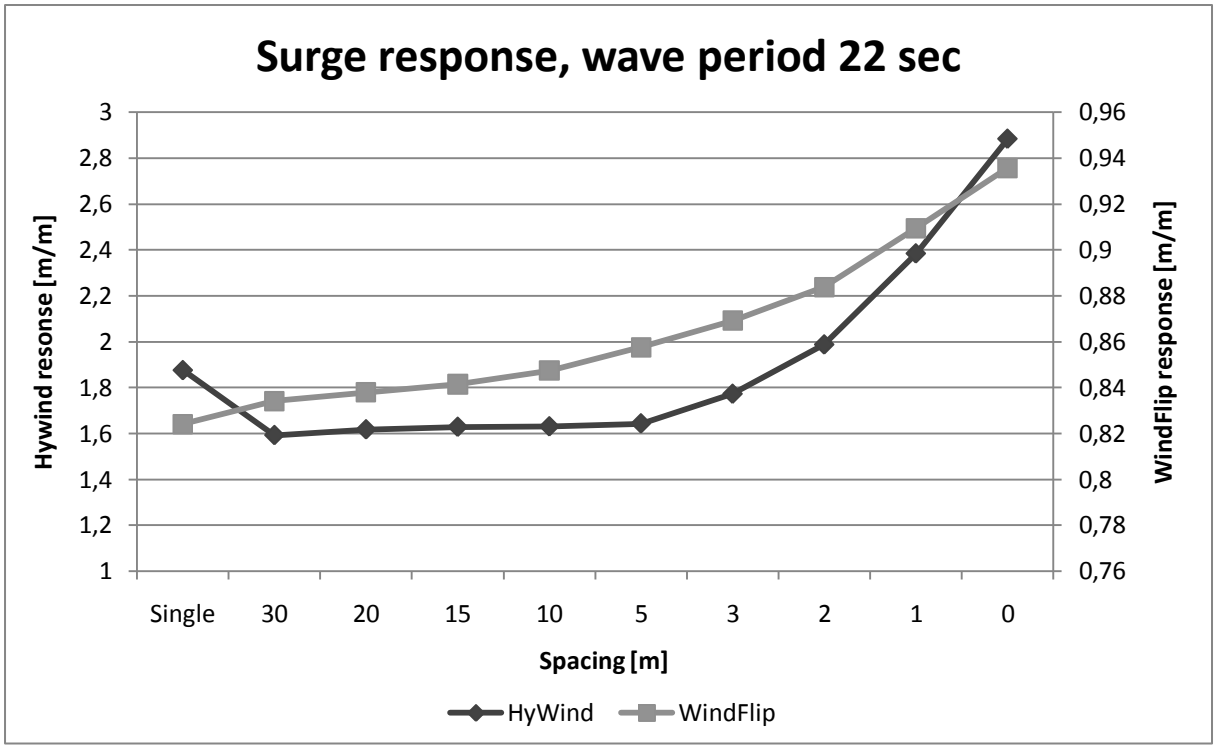

Graph 16 Surge response 22 sec wave period

We see the same increasing response trend for WindFlip for 22 seconds in Graph 16 (and Appendix N) as for 19 seconds in Graph 15. Hywind on the other hand show a different behaviour for 22 seconds period as the structures get closer. In the 19 second case the maximum response is at large distances, and the response decreases when Hywind is situated in the close wake of WindFlip. At 22 second period the responses for Hywind are increased as the structures move closer, and we have a response amplitude of 3 m/m in the case of zero spacing. This implies the structure moving 3 meters in x-direction per meter wave amplitude. We see that the response amplitude of WindFlip is close to 0.94 meters per meter wave amplitude, and regardless of how the phases angles are this situation will cause a collision of the structures.

When we compare the responses for 19 and 22 seconds for Hywind we see that the deviations are very large. This is shown in Graph 17 for surge and in Appendix O for heave and pitch.

We see that there is a significant increase in the surge response for Hywind when the spacing gets smaller and the waves are of 22 second period. For 19 seconds we have the opposite effect, hence a reduction as the spacing gets smaller. The reduction corresponds to what was found in chapter 2.2 and 6.3.1.

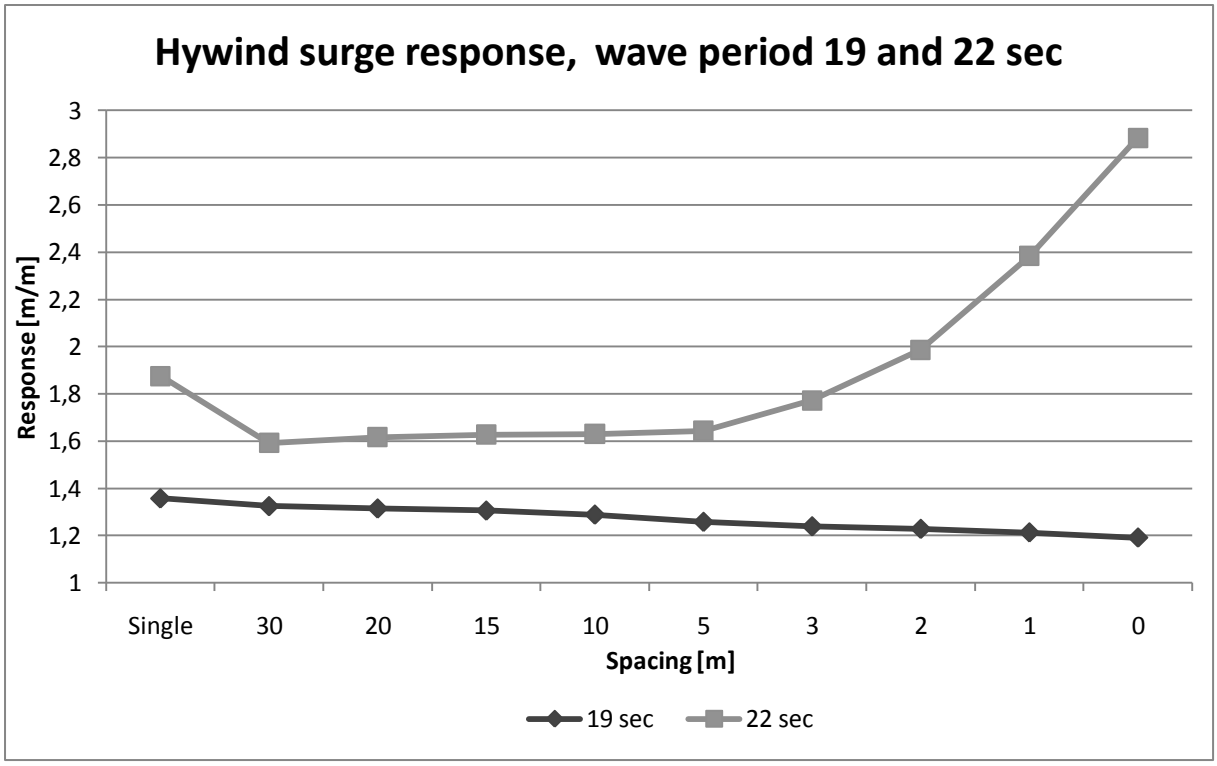

Graph 17 Hywind surge response for 19 and 22 seconds

As mentioned earlier the peak at 22 seconds could be because the interaction effects between the two structures alter the eigen frequency of the system, and by that cause Hywind to hit some sort of interaction induced resonance frequency at about 22 seconds. The effects on WindFlip are small, and the WindFlip RAOs are close to unchanged. Seeing as the displacement of WindFlip is about four times the displacement of Hywind, the responses to the waves are smaller in all cases, and most probably due to the size change the effects are small at 22 seconds as well.

However, as discussed in chapter 6.3.1 the jump in response for Hywind at 22 seconds is also occurring when the structures are placed in a side-by-side configuration far away from each other, where no interaction effects are expected. The magnitude of the deviation is smaller than for the zero spacing case, but still large enough to be noticed. In Graph 11 we see the deviation in surge response at about 22 seconds, and the reason for this is not properly understood.

One option is that the deviations are due to a numerical error in Wadam. As mentioned in 6.1 all the HydroD input correspond to what was agreed with DNV, and there are no obvious mistakes in the set up. However, the multibody analyses performed have proven not to be trivial, and there might be more limitations in the program than what was detected in setting up the analyses.

The WindFlip team has been notified that the results around 22 seconds are unreliable, and this should be looked more closely into to obtain an understanding for what is going on. As in chapter 4 many of the graphs in this chapter show an interesting behaviour at the end of our chosen wave range. Further studies should be performed for longer waves to get an impression of what goes on around the higher waves. Even though waves of higher periods than 23 seconds rarely occur in nature it is of great importance knowing what would happen if the structures were to be exposed to such waves in extreme situations.

7. Horizontal motion between WindFlip and Hywind

As the two structures are excited by the waves the horizontal distance between them varies. If the structures are not equal in size and shape their responses to the waves will be different, which again induces a variation in the distance between them. Both the amplitudes and the phase angles relative to the wave elevation will be changed due to altered geometry and size.

With changing distance between the structures the waves will be at different stages of the wave cycle when passing the structures at a given time instant. This will also introduce a difference in the motion characteristics of the structures. This part of the motion between the structures is dependent on the initial distance between them.

On the next page is a sketch (Figure 39) where the parameters discussed above are made clearer. A_{B1} and A_{B2} are the amplitudes of horizontal motion for body 1 (B1) and body 2 (B2) respectively, and A_w is the amplitude of the wave elevation and correspond to $-\zeta_a$ in formula 11-2.

x_{B2} denotes the distance between the cylinders origins along the x-axis. $\eta_{1_{B1}}$ and $\eta_{1_{B1}}$ are the surge motions, defined positive along the x-axis. $\eta_{5_{B1}}$ and $\eta_{5_{B1}}$ are the pitch motions, defined positive anti clockwise. ε_{B1} and ε_{B2} are the phase angle relative to the incident wave for body 1 and body 2 respectively.

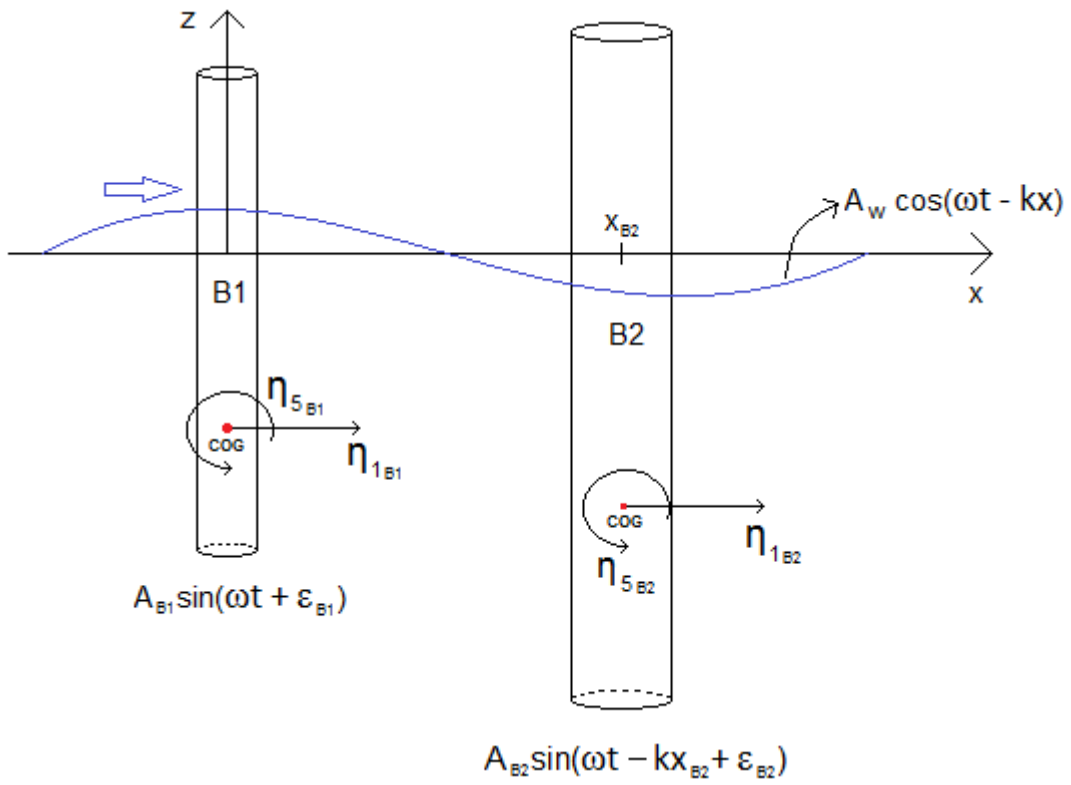

Figure 39 Two cylinders in a regular wave

The motion for one cylinder has been looked into in chapter 3.1. In chapter 3.1 only motions in roll and sway were evaluated, which means that heave is neglected and the problem is looked at in only 2-dimensions. The structures are symmetrical around the x-axis, and hence no motions should be induced in the y-direction by waves propagating in the x-direction in a potential theory analysis like the one performed in this thesis.

When we introduce two structures in close proximity of each other, the phase angles of the motions will be altered. The phase angles will change due to the interaction effects, and this needs to be taken into account in the motion equations. In Figure 39 the total horizontal motion equations for both structures are given, together with the wave elevation. These equations are derived from the incident wave potential for deep water waves. (Faltinsen 1990)

$$\varphi = \frac{g\zeta_a}{\omega} e^{kz} \, sin(\omega t - kx) \qquad \textbf{7-1}$$

The incident waves are found by using the dynamic free surface condition as (Faltinsen 1990)

$$\zeta = -\frac{1}{g}\frac{\partial \phi}{\partial t}\Big|_{z=0} = -\frac{1}{g}\frac{\partial}{\partial t}\frac{g\zeta_a}{\omega}\sin(\omega t - kx) = -\zeta_a \cos(\omega t - kx) \qquad \textbf{7-2}$$

The horizontal motion of each cylinder consists of a surge part and a pitch part. The total horizontal motion is a combination of these two components, and will change along the z-axis of the cylinders. In chapter 3.1 the horizontal motion of an arbitrary point on the cylinder was given as (Faltinsen 1990)

$$\eta_{horiz} = \eta_1 - \eta_5 * z = (\eta_{1a} - z\eta_{5a}) * \sin(\omega t - kx) \qquad \textbf{7-3}$$

where

$$\eta_1 = \eta_{1a}\sin(\omega t - kx) \text{ and } \eta_5 = \eta_{5a}\sin(\omega t - kx) \quad \textbf{7-4}$$

z is the vertical distance from the centre of gravity (COG) to the point we are looking at. In 7-3 we assume the surge and pitch motion to be 180 degrees out of phase. The pitch motion is in phase with the wave elevation, and the surge motion is 90 degrees out of phase with the wave elevation$\left(\cos(a) = -\sin(a - \frac{\pi}{2})\right)$. This assumption will give accurate answers for a structure freely floating without disturbances such as other structures or walls, when only the incident wave potential is taken into account, and when the wave period does not coincide with the structures eigen period in the motion modes taken into account. This simplification will no longer be valid when we are looking at several cylinders where radiation, diffraction and interaction are taken into account. The interaction effects may influence both amplitude and phase angle. The interactions impact on the phase angles may be an important parameter in finding the resulting horizontal distance between the two structures.

When the phase angles are to be taken into account the motions in surge and pitch direction are expressed as

$$\eta_1 = \eta_{1a}\sin(\omega t + \varepsilon_1) \text{ and } \eta_5 = \eta_{5a}\sin(\omega t + \varepsilon_5) \quad \textbf{7-5}$$

where ε_1 and ε_5 also includes the translation in x-direction if relevant (the $k * x$ term). The two equations in 7-5 can be combined into one single general expression representing the total horizontal motion at an arbitrary point, z, on the structure.

$$\eta_H = \eta_1 + z\eta_5 = \eta_{1a}\sin(\omega t + \varepsilon_1) + z\eta_{5a}\sin(\omega t + \varepsilon_5) \quad \textbf{7-6}$$

By rewriting the expression as

$$\eta_H = \eta_{1a}[\sin\omega t * \cos\varepsilon_1 + \cos\omega t * \sin\varepsilon_1] + z\eta_{5a}[\sin\omega t * \cos\varepsilon_5 + \cos\omega t * sin\varepsilon_5]$$

and by rearranging to

$$\eta_H = (\eta_{1a}\cos\varepsilon_1 + z\eta_{5a}\cos\varepsilon_5)\sin\omega t + (\eta_{1a}\sin\varepsilon_1 + z\eta_{5a}\sin\varepsilon_5)\cos\omega t \quad \textbf{7-7}$$

we may make use of the trigonometric addition theorem (Rottmann 2004)

$$a\sin x + b\cos x = \sqrt{a^2 + b^2}\sin(x + \varphi)\ ,\ \varphi = \arctan\frac{b}{a} + \begin{cases} 0 & if\ a \geq 0 \\ \pi & if\ a < 0 \end{cases} \quad \textbf{7-8}$$

which in our case leads to the expression for total horizontal motion:

$$\left.\begin{aligned} \eta_H &= \eta_{Ha} * \sin(\omega t + \varepsilon_H) \\ \eta_{Ha} &= \sqrt{(\eta_{1a}\cos\varepsilon_1 + z\eta_{5a}\cos\varepsilon_5)^2 + (\eta_{1a}\sin\varepsilon_1 + z\eta_{5a}\sin\varepsilon_5)^2} \\ \varepsilon_H &= \arctan\left(\frac{\eta_{1a}\sin\varepsilon_1 + z\eta_{5a}\sin\varepsilon_5}{\eta_{1a}\cos\varepsilon_1 + z\eta_{5a}\cos\varepsilon_5}\right) \end{aligned}\right\} \quad \textbf{7-9}$$

These expressions give us the combined surge/pitch motion at the vertical point z on a structure floating freely in regular waves. We have to be careful how we define the point z. Points above COG should be denoted –z according to the definition of pitch in Figure 39. As heave response has proven to be small compared to motion in horizontal direction for a cylinder, no motion in the z-direction

has been taken into account. The expression 7-9 is capable of giving the horizontal motion for any structure when the response in surge and pitch is known. However, for many structures, such as ships and barges, the combined heave/pitch motion (i.e. vertical motion) will be of much more importance than the surge motion. The principles behind finding the total motion vertical will be analogous with the method above for the 2-dimensional case, and the same goes for combined sway/roll motion.

If we were to evaluate waves coming in from other directions, such as 45 degrees, we would also have to include the motions in y-direction, and the analysis would become more complex. WindFlip and Hywind are intended to be placed in a tandem arrangement (Figure 21), WindFlip meeting the waves and WindFlip situated in the sheltered area downstream. Due to the symmetry around the x-axis the motions in y-direction will be less significant for waves propagating along the x-axis. However, real sea states do not have unidirectional waves like the one being analyzed here. Hence some motions in the y-direction will be induced in the structures. It is expected that these motions are of smaller amplitudes than the ones in x-direction as the main wave direction is planned to be along the x-axis. This, together with the structures being placed on the x-axis, lead us to believe that by only looking at motions in the x-directions we should obtain a good picture of the relative motion between the structures.

The motion between the structures is dependent on the chosen point on the structures we are looking at. The important thing to evaluate in the Hywind release operation is the minimum distance appearing between the two structures during the operation. By looking at the lowest and highest points on the structures we find the two points where the horizontal distance will be lowest. This is sketched in the Figure 40.

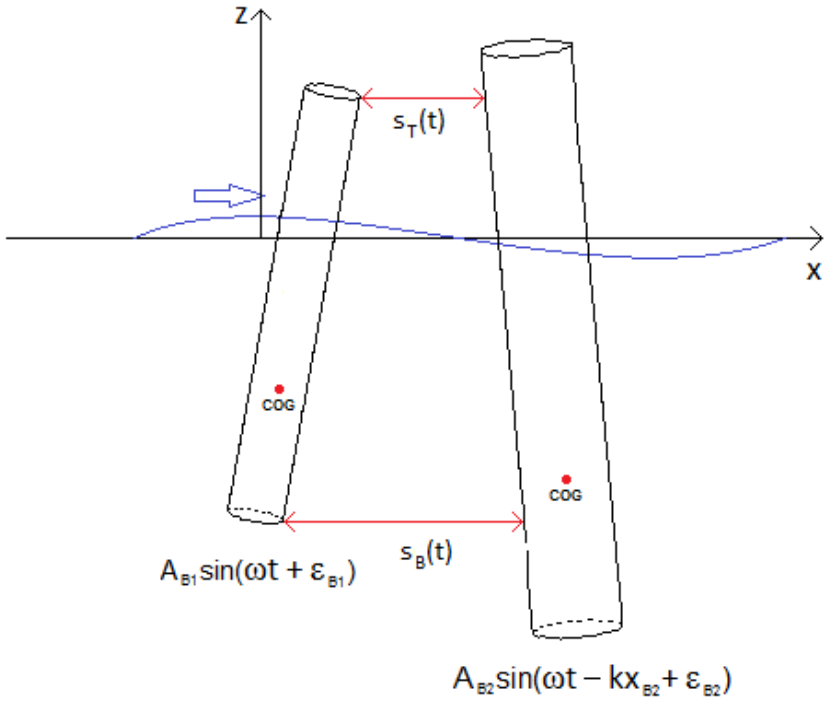

Figure 40 Horizontal spacing between two structures

By choosing the z-coordinates like in Figure 40, hence the top point of the lowest structure and the bottom point of the structure with the smallest draft, we can find the motions between the critical

points of the structures. The points are defined when both structures are vertical, and by that we introduce a small vertical error when the structures are rotated. However, the pitch motions are not large enough to give a significant displacement in the vertical direction, and this simplification will not introduce any large errors in the calculations.

To find an expression for the spacing at the two most critical points on the structures we have to look at the horizontal motion equations for both structures. By combining these two expressions and taking into account the horizontal distance between the structures we obtain the following expression (ref Figure 39)

$$s(t) = (x_{B2} - x_{B1}) + \eta_{H_{B2}} \sin(\omega t + \varepsilon_{H_{B2}} - k x_{B2}) - \eta_{H_{B2}} \sin(\omega t + \varepsilon_{H_{B1}} - k x_{B1}) \qquad \textbf{7-10}$$

In Figure 39 we have chosen to place the centre of Body 1 in the origin, and hence we can simplify the expression as follows

$$s(t)|_{x_{B1}=0} = x_{B2} + \eta_{H_{B2}} \sin(\omega t + \varepsilon_{H_{B2}} - k x_{B2}) - \eta_{H_{B1}} \sin(\omega t + \varepsilon_{H_{B1}}) \qquad \textbf{7-11}$$

To investigate possible collisions in both the top and bottom points of the cylinders we need two perform the calculation above twice. The η_H and ε_H are for both structures dependent on the vertical distance from COG for the evaluated point, and we end up with $s_T(t)$ for the top point, and $s_B(t)$ for the bottom point.

When using Postresp as a postprocessor for the Wadam results the phase angles for both bodies are given in the global coordinate system. In the analyses the input coordinate system of Hywind is situated so that it coincides with the global coordinate system. This implies that the distance term $(k * x_{B2})$ in 7-11 is unnecessary, and the expression is further simplified to

$$s(t) = x_{distance} + \eta_{H_{B2}} \sin(\omega t + \varepsilon_{H_{B2}}) - \eta_{H_{B1}} \sin(\omega t + \varepsilon_{H_{B1}}) \qquad \textbf{7-12}$$

The two last terms can be combined into a single term denoting the relative motion of both structures. By performing the same operation as in 7-8 we obtain

$$\begin{aligned} s(t) &= x_{distance} + \eta_{H_{tot}} * \sin(\omega t + \varepsilon_{H_{tot}}) \\ \eta_{H_{tot}} &= \sqrt{\left(\eta_{H_{B2}} \cos \varepsilon_{H_{B2}} - \eta_{H_{B1}} \cos \varepsilon_{H_{B1}}\right)^2 + \left(\eta_{H_{B2}} \sin \varepsilon_{H_{B2}} - \eta_{H_{B1}} \sin \varepsilon_{H_{B1}}\right)^2} \\ \varepsilon_{H_{tot}} &= \arctan\left(\frac{\eta_{H_{B2}} \sin \varepsilon_{H_{B2}} - \eta_{H_{B1}} \sin \varepsilon_{H_{B1}}}{\eta_{H_{B2}} \cos \varepsilon_{H_{B2}} - \eta_{H_{B1}} \cos \varepsilon_{H_{B1}}}\right) \end{aligned} \qquad \textbf{7-13}$$

$s(t)$ in expression 7-3 gives us the distance at a given point z on the structures when the structures are situated $x_{distance}$ away from each other. The expression above is useful in finding the horizontal distance between Hywind and WindFlip during the release procedure. By going through the wave periods and distances that have been analyzed by Wadam we can find out whether or not the structures will collide at some point in the release operation.

Two Matlab scripts have been made to evaluate all possible combinations of wave period and distance between the structures. The scripts are attached in Appendix A and use the output from Postresp which is also attached as a spreadsheet in Appendix A. The first script makes a visualization of two structures of equivalent size as Hywind and WindFlip, and is called VisualizationHyFlip.m. The

script needs to be given a wave period and initial spacing for the visualization. After this has been specified the script will find the relevant motion amplitudes and phase angles from the Wadam results and use these values to simulate the motions for the two structures together with incident waves. By visually inspecting the animations we can get an indication on whether or not the structures will collide under the prescribed circumstances. Some VTF- files from the visualization are attached in Appendix C. Below are a couple of snap shots from the visualizations given.

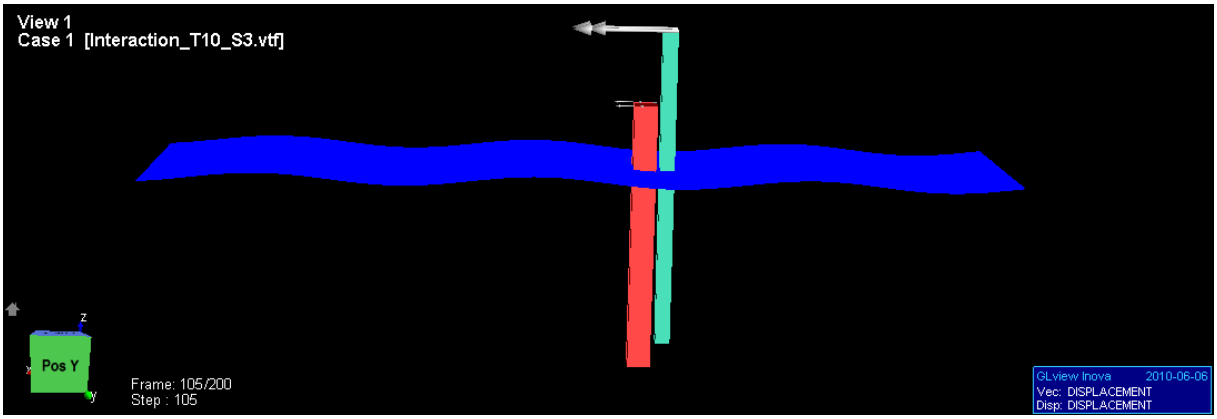

Figure 41 Visualization with 3 m spacing and wave period 10 sec

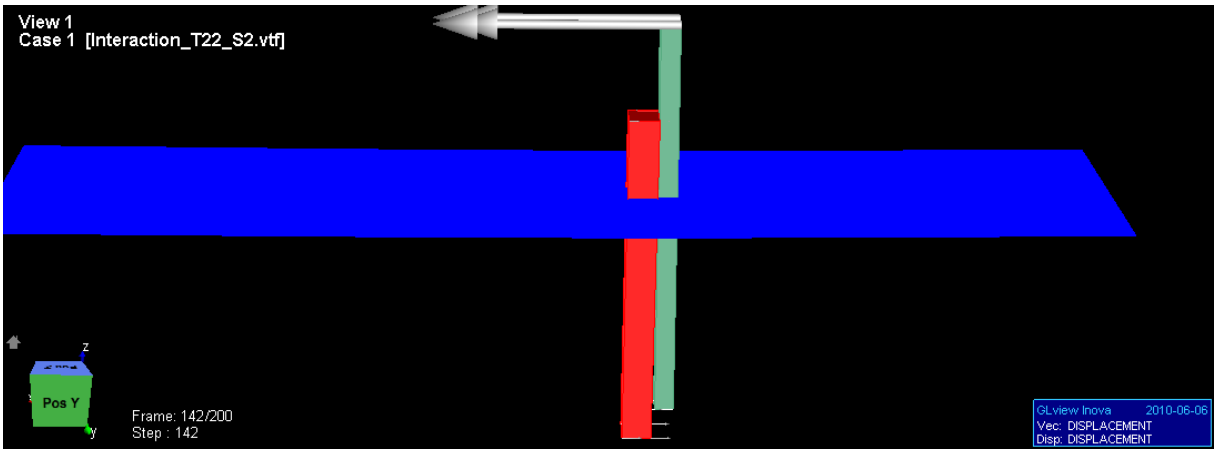

Figure 42 Visualization with 2 m spacing and wave period 22 sec

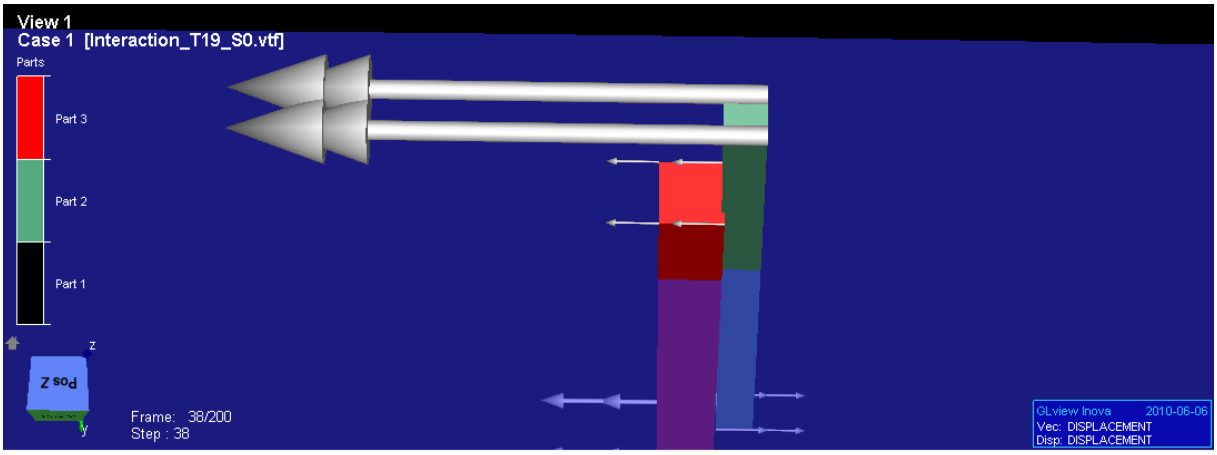

Figure 43 Visualization with 0 m spacing and wave period 19 sec

When looking at the relative motions between two bodies, where both amplitudes and phase angles might be different, numbers and graphs are not so easy to relate to the physical motions. By making

visualizations like these we obtain a good picture of how the total motion picture look, and can get an impression of where we might detect problems. We can then look more closely into the situations that look interesting from the visualizations.

Figure 41 shows the two structures in waves with a period of 10 seconds. From chapter 6.3.1, and the corresponding appendix, we see that the responses are low at this frequency. This is also shown by the vector arrows, which are significantly smaller than the ones in Figure 42 for 22 second period and in Figure 43 for 19 second period. There is no contact between the two structures in the case of 3 m spacing and 10 seconds, and hence we characterize this situation to be safe.

Figure 42 shows the case of 22 second period and 2 m spacing. Waves with 22 second period are potentially the worst scenario for the release process, and by inspecting the visualization we see that we are very close to a collision between the top points during this situation. In the case in Figure 43, which is the release position in 19 second period waves, we will have a collision between the structures. This is however to be expected. When we have initially zero spacing just infinitesimal differences in the motion characteristics will give collision. Also here the top point is the most exposed point, and this relates to the center of gravity being placed below the midpoint of the structures.

It is worth noting from the visualization that as the wave periods, and hence wave lengths, increase the motion characteristics become more synchronized. When the wave lengths are much longer than the size of the structures similar phase angles are to be expected as the structures will follow the waves closely. The interaction effects found by potential theory do not alter this to a great extent, and the structures show quite similar motions when they are close. As mentioned in the previous chapter no viscous effects are taken into account, and looking into how the viscosity alter the phase angles of the motions and their amplitudes is something that should be investigated further.

To be able to get an overview of how the different spacings and periods affect the relative motion between the structures a second Matlab script has been made. This is called relativeMotion.m and is attached in Appendix A. The output from the program is plots showing the minimum top and bottom spacing occurring for each wave period for all the examined spacings. The graphs are given on the following three pages. The first two graphs show all spacings, and we can quickly eliminate spacings over 5 meters as a risk for our wave period range. To make the smaller spacings more apparent equivalent plots have been made with only the smaller spacings.

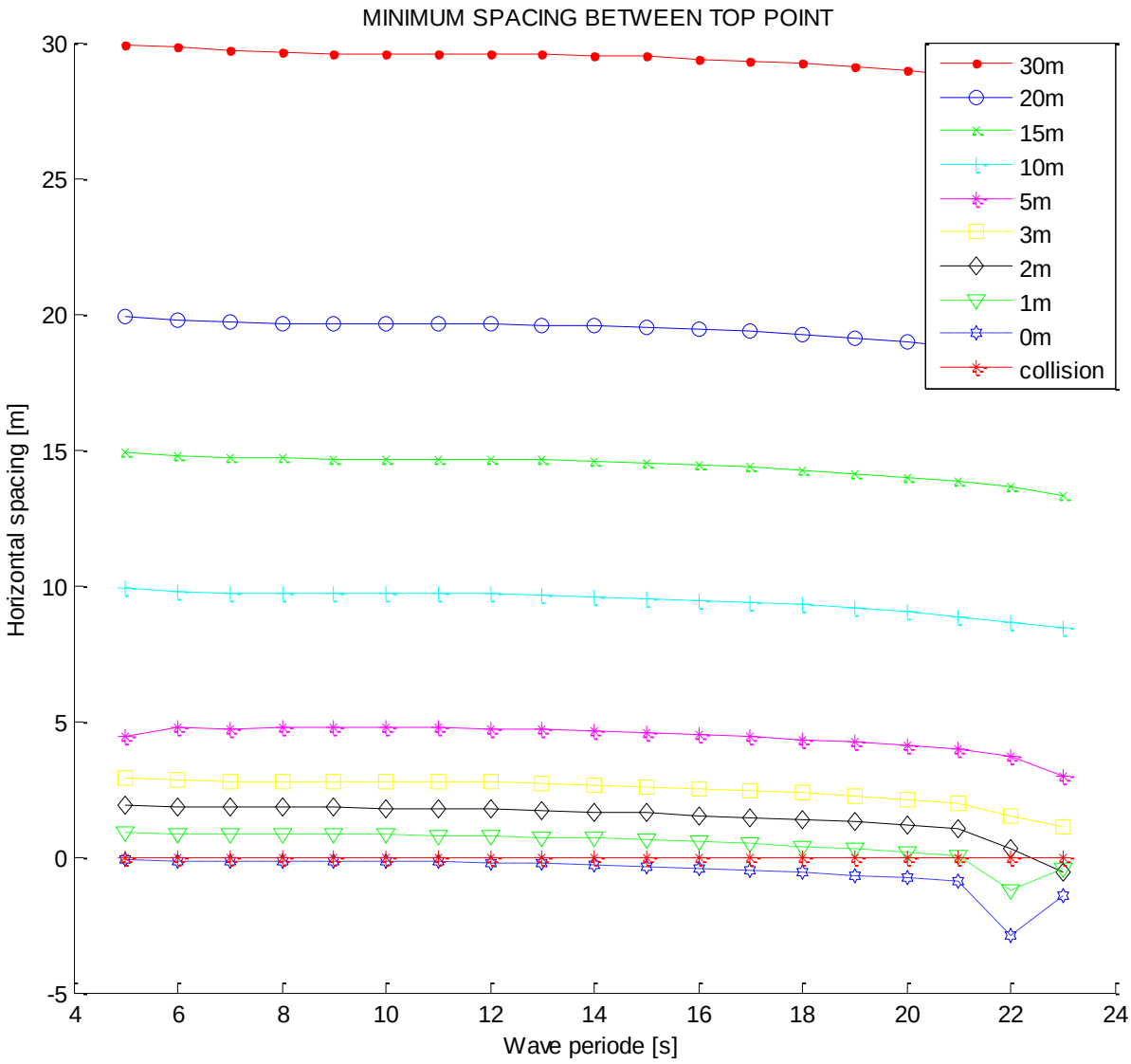

Graph 18 Horizontal spacing between top of WindFlip and Hywind for all spacings examined

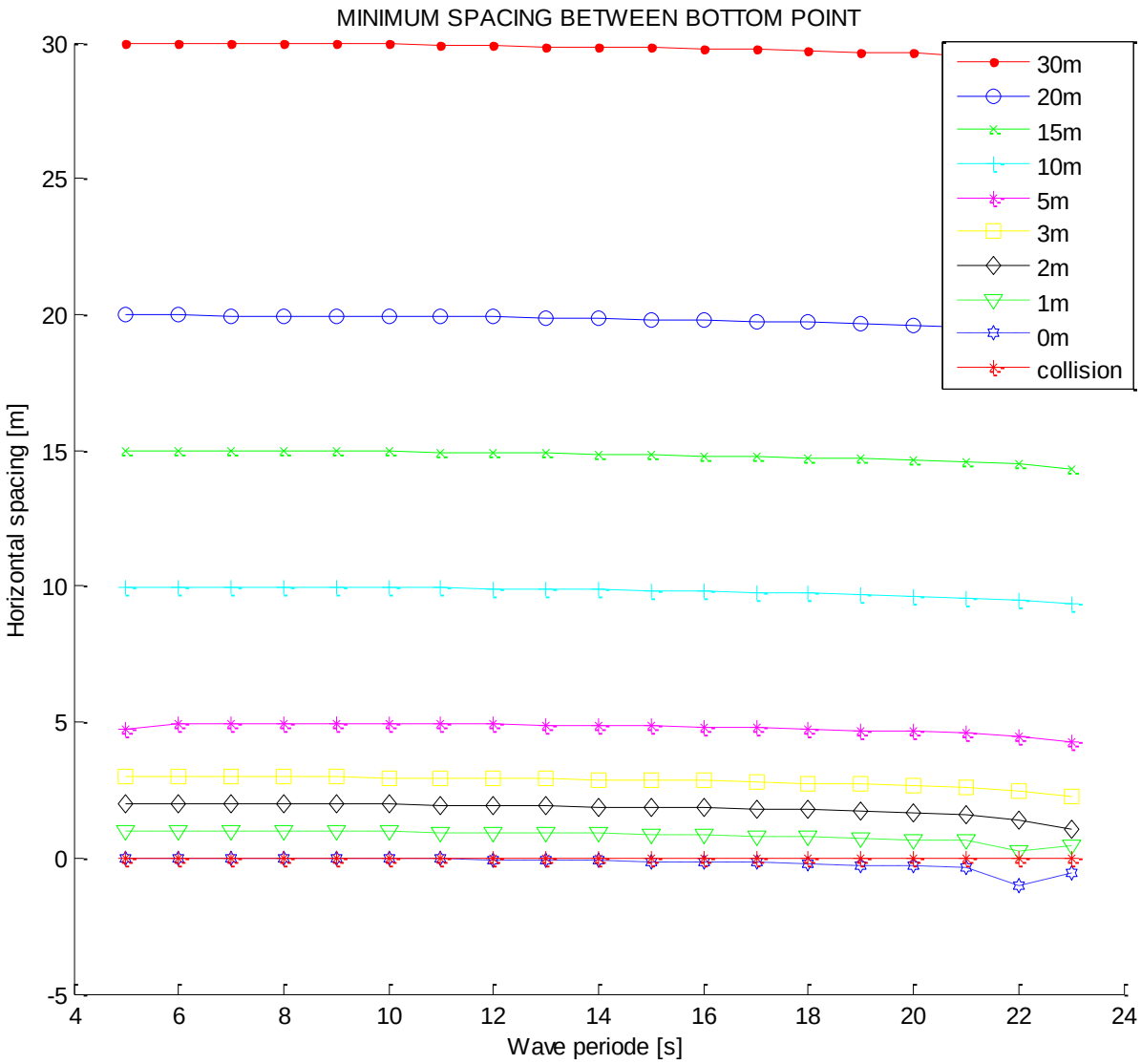

Graph 19 Horizontal spacing between bottom of Hywind and WindFlip for all spacings examined

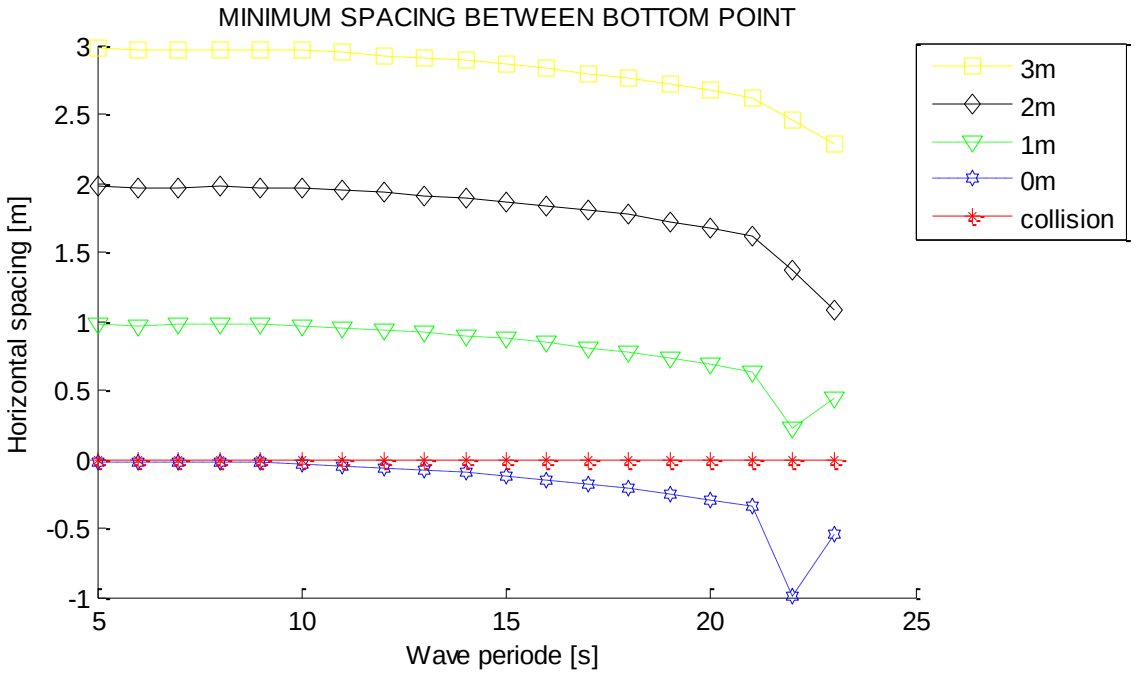

Graph 20 Horizontal spacing between bottom of WindFlip and Hywind for low spacing

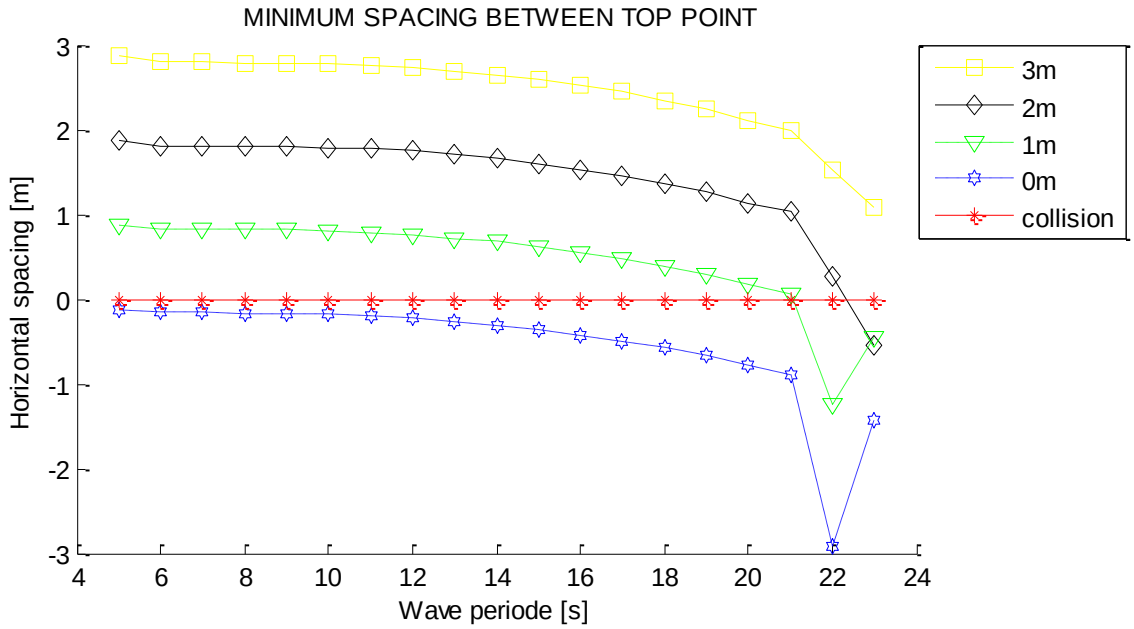

Graph 21 Horizontal spacing between top of Hywind and WindFlip for low spacings

From these graphs we note that we will have a collision for zero spacing at all wave periods, as mentioned and expected in chapter 6.3.2. The cases of 1 and 2 meter spacing give no collision for wave periods lower than 21 meters, whilst 3 meters spacing will not lead to collision in any our period range.

These plots are based on the RAOs for the responses and are hence valid for wave amplitude of 1 meter. The responses are assumed linear to the wave elevations, and to find responses for other wave amplitude we merely have to multiply the wanted wave amplitude to our response RAO value

for each wave period. The scripts are given to Torbjørn Mannsåker, which is responsible for the hydrodynamics in WindFlip AS. By using the function in 7-9, which is an RAOs for the motions, and combining them with wave spectrums, response spectrums for the relative spacing are easily found. The response spectrums are to be used to perform statistical analyses on the collision risk in different sea states. By comparing different wave spectrums with varying significant wave height and peak period, acceptance limits for sea state during the release operation can be set.

8. Conclusion

After looking into different effects arising for the interaction between circular cylinders in a fluid and the interaction between several floating bodies in waves, a suggestion for an arrangement that will give the lowest motions of the floating bodies has been suggested. The tandem arrangement, where one cylinder is placed in the wake of the other, seems to be an obvious choice for the launch and release process of Hywind from WindFlip. By placing Hywind in the wake region of the WindFlip barge the wave forces on Hywind should be minimized, and hence its motions reduced in a critical phase.

The reduction in the responses for the lee-side cylinder is supported by numerical potential theory multibody analyses. The numerical analyses show an increase in motion for the weather side structure (WindFlip) as the spacing is reduced, and shows at the same time a decrease in the responses for the lee-side structure (Hywind). Visualizations of the free surface around the structures show a reduction in wave amplitudes behind the weather side cylinder. The lower waves should cause a reduction in the motions of the lee-side cylinder, and hence also supports the findings from the multibody analyses.

The interaction effects found in the analyses are not very prominent in the total motion responses. The incident wave, radiation and diffraction potential for the wave field are used to find the motions responses, and no viscosity is included. It is believed that the viscosity will affect the interaction to a greater extent than the wave loads accounted for in this thesis, though wave resonance effects may occur, and it is recommended that the viscous effects are evaluated.

9. Discussion and further work

All the analyses in this thesis refer to motions in only two dimensions. For the multibody analyses unidirectional waves are used along the x-axis, and the responses in heave, surge and pitch are evaluated. When the waves are unidirectional along the x-axis the motions induced in y-direction are insignificant when using potential theory, and looking away from them should not cause any problems. In real sea states however, the waves will also induce motions in sway, roll and yaw degree of freedom, in addition to heave, pitch and surge. The motions in the y-direction might be important for the resulting motions, and when the chances of collision are evaluated this should be looked into.

The structures evaluated have only been analyzed in a tandem arrangement with WindFlip as weather side cylinder. Even though the release is planned to be performed in this tandem configuration, unexpected events may lead to the waves attacking from other directions. Waves approaching from various directions should be looked into to evaluate how the structures will respond to wave loads if the release does not go according to plan. Both side-by-side and staggered arrangements will probably induce larger motions on the structures than the tandem arrangement, and should be evaluated.

To be able to predict the behavior of the structures during the release, an appropriate wave spectrum should be applied, instead of the regular waves in this thesis. A sea state includes waves of different periods and heights, and will give a better picture of how the release operation will act out in the area where the spectrum is applicable.

The wave period range of the analyses in this thesis is limited to 5-23 seconds. We notice in many of the graphs regarding WindFlip and Hywind that the responses undergo quite a lot of changes around the longer periods. Knowing what goes on outside the applied wave range of this thesis should be looked into. Even though the waves at periods above 23 seconds are very long and not usually occur in nature, extreme situations may happen. Not knowing how WindFlip and Hywind will respond to these situations could be critical if such a situation at some point was to occur. Hence analyses containing waves of longer periods should be looked into to clarify the consequences if extreme circumstances were to take place.

Currents are also a possible complication during the release procedure. We know that Hywind will be exposed to vortex induced vibrations (VIV) at 2-3 knots (Moxnes 2009), and hence strong currents will represent a problem during release. To take VIV into account the potential theory solver Wadam can no longer be used, and a computational fluid dynamics (CFD) analysis would have to be performed. For the Hywind/WindFlip case this type of analysis would require a lot of computational resources and time. More extensive model testing will be able to investigate the current issue, and could be performed as an alternative to CFD analyses. However, model testing will induce errors due to scale effects, and how well the viscous effects will be modeled is hard to predict.

Viscous effects are also present when no steady current is looked into. Long waves give a large Keulegan-Carpenter number, meaning that the flow will spend a long time passing the structure before it returns. We may then look at the wave as a current when it passes, and a turbulent flow behind around the structures may arise. This will lead to viscous interaction effects, which might be important when looking at the total motion of the structures. As mentioned in the previous section a CFD analysis should be performed in order to see the effect of the viscosity.

A single mooring line will most likely be attached to the WindFlip vessel during the launch and release operation. This induces a restoring force and will change the motion characteristics of WindFlip. To what extent the mooring line will alter the movements of the structure is not easy to predict accurately, and this is something that could be taken into account in further development of the analyses performed in this thesis, where both bodies are freely floating.

10. Nomenclature

G	Gap size/spacing, length of the opening between cylinders
T	Length between cylinder centres for side-by-side configurations
S	Length between cylinder centres for tandem configurations
k	Wave number, $k = \frac{\lambda}{2\pi}$
λ	Wave length
ω	Wave frequency, $\omega = \frac{2\pi}{T}$ [rad/sec]
T	Wave period [sec]
COB	Centre of buoyancy (measured from bottom of structure)
COG	Centre of gravity (measured from bottom of structure)
GM	Metacentre height
D	Diameter of cylinder
d	Draft of cylinder
L	Length of cylinder
RAO	Response Amplitude Operator
A_{22}	Added mass, sway direction
A_{33}	Added mass, heave direction
A_{44}	Added mass, roll direction
A_{24} , A_{42}	Coupled added mass, sway/roll

C_{33}	Restoring coefficient, heave direction
C_{44}	Restoring coefficient, roll direction
η_1	Motion, surge direction
$\bar{\eta}_1$	Amplitude of motion, sway direction
η_2	Motion, sway direction
$\bar{\eta}_2$	Amplitude of motion, sway direction
η_3	Motion, heave direction
$\bar{\eta}_3$	Amplitude of motion (displacement), heave direction
η_4	Motion, roll direction
$\bar{\eta}_4$	Amplitude of motion, roll direction
η_5	Motion, pitch direction
$\bar{\eta}_5$	Amplitude of motion, pitch direction
F_1	Exciting force, surge direction
F_2	Exciting force, sway direction
F_3	Exciting force, heave direction
F_4	Exciting force, roll direction
F_5	Exciting force, pitch direction
U	Velocity
p	Dynamic pressure
n_i	Unit normal vector
A_w	Water plane area/Wave amplitude

11. References

Agarwal, A.K., and A.K. Jain. “Dynamic behaviour of offshore spar platforms under regular sea waves.” *Ocean Engineering, Volume 30, Issue 4*, 2003: 487-516 .

Ali, M.T. «On hydrodynamic interaction between several freely floating vertical cylinders in waves.» *OMAE Offshore Technology Symposium Database*, 2005.

Det Norske Veritas. «SESAM User Manual HydroD.» 5 Januar 2010: 95.

—. «SESAM User Manual Wadam.» 2 March 2009: 2.19.

Faltinsen, Odd Magnus. *Sea Loads on Ships and Offshore Structures.* Cambridge University Press, 1990.

Jonkman, J.M. «Dynamics of Offshore Floating Wind Turbines - Model Development and Verification.» *Wind Energy, Volume 12 Issue 5*, 2009: 459 - 492.

Kim, C.H. «The hydrodynamic interaction between two cylindrical bodies floating in beam sea.» *Sea Grant Report NOAA-2-35249, Stevens Institute of Technology* , 1972: 65.

Larsen, Carl Martin. *Marin Dynamikk.* Trondheim: Department of Marine Technology, NTNU, 2007.

Mannsåker, Torbjørn. «Private correspondence.» 2009.

—. «Private correspondence.» Trondheim, May 2010.

Moxnes, Simen. *Flytende vindmøller - Hywind.* Marine Technology Conference (NPF), Trondheim. November 2009.

Newman, J.N. *Marine Hydrodynamics.* The MIT Press, Cambridge, Massachusetts, 1977.

Pettersen, Bjørnar. *Marin Teknikk 3 - Hydrodynamikk.* Trondheim: Department of Marine Technology, NTNU, 2007.

Rottmann, Karl. *Matematisk formelsamling.* Spektrum forlag, 2004.

Sumer, B.M, and J. Fredsøe. “Hydrodynamics Around Cylindrical Structures.” *Advanced Series on Ocean Engineering , Vol 12*, 1997.

Sumner, D., M.D. Richards, and O.O. Akosile. “Two staggered circular cylinders of equal diameter in cross-flow.” *Journal of Fluids and Structures, Volume 20, Issue 2*, 2005: 255-276 .

Tao, Longbin. *Lectured material for MAR8021 Advanced Offshore Engineering.* University of Newcastle upon Tyne, Newcastle. May 2009.

White, Frank M. *Fluid Mechanics, fifth edition.* Mc Graw Hill, 2005.

Zdravkovich, M.M. *Flow Around Circular Cylinders volume 2: Applications.* Oxford Science Publications, 2003.

—. *Flow around cirkular cylinders volume 1: Fundamentals.* Oxford Sciense Publications, 1997.

Zhao, M., L. Cheng, B. Teng, og G. Dong. «Hydrodynamic forces on dual cylinders of different diameter in steady current.» *Journal of Fluids and Structures, Volume 23, Issue 1*, 2007: 59-83.

List of figures

List of graphs

List of tables

Appendices

Appendix A: Matlab files

Appendix B: Main dimensions

Appendix C: Visualization

Appendix D: Heave and pitch responses for 60 degrees trim

Appendix E: Heave and pitch responses for 85 degrees trim

Appendix F: Comparing 3-20 seconds RAOs for two tandem arranged cylinders

Appendix G: Comparing 0.5-3 seconds RAOs for two tandem arranged cylinders

Appendix H: Wadam shortcomings discovered in the multibody analyses

Appendix I: Heave and pitch reference response

Appendix J: Hywind and WindFlip resonance runs

Appendix K: Spreadsheet for Hywind and WindFlip multibody analyses

Appendix L: Heave and pitch RAOs with and without interaction effects

Appendix M: Interaction effects at 19 seconds period

Appendix N: Interaction effects at 22 seconds period

Appendix O: Comparing Hywind for waves of 19 and 22 seconds

Appendix A Matlab files

All Matlab files are found on the attached CD, in the folder “Appendix A”. The scripts for visualization of the interacting cylinders, and the relative horizontal motion are given underneath.

```
%%%%%%%%%%%%%%%%%%%%%%%%%%%%%%%%%%%%%%%%%%%%%%%%%%%%%%%%%%%%%%%%%%%%%%%%%%%%%%%%
%  FINDING THE TOTAL HORIZONTAL MOTION BETWEEN TWO BODIES                        %
%                                                                                %
%  by Susanne Rusnes                                                             %
%  Norwegian University of Science and Technology                                %
%  June 2010                                                                     %
%%%%%%%%%%%%%%%%%%%%%%%%%%%%%%%%%%%%%%%%%%%%%%%%%%%%%%%%%%%%%%%%%%%%%%%%%%%%%%%%

clc
clear all
close all

%--- Reading input from Wadam analyses ---%

amplHW = xlsread('Compare_HyFlip.xlsx','Amplitude','C3:N59');
amplWF = xlsread('Compare_HyFlip.xlsx','Amplitude','C63:N119');

epsHW = xlsread('Compare_HyFlip.xlsx','Amplitude','Q3:AB59');
epsWF = xlsread('Compare_HyFlip.xlsx','Amplitude','Q63:AB119');

length_batch = length(amplHW(:,1))/3;

%--- Parameters for the structures and the visualization ---%

waveHeight = 2;                    % wave height, twice the amplitude
wa = waveHeight/2;                 % wave amplitude
g = 9.81;                          % acceleration of gravity


%- Hywind

length_1 = 190;                   % length of buoy
depth_1 = 110;                    % depth of buoy
freeb_1 = length_1 - depth_1;     % freeboard
diameter_1 = 8.75;                % diameter of buoy

B1L = diameter_1;                 % characteristic length of body 1
B1dist = 75;                      % distance between COG and sea surface of
body 1
top_1 = B1dist + freeb_1;         % point of motion, from COG, positive
upwards of body 1
bottom_1 = length_1 - top_1;

%- WindFlip

length_2 = 160;                  % length of buoy
depth_2 = 124;                   % depth of buoy
freeb_2 = length_2 - depth_2;    % freeboard
diameter_2 = 17.17;              % diameter of buoy

B2L = 13.6652;                   % characteristic length of body 2
```

```
B2dist = 70.17;                 % distance between COG and sea surface of
body 2
top_2 = B2dist + freeb_2;       % point of motion, from COG, positive
upwards of body 1
bottom_2 = length_2 - top_2;

%--- Wadam Input: Phase angles and amplitudes of motion in x- and z-
direction ---%

distance = [30 20 15 10 5 3 2 1 0];      % distance between the centres of
the two bodies
ss = length(distance);

space_min_top = zeros(1,ss);
space_min_bottom = zeros(1,ss);

result_bottom = zeros(ss,length_batch);
result_top = zeros(ss,length_batch);

for dist=1:ss
    spacing = distance(dist);                    %distance between the body
surfaces
    origins = distance(dist) + B1L/2 + B2L/2;

    for batch = 1:length_batch

        %- Hywind/Body 1

        B1w_eta3 = amplHW(batch,dist+3);                  % heave amplitude
        B1w_eta1 = amplHW(batch+2*length_batch,dist+3);   % surge amplitude
        B1w_eta5 = amplHW(batch+length_batch,dist+3);     % pitch amplitude

        B1w_eps3 = epsHW(batch,dist+3);               % phase angle degrees
        B1w_eps1 = epsHW(batch+2*length_batch,dist+3);% phase angle degrees
        B1w_eps5 = epsHW(batch+length_batch,dist+3);  % phase angle degrees


        %- WindFlip/Body 2

        B2w_eta3 = amplWF(batch,dist+3);                  % heave amplitude
        B2w_eta1 = amplWF(batch+2*length_batch,dist+3);   % surge amplitude
        B2w_eta5 = amplWF(batch+length_batch,dist+3);     % pitch amplitude

        B2w_eps3 = epsWF(batch,dist+3);               % phase angle degrees
        B2w_eps1 = epsWF(batch+2*length_batch,dist+3);% phase angle degrees
        B2w_eps5 = epsWF(batch+length_batch,dist+3);  % phase angle degrees


        %--- Defining variables of the sea state ---%


        Tw = amplHW(batch,1);             % wave period
        lambda = 1.56*Tw^2;               % wave length
        k = 2*pi() / lambda;              % wave number
        omegaWave = 2*pi/Tw;              % wave frequency

        %--- Motion amplitudes in COG-coordinates for body 1---%
```

```
B1eta3A = B1w_eta3;                          % heave amplitude
B1eta5A = B1w_eta5;                          % pitch amplitude
B1eta1A = B1w_eta1 - B1dist*B1eta5A;         % surge amplitude


B1eps3 = B1w_eps3*pi()/180;                  % phase angle radians
B1eps1 = B1w_eps1*pi()/180;                  % phase angle radians
B1eps5 = B1w_eps5*pi()/180;                  % phase angle radians


%--- Motion amplitudes in COG-coordinates for body 2---%

B2eta3A = B2w_eta3;                          % heave amplitude
B2eta5A = B2w_eta5;                          % pitch amplitude
B2eta1A = B2w_eta1 - B2dist*B2eta5A;         % surge amplitude


B2eps3 = B2w_eps3*pi()/180;                  % phase angle radians
B2eps1 = B2w_eps1*pi()/180;                  % phase angle radians
B2eps5 = B2w_eps5*pi()/180;                  % phase angle radians


%--- Coefficients for motion of the top point of Hywind ---%

B1A_top = (B1eta1A*cos(B1eps1)) +(-top_2*B1eta5A*cos(B1eps5));
B1B_top = (B1eta1A*sin(B1eps1)) +(-top_2*B1eta5A*sin(B1eps5));

B1etaTot_top = sqrt(B1A_top^2 + B1B_top^2);
B1epsilon_top = atan2(B1B_top,B1A_top);

%--- Coefficients for motion of the bottom of Hywind ---%

B1A_bottom= (B1eta1A*cos(B1eps1)) +(bottom_1*B1eta5A*cos(B1eps5));
B1B_bottom= (B1eta1A*sin(B1eps1)) +(bottom_1*B1eta5A*sin(B1eps5));

B1etaTot_bottom = sqrt(B1A_bottom^2 + B1B_bottom^2);
B1epsilon_bottom = atan2(B1B_bottom,B1A_bottom);


%--- Coefficients for motion of the top point of WindFlip ---%

B2A_top = (B2eta1A*cos(B2eps1)) +(-top_2*B2eta5A*cos(B2eps5));
B2B_top = (B2eta1A*sin(B2eps1)) +(-top_2*B2eta5A*sin(B2eps5));

B2etaTot_top = sqrt(B2A_top^2 + B2B_top^2);
B2epsilon_top = atan2(B2B_top,B2A_top);

%--- Coefficients for  motion of the bottom of WindFlip ---%

B2A_bottom =(B2eta1A*cos(B2eps1)) +(bottom_1*B2eta5A*cos(B2eps5));
B2B_bottom =(B2eta1A*sin(B2eps1)) +(bottom_1*B2eta5A*sin(B2eps5));

B2etaTot_bottom = sqrt(B2A_bottom^2 + B2B_bottom^2);
B2epsilon_bottom = atan2(B2B_bottom,B2A_bottom);

%--- Relative motion between structures, top ---%
```

```
        A_top = (B2etaTot_top*cos(B2epsilon_top)) -
(B1etaTot_top*cos(B1epsilon_top));
        B_top = (B2etaTot_top*sin(B2epsilon_top)) -
(B1etaTot_top*sin(B1epsilon_top));

        eta_top = sqrt(A_top^2 + B_top^2);
        eps_top = atan2(B_top,A_top);

        %--- Relative motion between structures, bottom ---%

        A_bottom = (B2etaTot_bottom*cos(B2epsilon_bottom)) -
(B1etaTot_bottom*cos(B1epsilon_bottom));
        B_bottom = (B2etaTot_bottom*sin(B2epsilon_bottom)) -
(B1etaTot_bottom*sin(B1epsilon_bottom));

        eta_bottom = sqrt(A_bottom^2 + B_bottom^2);
        eps_bottom = atan2(B_bottom,A_bottom);

        %--- Horizontal distance between the two bodies ---%

        for i = 1:50;
            tid(i) = (i-1);
            s_top(i) = spacing + eta_top*sin(omegaWave*tid(i)+eps_top);
            s_bottom(i) = spacing +
eta_bottom*sin(omegaWave*tid(i)+eps_bottom);
        end

        result_bottom(dist,batch) = min(s_bottom);
        result_top(dist,batch) = min(s_top);
        periods(batch)=round(Tw);
        zeros(batch) = 0;
    end
end

disp('¤¤¤¤¤¤¤¤¤¤¤¤¤¤¤¤¤¤¤¤¤¤¤¤¤¤¤¤¤¤¤¤¤¤¤¤¤¤¤¤¤¤¤¤¤¤¤¤¤¤¤¤¤¤¤¤¤¤¤¤¤¤¤¤');
disp('¤  SPACING BETWEEN HYWIND AND WINDFLIP            ');
disp('¤  By Susanne Rusnes, June 2010           ');
disp('¤ ____________________________________________________________ ');
disp('¤  Minimum horizontal spacing between Hywind and WindFlip      ');
disp('¤  Wave period range:                                          ');
disp('¤  5-23 second, 1 second increments                            ');
disp('¤                                                              ');
disp('¤  Initial spacing distances:                                  ');
disp('¤  30, 20, 15, 10, 5, 3, 2, 1, 0 meters                        ');
disp('¤______________________________________________________________');
disp(' Wait for it....');

%--- Plotting the spacing graphs ---%

%- Gives both plots in same window
subplot(2,1,1);
hold on;
plot(periods(:),result_bottom(1,:), 'r.-');
plot(periods(:),result_bottom(2,:), 'bo-');
plot(periods(:),result_bottom(3,:), 'gx-');
plot(periods(:),result_bottom(4,:), 'c+-');
plot(periods(:),result_bottom(5,:), 'm*-');
plot(periods(:),result_bottom(6,:), 'ys-');
plot(periods(:),result_bottom(7,:), 'kd-');
```

```
plot(periods(:),result_bottom(8,:), 'gv--');
plot(periods(:),result_bottom(9,:), 'bh--');
plot(periods(:), zeros(:), 'r*-');
hold off;
title('MINIMUM SPACING BETWEEN BOTTOM POINT');
xlabel('Wave periode [s]');
ylabel('Horizontal spacing [m]');
legend('30m','20m','15m','10m','5m','3m','2m','1m','0m','collision');
% legend('3m','2m','1m','0m','collision');

subplot(2,1,2);
hold on;
plot(periods(:),result_top(1,:), 'r.-');
plot(periods(:),result_top(2,:), 'bo-');
plot(periods(:),result_top(3,:), 'gx-');
plot(periods(:),result_top(4,:), 'c+-');
plot(periods(:),result_top(5,:), 'm*-');
plot(periods(:),result_top(6,:), 'ys-');
plot(periods(:),result_top(7,:), 'kd-');
plot(periods(:),result_top(8,:), 'gv--');
plot(periods(:),result_top(9,:), 'bh--');
plot(periods(:), zeros(:), 'r*-');
hold off;
title(' MINIMUM SPACING BETWEEN TOP POINT');
xlabel('Wave periode [s]');
ylabel('Horizontal spacing [m]');
legend('30m','20m','15m','10m','5m','3m','2m','1m','0m','collision');
% legend('3m','2m','1m','0m','collision');

%- Gives the two figures in seperate windows

% figure(1);
% hold on;
% plot(periods(:),result_bottom(1,:), 'r.-');
% plot(periods(:),result_bottom(2,:), 'bo-');
% plot(periods(:),result_bottom(3,:), 'gx-');
% plot(periods(:),result_bottom(4,:), 'c+-');
% plot(periods(:),result_bottom(5,:), 'm*-');
% plot(periods(:),result_bottom(6,:), 'ys-');
% plot(periods(:),result_bottom(7,:), 'kd-');
% plot(periods(:),result_bottom(8,:), 'gv--');
% plot(periods(:),result_bottom(9,:), 'bh--');
% plot(periods(:), zeros(:), 'r*-');
% hold off;
% title('MINIMUM SPACING BETWEEN BOTTOM POINT');
% xlabel('Wave periode [s]');
% ylabel('Horizontal spacing [m]');
% % legend('30m','20m','15m','10m','5m','3m','2m','1m','0m','collision');
% legend('3m','2m','1m','0m','collision');
%
% figure(2);
% hold on;
% plot(periods(:),result_top(1,:), 'r.-');
% plot(periods(:),result_top(2,:), 'bo-');
% plot(periods(:),result_top(3,:), 'gx-');
% plot(periods(:),result_top(4,:), 'c+-');
% plot(periods(:),result_top(5,:), 'm*-');
% plot(periods(:),result_top(6,:), 'ys-');
% plot(periods(:),result_top(7,:), 'kd-');
% plot(periods(:),result_top(8,:), 'gv--');
% plot(periods(:),result_top(9,:), 'bh--');
```

```
% plot(periods(:), zeros(:), 'r*-');
% hold off;
% title(' MINIMUM SPACING BETWEEN TOP POINT');
% xlabel('Wave periode [s]');
% ylabel('Horizontal spacing [m]');
% % legend('30m','20m','15m','10m','5m','3m','2m','1m','0m','collision');
% legend('3m','2m','1m','0m','collision');

disp(' Program normal end');
```

```
%%%%%%%%%%%%%%%%%%%%%%%%%%%%%%%%%%%%%%%%%%%%%%%%%%%%%%%%%%%%%%%%%%%%%%%%%%%%%%%%
%  FINDING THE TOTAL HORIZONTAL MOTION BETWEEN HYWIND AND WINDFLIP                 %
%                                                                                  %
%  by Susanne Rusnes                                                               %
%  Norwegian University of Science and Technology                                  %
%  June 2010                                                                       %
%%%%%%%%%%%%%%%%%%%%%%%%%%%%%%%%%%%%%%%%%%%%%%%%%%%%%%%%%%%%%%%%%%%%%%%%%%%%%%%%

clc
clear all
close all

%--- Reading input from Wadam analyses ---%

amplHW = xlsread('Compare_HyFlip.xlsx','Amplitude','C3:N59');
amplWF = xlsread('Compare_HyFlip.xlsx','Amplitude','C63:N119');

epsHW = xlsread('Compare_HyFlip.xlsx','Amplitude','Q3:AB59');
epsWF = xlsread('Compare_HyFlip.xlsx','Amplitude','Q63:AB119');

length_batch = length(amplHW(:,1))/3;

%--- Parameters for the structures and the visualization ---%

periode = 19;                           % choose wave period
distance = 0;                           % chose initial spacing

waveHeight = 2;                         % wave height, twice the amplitude
wa = waveHeight/2;                      % wave amplitude
g = 9.81;                               % acceleration of gravity


%- Hywind

length_1 = 190;                         % length of buoy
depth_1 = 110;                          % draft of buoy
freeb_1 = length_1 - depth_1;           % height above
diameter_1 = 8.75;                      % diameter of buoy

B1L = diameter_1;                       % characteristic length of body 1
B1dist = 75;                            % distance between COG and sea surface
of body 1
top_1 = B1dist + freeb_1;               % point of motion, from COG, positive
upwards of body 1
bottom_1 = length_1 - top_1;

%- WindFlip

length_2 = 160;                         % length of buoy
depth_2 = 124;                          % depth of buoy
freeb_2 = length_2 - depth_2;           % freeboard
diameter_2 = 13.6652;                   % diameter of buoy

B2L = 13.6652;                          % characteristic length of body 2
B2dist = 70.17;                         % distance between COG and sea surface
of body 2
top_2 = B2dist + freeb_2;               % point of motion, from COG, positive
upwards of body 1
```

```
bottom_2 = length_2 - top_2;

% --- checking for valid distance value ---%

if distance == 30;
    kolonne = 4;
elseif distance == 20;
    kolonne = 5;
elseif distance == 15;
    kolonne = 6;
elseif distance == 10;
    kolonne = 7;
elseif distance == 5;
    kolonne = 8;
elseif distance == 3;
    kolonne = 9;
elseif distance == 2;
    kolonne = 10;
elseif distance == 1;
    kolonne = 11;
elseif distance == 0;
    kolonne = 12;
else disp ('ERROR: Not valid distance. Please chose 30, 25, 20, 5, 3, 2, 1
or 0 m.')
end

% disp(['Chosen spacing: ' NUM2STR(distance)]);

%--- Checking for valid period ---%

if periode > 23;
    disp('ERROR: Wave period range exceeded, please choose value between 5
and 23 sec');
elseif periode < 5;
    disp('ERROR: Wave period range exceeded, please choose value between 5
and 23 sec');
end

% disp(['Chosen periode: ' NUM2STR(periode)]);

batch = periode - 4;

spacing = distance;                         %distance between the body surfaces
origins = distance + B1L/2 + B2L/2;


%--- Wadam Input: Phase angles and amplitudes of motion ---%

%- Hywind/Body 1

B1w_eta3 = amplHW(batch,kolonne);                    % heave amplitude
B1w_eta1 = amplHW(batch+2*length_batch,kolonne);     % surge amplitude
B1w_eta5 = amplHW(batch+length_batch,kolonne);       % pitch amplitude

B1w_eps3 = epsHW(batch,kolonne);                     % phase angle, degrees
B1w_eps1 = epsHW(batch+2*length_batch,kolonne);      % phase angle, degrees
B1w_eps5 = epsHW(batch+length_batch,kolonne);        % phase angle, degrees

%- WindFlip/Body 2
```

```
B2w_eta3 = amplWF(batch,kolonne);                    % heave amplitude
B2w_eta1 = amplWF(batch+2*length_batch,kolonne);     % surge amplitude
B2w_eta5 = amplWF(batch+length_batch,kolonne);       % pitch amplitude

B2w_eps3 = epsWF(batch,kolonne);                     % phase angle, degrees
B2w_eps1 = epsWF(batch+2*length_batch,kolonne);      % phase angle, degrees
B2w_eps5 = epsWF(batch+length_batch,kolonne);        % phase angle, degrees


%--- Defining variables of the sea state ---%

Tw = periode;           % wave period
lambda = 1.56*Tw^2;     % wave length
k = 2*pi() / lambda;    % wave number
omegaWave = 2*pi/Tw;    % wave frequency
deltaT = 1;             % time increment

%--- Motion amplitudes in COG-coordinates for body 1---%

B1eta3A = B1w_eta3;                     % heave amplitude
B1eta5A = B1w_eta5;                     % pitch amplitude
B1eta1A = B1w_eta1 - B1dist*B1eta5A;    % surge amplitude (COG)


B1eps3 = B1w_eps3*pi()/180;             % phase angle, radians
B1eps1 = B1w_eps1*pi()/180;             % phase angle, radians
B1eps5 = B1w_eps5*pi()/180;             % phase angle, radians

%--- Motion amplitudes in COG-coordinates for body 2---%

B2eta3A = B2w_eta3;                     % heave amplitude
B2eta5A = B2w_eta5;                     % pitch amplitude
B2eta1A = B2w_eta1 - B2dist*B2eta5A;    % surge amplitude


B2eps3 = B2w_eps3*pi()/180;             % phase angle, radians
B2eps1 = B2w_eps1*pi()/180;             % phase angle, radians
B2eps5 = B2w_eps5*pi()/180;             % phase angle, radians

%--- Coefficients for calculation of total horizontal motion ---%
%- Hywind top point

B1A_top = (B1eta1A*cos(B1eps1)) + (-top_1*B1eta5A*cos(B1eps5));
B1B_top = (B1eta1A*sin(B1eps1)) + (-top_1*B1eta5A*sin(B1eps5));

B1etaTot_top = sqrt(B1A_top^2 + B1B_top^2);
B1epsilon_top = atan2(B1B_top,B1A_top);

%- Bottom point of Hywind
B1A_bottom = (B1eta1A*cos(B1eps1)) + (bottom_1*B1eta5A*cos(B1eps5));
B1B_bottom = (B1eta1A*sin(B1eps1)) + (bottom_1*B1eta5A*sin(B1eps5));

B1etaTot_bottom = sqrt(B1A_bottom^2 + B1B_bottom^2);
B1epsilon_bottom = atan2(B1B_bottom,B1A_bottom);

%- Top of WindFlip
B2A_top = (B2eta1A*cos(B2eps1)) + (-top_2*B2eta5A*cos(B2eps5));
```

```
B2B_top = (B2eta1A*sin(B2eps1)) + (-top_2*B2eta5A*sin(B2eps5));

B2etaTot_top = sqrt(B2A_top^2 + B2B_top^2);
B2epsilon_top = atan2(B2B_top,B2A_top);

%- Bottom of WindFlip
B2A_bottom = (B2eta1A*cos(B2eps1)) + (bottom_2*B2eta5A*cos(B2eps5));
B2B_bottom = (B2eta1A*sin(B2eps1)) + (bottom_2*B2eta5A*sin(B2eps5));

B2etaTot_bottom = sqrt(B2A_bottom^2 + B2B_bottom^2);
B2epsilon_bottom = atan2(B2B_bottom,B2A_bottom);


%----------------- VISUALIZING THE BODIES MOTIONS ---------------%

%--- Geometry for sea ---%

time = 200;              % duration of animation
NB = 500;                % divisions of the sea surface
seaLength = 300;
seaWidth = 100;

%--- Writing results to screen ---%

disp('¤¤¤¤¤¤¤¤¤¤¤¤¤¤¤¤¤¤¤¤¤¤¤¤¤¤¤¤¤¤¤¤¤¤¤¤¤¤¤¤¤¤¤¤¤¤¤¤¤¤¤¤¤¤¤¤¤¤¤¤¤¤¤¤');
disp('¤  MOTIONS FOR HYWIND AND WINDFLIP             ');
disp('¤  By Susanne Rusnes, June 2010             ');
disp('¤ ____________________________________________________________ ');
disp('¤  Realitive motion between Hywind and WindFlip      ');
disp('¤  ');
disp(['¤  Wave periode in seconds:                          '
num2str(periode) ]);
disp(['¤  Spacing in x-direction in meters:                 '
num2str(spacing) ]);
disp(['¤  Distance between the structures origins in meters:  '
num2str(origins) ]);
disp('¤                                          ');
disp('¤  Run Interaction_T19_S0.vtf in GLview to see simulation        ');
disp('¤______________________________________________________________');
disp('¤                                                              ');
disp(' Wait for it....');

file = fopen('Interaction_T19_S0.vtf','w');    % opening a VTF file for
writing
fprintf(file,'*VTF-1.00\n\n');

%-- Defining the nodes --%

% Defining the nodes for the ocean
fprintf(file, '*NODES 1\n');
x = -200;
dx = (seaLength-x)/NB;

for i=1:(NB+1);
        fprintf(file, '%f %f %i \n', x, 0, 0);
        fprintf(file, '%f %f %i \n', x, seaWidth, 0);
        x = x + dx; %dx * i;
end
```

```
% Defining the nodes for buoy 1

fprintf(file, '\n\n');
fprintf(file, '*NODES 2\n');

xDir_1 = 0;                     % placement in x-direction
yDir_1 = 50;                    % placement in y-direction

fprintf(file, '%f %f %f \n', xDir_1-(diameter_1/2), yDir_1+(diameter_1/2),
-depth_1);
fprintf(file, '%f %f %f \n', xDir_1-(diameter_1/2), yDir_1-(diameter_1/2),
-depth_1);
fprintf(file, '%f %f %f \n', xDir_1+(diameter_1/2), yDir_1-(diameter_1/2),
-depth_1);
fprintf(file, '%f %f %f \n', xDir_1+(diameter_1/2), yDir_1+(diameter_1/2),
-depth_1);
fprintf(file, '%f %f %f \n', xDir_1-(diameter_1/2), yDir_1+(diameter_1/2),
freeb_1);
fprintf(file, '%f %f %f \n', xDir_1-(diameter_1/2), yDir_1-(diameter_1/2),
freeb_1);
fprintf(file, '%f %f %f \n', xDir_1+(diameter_1/2), yDir_1-(diameter_1/2),
freeb_1);
fprintf(file, '%f %f %f \n', xDir_1+(diameter_1/2), yDir_1+(diameter_1/2),
freeb_1);

% Defining the nodes for buoy 2

fprintf(file, '\n\n');
fprintf(file, '*NODES 3\n');

xDir_2 = xDir_1+origins;        % placement in x-direction
yDir_2 = 50;                    % placement in y-direction

fprintf(file, '%f %f %f \n', xDir_2-(diameter_2/2), yDir_2+(diameter_2/2),
-depth_2);
fprintf(file, '%f %f %f \n', xDir_2-(diameter_2/2), yDir_2-(diameter_2/2),
-depth_2);
fprintf(file, '%f %f %f \n', xDir_2+(diameter_2/2), yDir_2-(diameter_2/2),
-depth_2);
fprintf(file, '%f %f %f \n', xDir_2+(diameter_2/2), yDir_2+(diameter_2/2),
-depth_2);
fprintf(file, '%f %f %f \n', xDir_2-(diameter_2/2), yDir_2+(diameter_2/2),
freeb_2);
fprintf(file, '%f %f %f \n', xDir_2-(diameter_2/2), yDir_2-(diameter_2/2),
freeb_2);
fprintf(file, '%f %f %f \n', xDir_2+(diameter_2/2), yDir_2-(diameter_2/2),
freeb_2);
fprintf(file, '%f %f %f \n', xDir_2+(diameter_2/2), yDir_2+(diameter_2/2),
freeb_2);


% Defining the elements for the ocean

fprintf(file, '\n\n');
fprintf(file, '*ELEMENTS 1\n');
fprintf(file, '%%NODES #1\n');
fprintf(file, '%%COLORS 0 0 255\n');
fprintf(file, '%%QUADS\n');
```

```
teller =1;
for i= 1:NB;
    e1 = teller;
    e2 = teller + 2;
    e3 = teller + 3;
    e4 = teller + 1;

    teller = teller + 2;

    fprintf(file, '%i %i %i %i \n', e1, e2, e3, e4);
end

% Defining the elements for buoy 1

fprintf(file, '\n\n');
fprintf(file, '*ELEMENTS 2\n');
fprintf(file, '%%NODES #2\n');
fprintf(file, '%%COLORS 0.5 0.5 0.5\n');
fprintf(file, '%%HEXAHEDRONS\n');

fprintf(file, '%i %i %i %i %i %i %i %i\n' , 1, 2, 3, 4, 5, 6, 7, 8);


% Defining the elements for buoy 2

fprintf(file, '\n\n');
fprintf(file, '*ELEMENTS 3\n');
fprintf(file, '%%NODES #3\n');
fprintf(file, '%%COLORS 0.5 0.5 0.5\n');
fprintf(file, '%%HEXAHEDRONS\n');

fprintf(file, '%i %i %i %i %i %i %i %i\n' , 1, 2, 3, 4, 5, 6, 7, 8);


% Defining which components to run

fprintf(file, '\n\n');
fprintf(file, '*GLVIEWGEOMETRY 1\n');
fprintf(file, '%%ELEMENTS\n');
fprintf(file, '1 2 3\n');


% Ocean movements

tiden=0;
t=0 ;
j=0 ;
p=0;

for t = 1:time;

    tiden = tiden + 1;

    fprintf(file, '\n\n');
    fprintf(file, '*RESULTS %i\n', tiden);
    fprintf(file, '%%DIMENSION 3\n');
    fprintf(file, '%%PER_NODE #1\n');
```

```
    for j = 1:(NB+1);
        zetaTot(j) = (waveHeight/2) * cos(omegaWave*tiden + k*dx*(j-200));

        fprintf(file, '0.0  0.0     %f\n', zetaTot(j));
        fprintf(file, '0.0  0.0     %f\n', zetaTot(j));
    end
end

% Buoy 1 movements

bevLow = 0;
bevTop = 0;

for t=0:time

    tiden = tiden + 1;

    fprintf(file, '\n\n');
    fprintf(file, '*RESULTS %i\n', tiden);
    fprintf(file, '%%DIMENSION 3\n');
    fprintf(file, '%%PER_NODE #2\n');

    bevLow = B1etaTot_bottom *  sin(omegaWave*tiden + B1epsilon_bottom);
    bevTop = B1etaTot_top *  sin(omegaWave*tiden + B1epsilon_top);
    BevHiv = 0;

    fprintf(file, '%f %f %f \n', bevLow, 0., BevHiv);
    fprintf(file, '%f %f %f \n', bevLow, 0., BevHiv);
    fprintf(file, '%f %f %f \n', bevLow, 0., BevHiv);
    fprintf(file, '%f %f %f \n', bevLow, 0., BevHiv);
    fprintf(file, '%f %f %f \n', bevTop, 0., BevHiv);
    fprintf(file, '%f %f %f \n', bevTop, 0., BevHiv);
    fprintf(file, '%f %f %f \n', bevTop, 0., BevHiv);
    fprintf(file, '%f %f %f \n', bevTop, 0., BevHiv);

end


% Buoy 2 movements

bevLow = 0;
bevTop = 0;
BevHiv = 0;

x_diff = xDir_2 - xDir_1;

for t=0:time

    tiden = tiden + 1;

    fprintf(file, '\n\n');
    fprintf(file, '*RESULTS %i\n', tiden);
    fprintf(file, '%%DIMENSION 3\n');
    fprintf(file, '%%PER_NODE #3\n');

    bevLow = B2etaTot_bottom *  sin(omegaWave*tiden + B2epsilon_bottom);
    bevTop = B2etaTot_top *  sin(omegaWave*tiden + B2epsilon_top);
    BevHiv = 0;
```

```
    fprintf(file, '%f %f %f \n', bevLow, 0., BevHiv);
    fprintf(file, '%f %f %f \n', bevLow, 0., BevHiv);
    fprintf(file, '%f %f %f \n', bevLow, 0., BevHiv);
    fprintf(file, '%f %f %f \n', bevLow, 0., BevHiv);
    fprintf(file, '%f %f %f \n', bevTop, 0., BevHiv);
    fprintf(file, '%f %f %f \n', bevTop, 0., BevHiv);
    fprintf(file, '%f %f %f \n', bevTop, 0., BevHiv);
    fprintf(file, '%f %f %f \n', bevTop, 0., BevHiv);

end


% Which results to run in each time step

    tall1=1;
    tall2=(time+1);
    tall3=((2*time)+1);

    fprintf(file, '\n\n');

    fprintf(file, '*GLVIEWVECTOR 1\n');
    fprintf(file, '%%NAME \"DISPLACEMENT\" \n');

    for o=1:(time);
        fprintf(file, '%%STEP %i\n', tall1);
        fprintf(file, '%i %i %i\n', tall1, tall2, tall3);

        tall1 = tall1 + 1;
        tall2 = tall2 + 1;
        tall3 = tall3 + 1;
    end

fclose(file);
disp(' VTF-file completed');
```

Appendix B Main dimensions

Main Dimensions WindFlip

WindFlip Local Coordinate System (WLC):

X, longitudinal, 0 at stern
y, transverse, 0 on CL
z, normal on baseline, 0 on baseline

WindFlip Global Coordinate system (WGC):

Same origin as local coordinate system. But rotated so n_Z is normal to free surface

Hywind Local Coordinate system (HLC):

Origin on centre axis and keel level. n_Z parallel with the centre axis

Hywind Global Coordinate System (HGC):

Origin on centre axis and at keel level. n_Z normal to free surface

Hywind CG Coordinate System (HCGC)

Origin in the Centre of Gravity. N_Z normal to free surface

ShipX Coordinate System (SXC):

Placed with z-axis passing through COG and with origin in the still water plane. X-axis is positive towards bow.

HyrdoD Global coordinate System (HGC)

Placed so that the z-axis goes through origin of HydroD input coordinate system.

The HydroD input coordinate system is for WindFlip equivalent to the windflip local coordinate system.

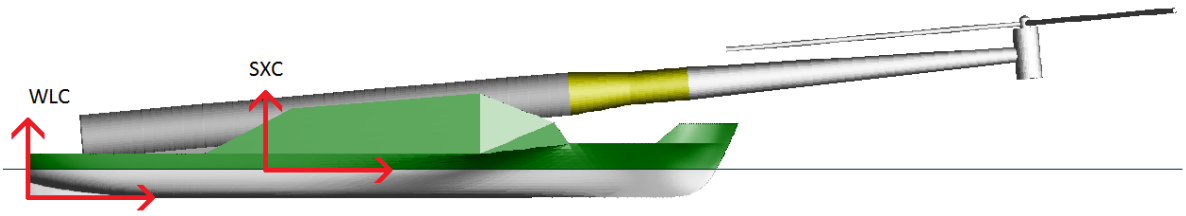

SXC and WLC coordinate systems

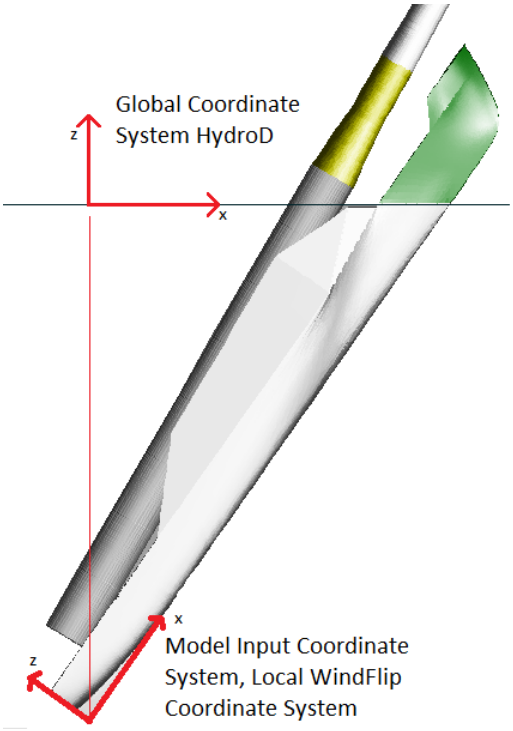

WLC and HGC coordinate systems

Transit (WLC): Length: 140 m Beam: 27.8 m Draft: 5.7 m Height (keel to top tanks): 20.7 m Displacement, volume: 11 615 m^3 Displacement, mass: 11 906 tons Transit Speed: 6 knots COB: (51.818, 0, 3.241) m COG: (51.79, 0, 12.30) m GMT: 1.79 m GML: 248.16 m Pitch, Moment Of Inertia: 59.57 ***	**Launch (WLC):** Draft: 120 m Height: 40 m Displacement, Volume: 27 777 m^3* Displacement, Weight: 28 472 tons* Trim Angle: 85 deg COB: (61.814, 0, 8.901) COG: (53.83, 0, 8.22) GML: 8.17 m GMT: 8.03 m Pitch, R.gyr: 71.67 m ***
Wind Turbine on WindFlip (WLC): Inclination angle: 5 deg COG: (40.3041, 0, 14.7766) m Weight: 6500 tons Blade tip pos: (228, +-52.2, 37.6) m Nacelle pos: (210.1, 0, 23.7) m In SXC Blade Tip pos: (172.9, 0, 31.9) m Nacelle Pos: (157.93, 0, 18) m	**Wind Turbine, free floating (HLC):** Draft: 110 m Height: 80 m Blade Length: 60 m Displacement, Volume: 6341.46 m^3 Displacement, Weight: 6500 tons Diameter, Substructure= 8.75 m Height, Substructure= 98 m Diameter, Waterline=6.5 m COG: (0, 0, 30) COB: (0, 0, 52.86) m GMT: 22.86 m** GML: 22.86 m** Pitch, R.gyr=47.96 m
Test Model, Transit (WLC): Scale Ratio: 1:45 Length: 3.11 m Beam: 0.62 m Draft: 0.13 m Model weight: 57.28 kg Displacement, volume: 0.126 m^3 Displacement, mass: I26.87 kg COB: (1.151, 0, 0.072) m COG: (1.151, 0, 0.273) m, includes turbine GML: 0.0398 m GMT: 5.515 m Pitch, R_{GYR}: 1.324 ***	**Test Model, Launch (WLC):** Draft: 2.67 m Height: 0.889 m Displacement, Volume: 0.304 m^3* Displacement, Weight: 304 kg* Trim Angle: 85 deg COB: (1.374, 0, 0.1978) COG: (1.196, 0, 0.183) GML: 0.182 m GMT: 0.178 m Pitch, R_{Gyr}: 1.593 m ***

* Displacement of ship alone. Not including the displaced volume of wind turbine

** Only the difference between COB and COG, no addition from waterline

*** Both ship and wind turbine

Transfer Functions

ShipX

The transfer functions from ShipX are defined in the SXC coordinate system. All transfer functions in from ShipX are normalized using the wave amplitude. The rotational transfer functions are given with dimension radians/meter.

HydroD

The transfer functions from HydroD are defined in the HGC coordinate system. All transfer functions are normalized on wave amplitude and the rotational DOF's are given with dimension radians/meter.

Appendix C Visualization

VTF files are found on the CD in the folder “Appendix C” for different the following cases:

Single cylinder from 3.2.1 :	SmallCylinderHeave.vtf
Small and large volume cylinder from 3.2.2:	LargeSmallCylinders.vtf
	LargeSmallCorrected.vtf
Hywind and WindFlip from 3.2.3:	HyFlip.vtf
Sea surface from chapter 5.2:	x3m_1_43_Hz.vtf
	X5m_1_43_Hz.vtf
Horizontal motion from chapter 7:	Interaction_T10_S3.vtf
	Interaction_T19_S0.vtf
	Interaction_T19_S2.vtf
	Interaction_T22_S2.vtf

Appendix D Heave and pitch responses for 60 degrees trimmed model

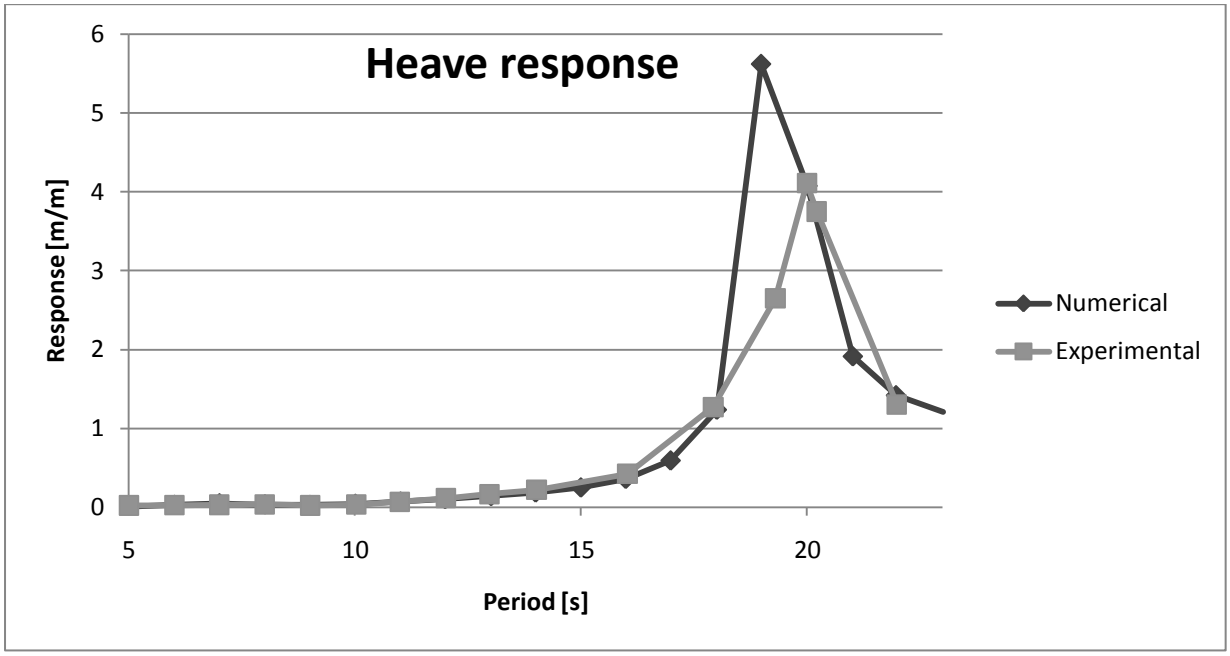

Graph 22 Heave response for attached model, 60 degrees trim

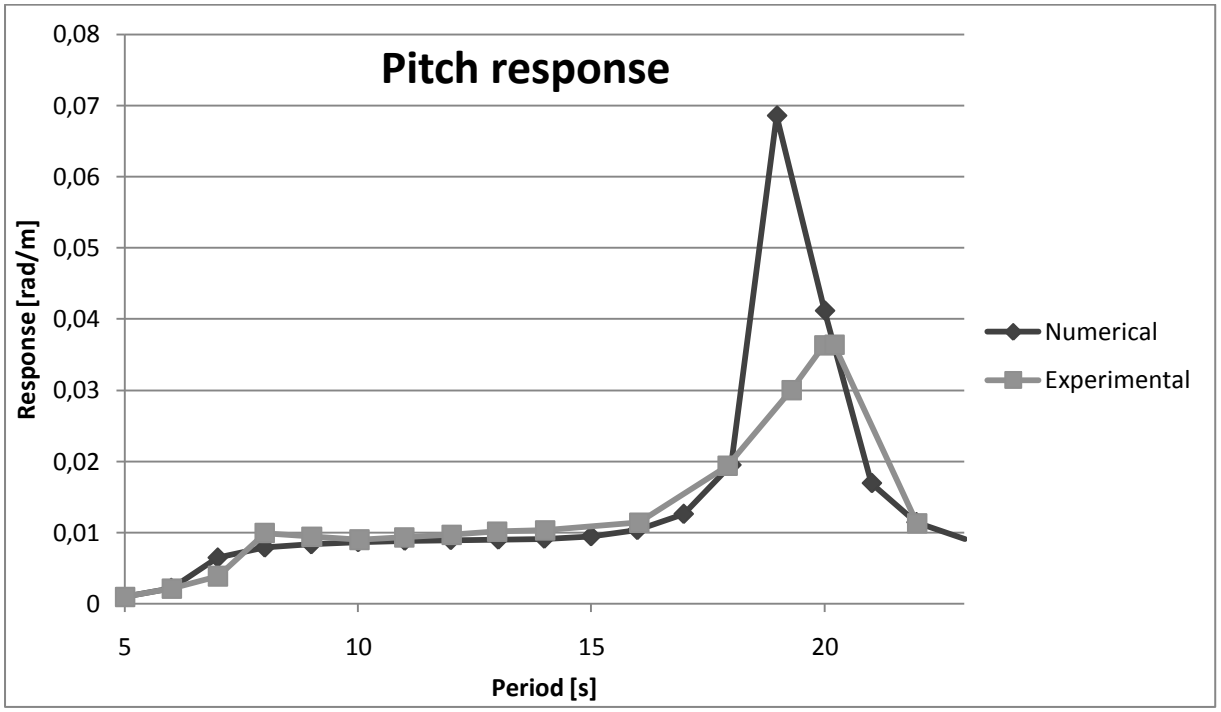

Graph 23 Pitch response for attached model, 60 degrees trim

Appendix E Heave and pitch responses for 85 degrees trimmed model

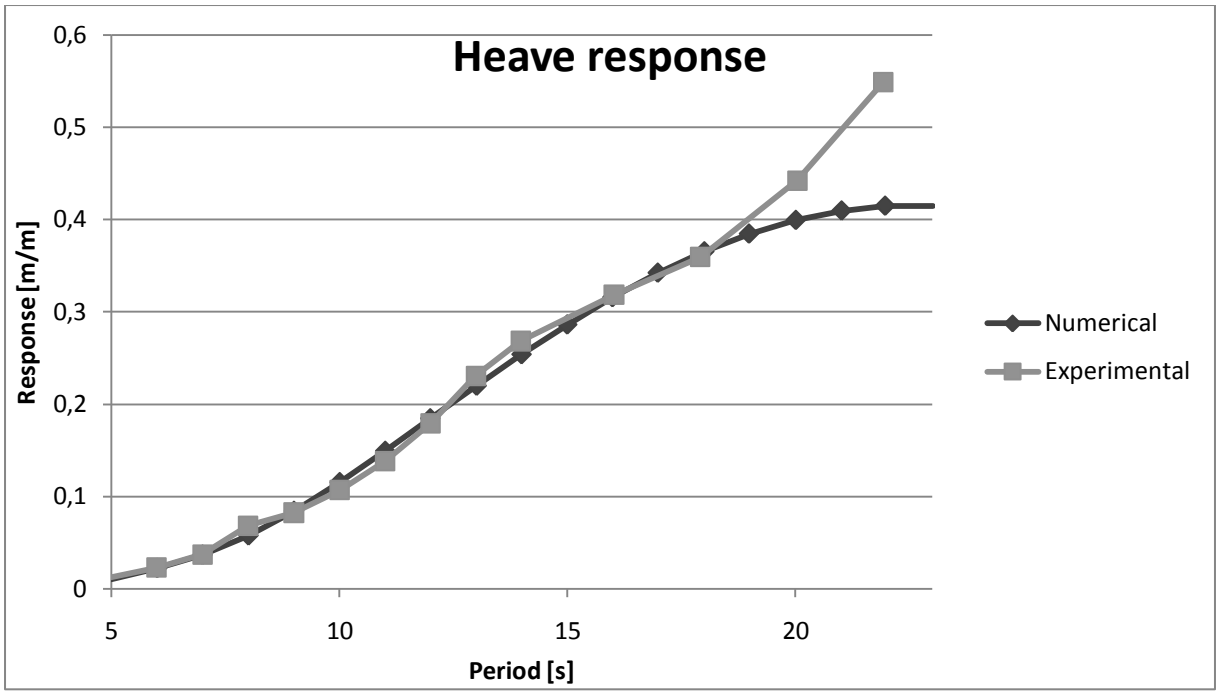

Graph 24 85 degrees trim, heave

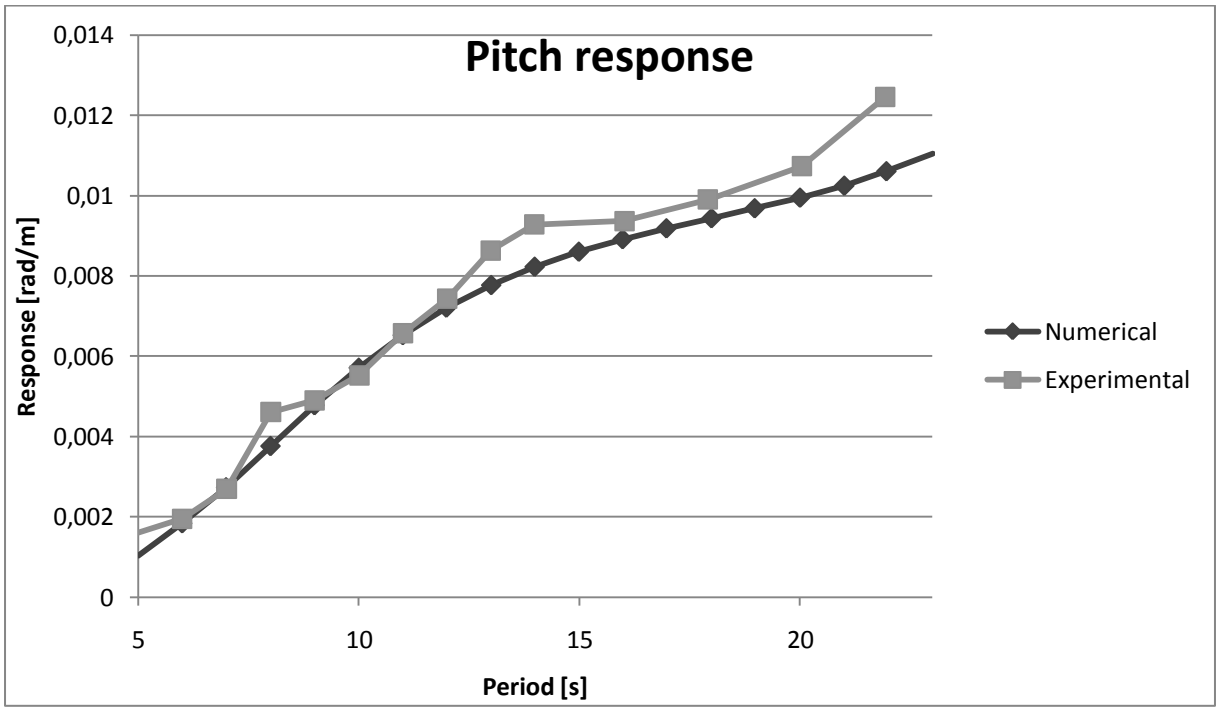

Graph 25 85 degrees trim, pitch

Appendix F Comparing 3-20 seconds RAOs for two tandem arranged cylinders

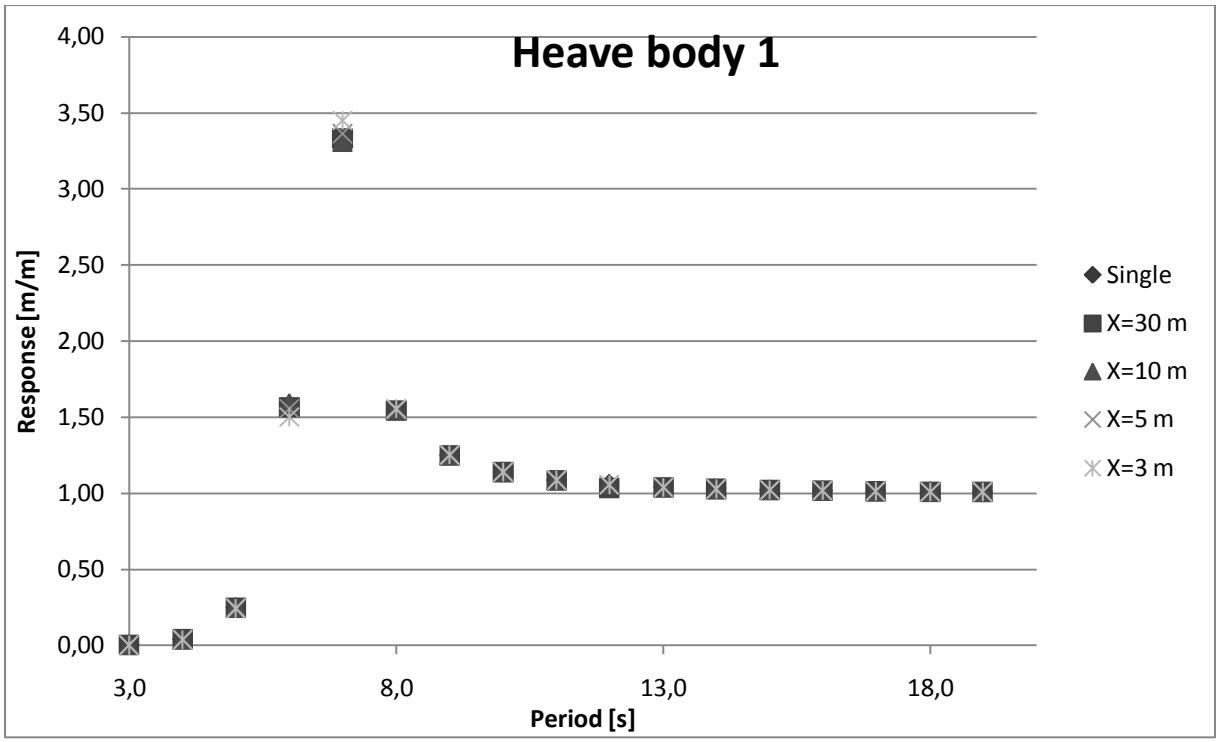

Graph 26 Heave response weather side cylinder

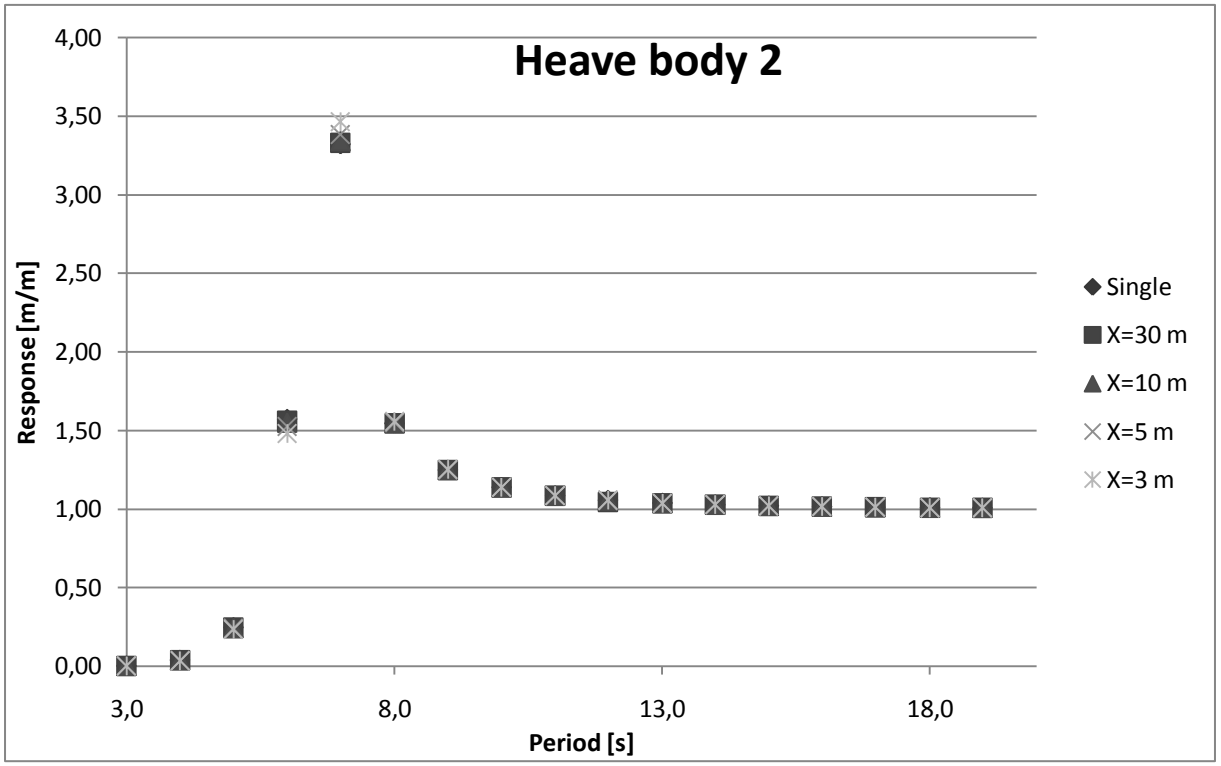

Graph 27 Heave response lee-side cylinder

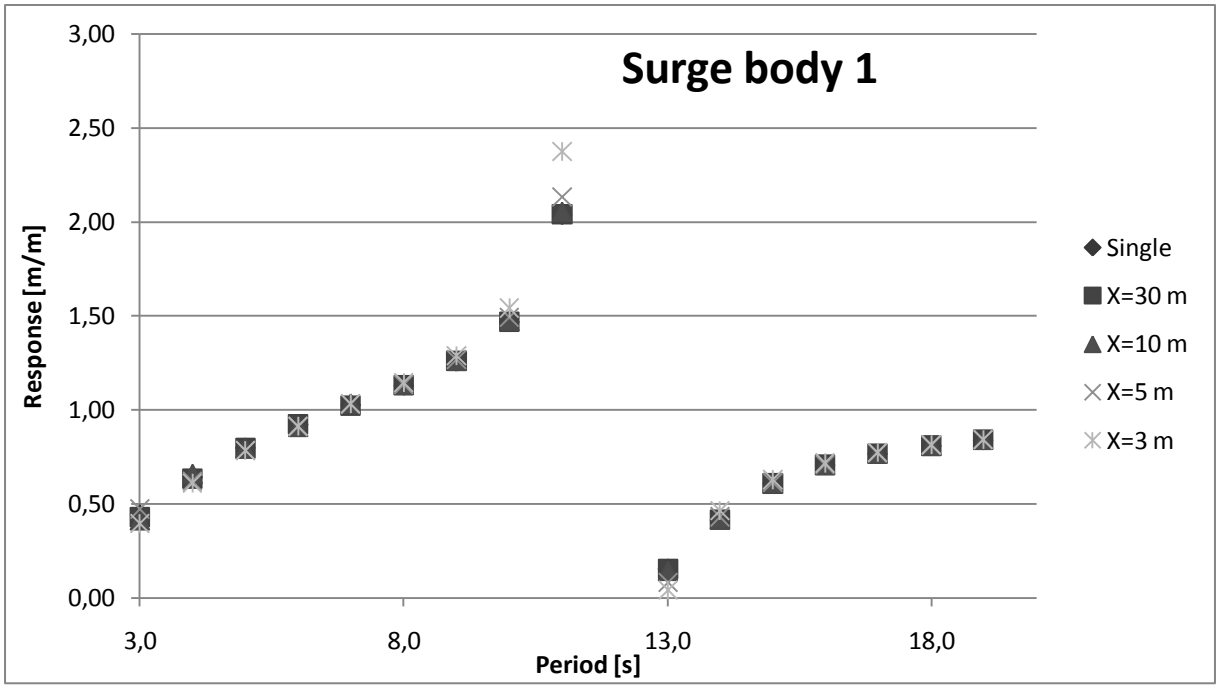

Graph 28 Surge response weather side cylinder

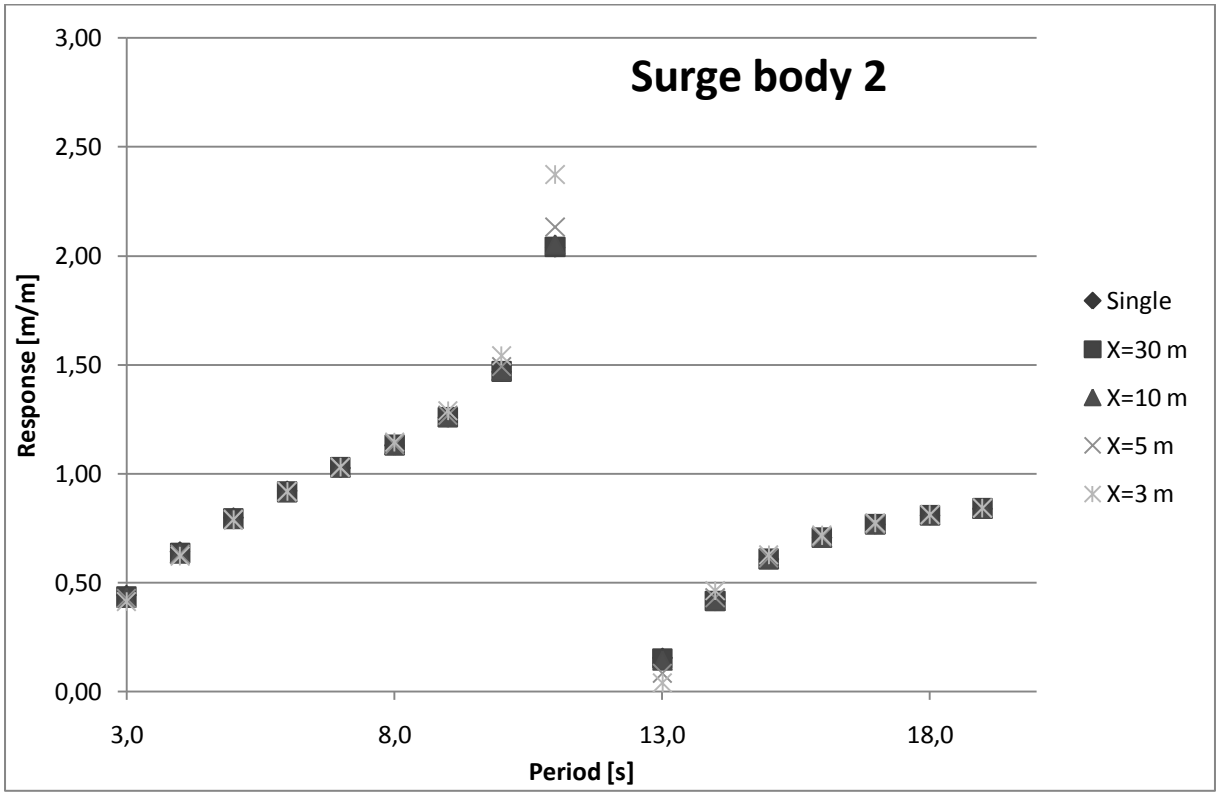

Graph 29 Surge response lee-side cylinder

Appendix G Comparing 0.5 to 3 seconds RAOs for two tandem arranged cylinders

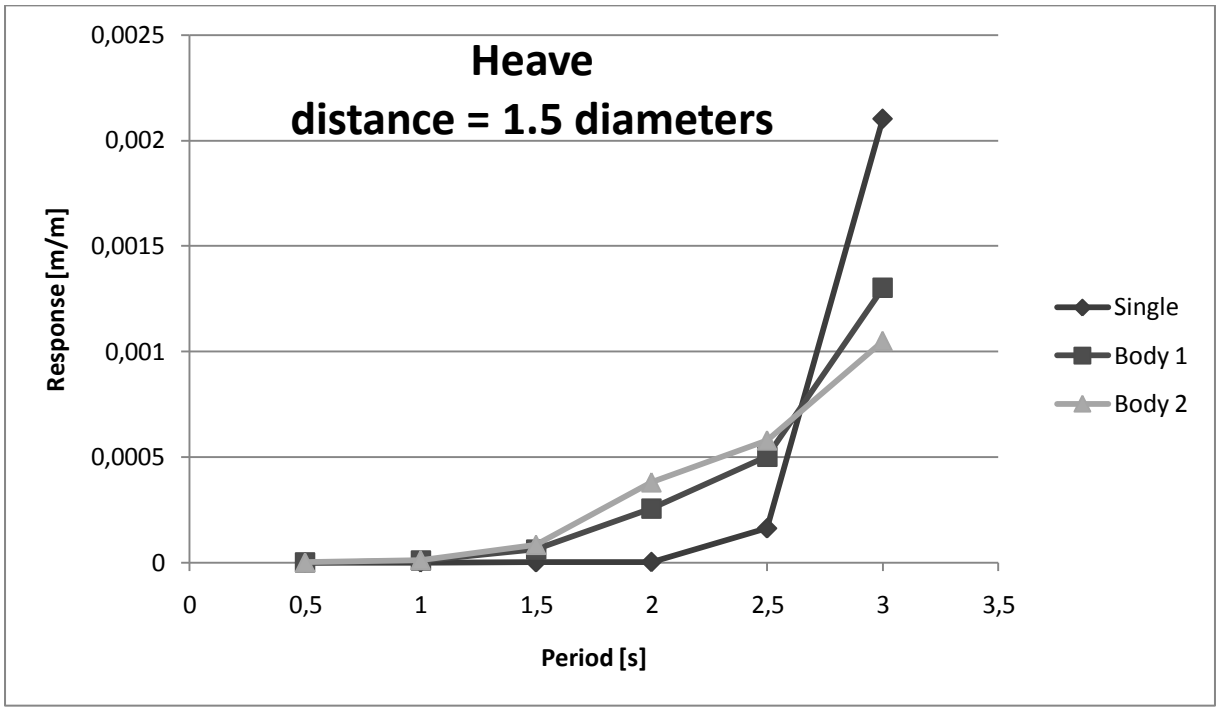

Graph 30 Heave response, multibody cylinders of distance 1.5 diameters

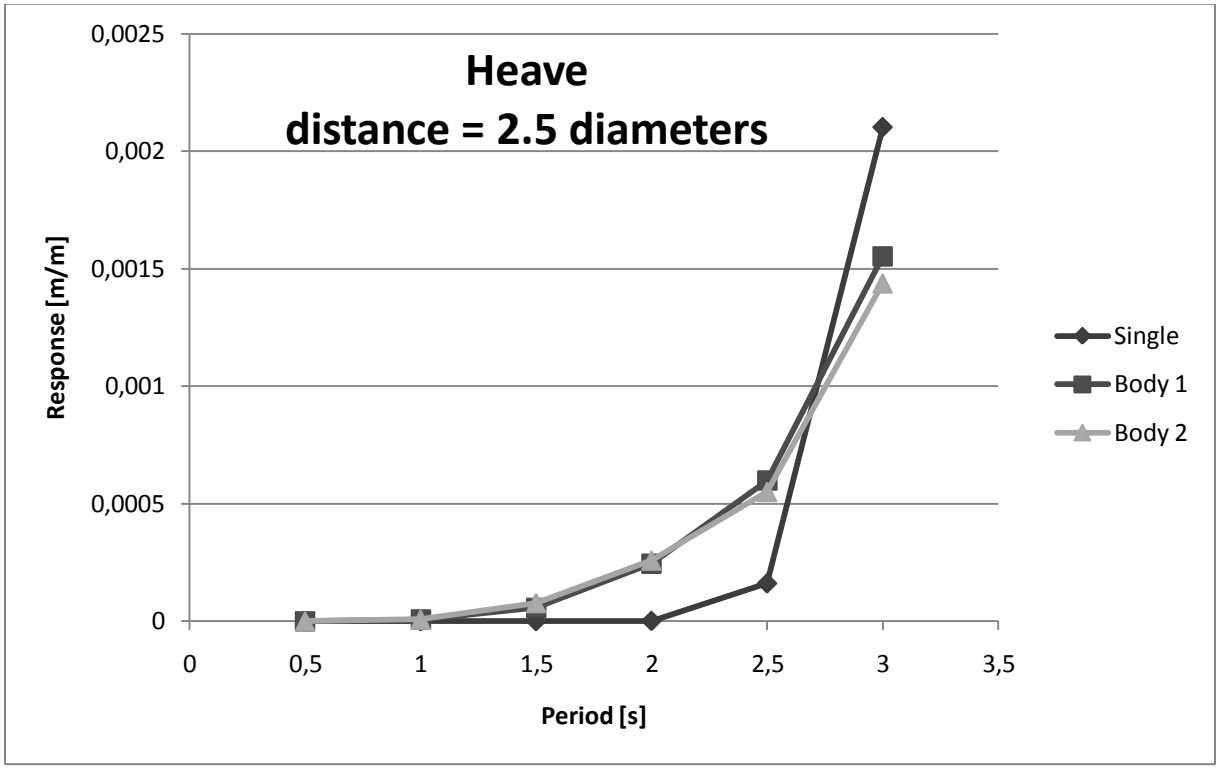

Graph 31 Heave response, multibody cylinders of distance 2.5 diameters

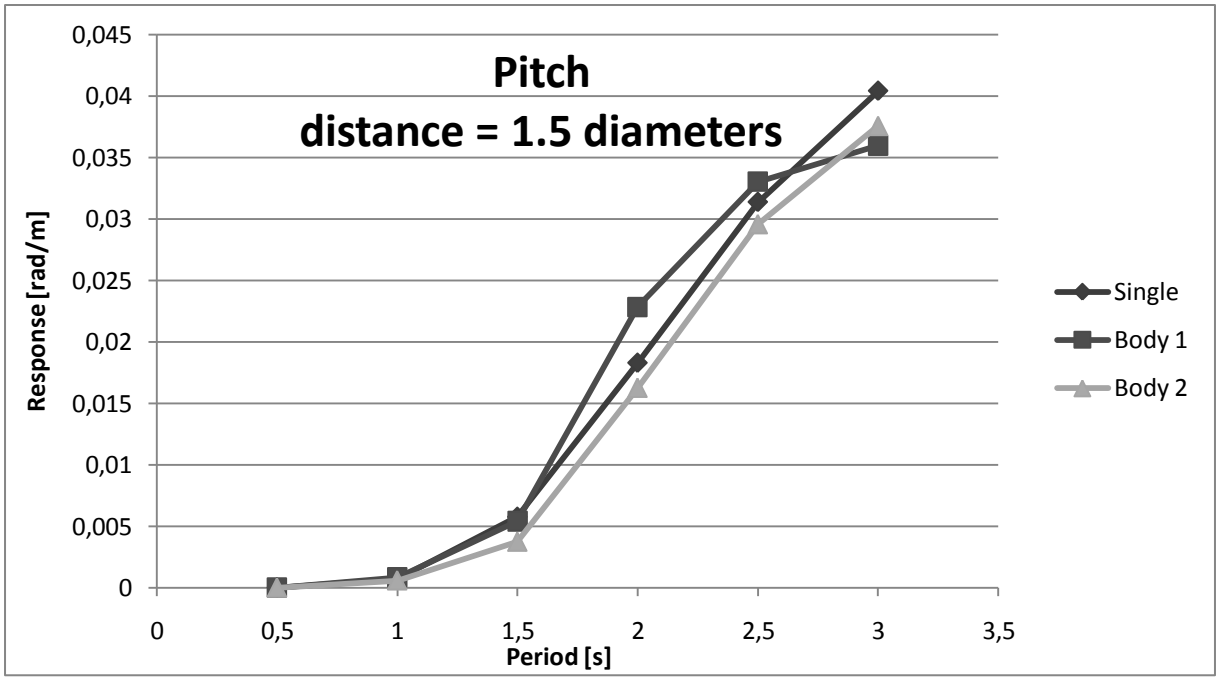

Graph 32 Pitch response, multibody cylinders of distance 1.5 diameters

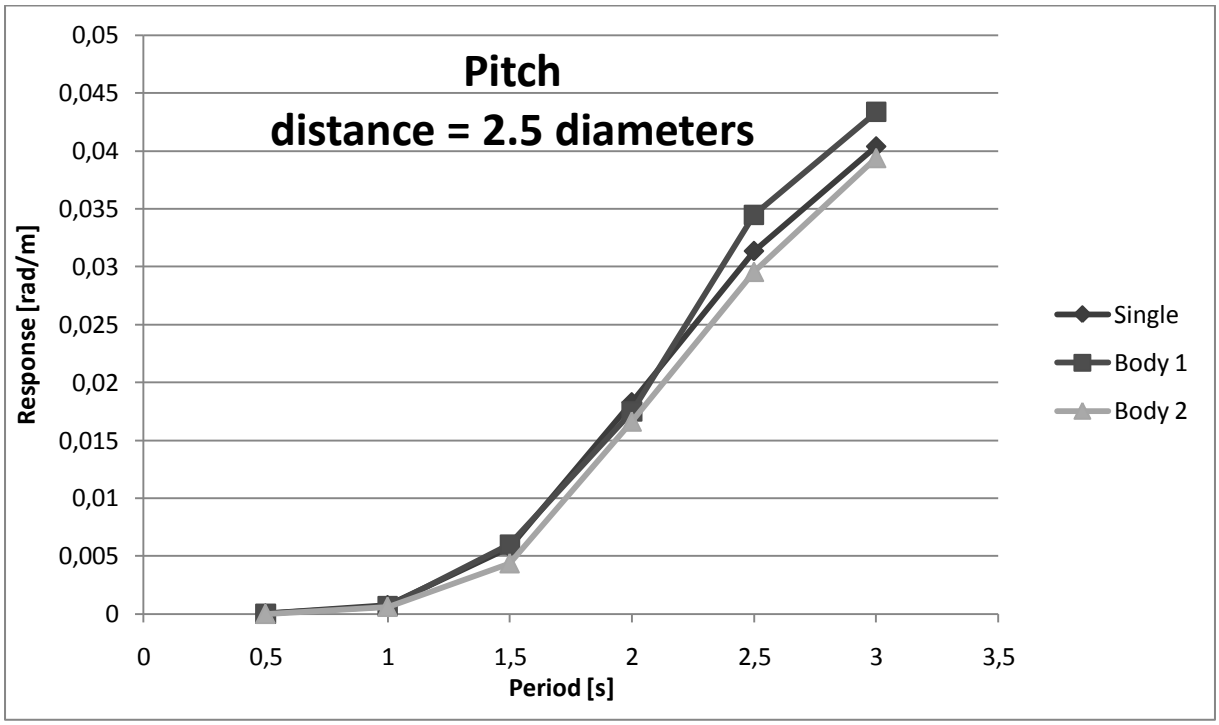

Graph 33 Pitch response, multibody cylinders of distance 2.5 diameters

Appendix H Wadam shortcomings discovered in the multibody analysis

After spending more than two weeks searching for errors in the multibody analysis set-up DNV Support was contacted and presented with the issues encountered. I had then run a multibody set up with a common coordinate system as shown in Figure 32 in chapter 6.1, and also below.

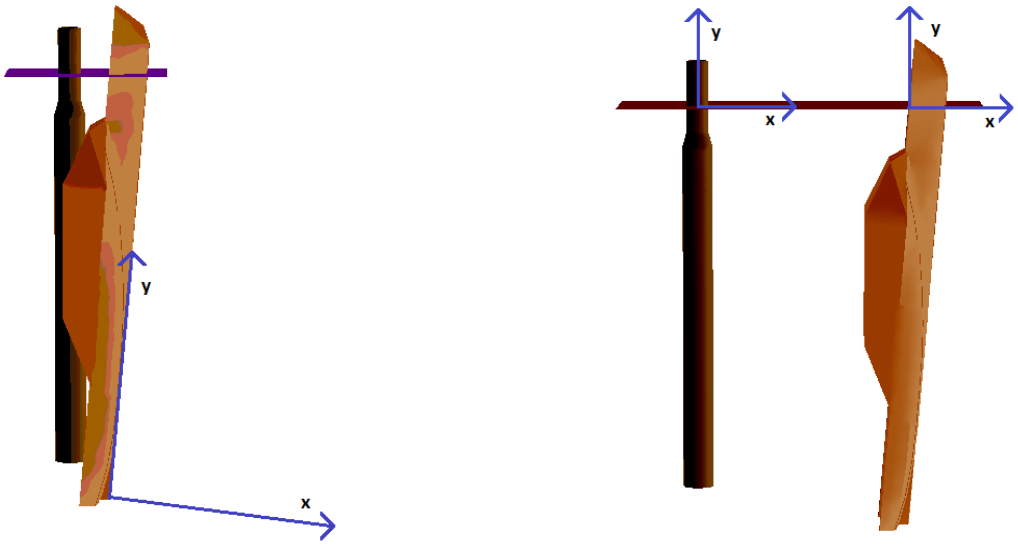

In the user manual for HydroD we find the following statement:

"The description of a multi-body analysis in the user manual for Wadam describes three coordinate systems, the input system, the body system and the global system. When running from HydroD, the body system is identical to the input system of the model. The results from the multi-body models are reported separately, in the body system for each model. "(Det Norske Veritas 2010)

This implies that our input system, placed at the stern of WindFlip, is defined the body coordinate system. Further we find the following regarding multibody analysis in the Wadam user manual:

"A hierarchical set of coordinate systems is introduced in which the individual structures and their input models are specified. The coordinate systems applied in a multi-body analysis are therefore different from those of a single-body analysis; see Figure 2.21. The coordinate systems are defined as follows:

- *The global coordinate system (X_{glo}, Y_{glo}, Z_{glo}) is a right handed cartesian coordinate system with its origin at the still water level and with the z-axis normal to the still water level and the positive z-axis pointing upwards.*
- *The individual body coordinate systems (x_B, y_B, z_B) of each structure are specified relative to the global coordinate system.*
- *The input coordinate system (x_{inp}, y_{inp}, z_{inp}) of each input model included in a body is specified relative to the body coordinate system of that body.*

The body independent coordinates are described in the global coordinate system, e.g. the fluid kinematics evaluation points.

The coordinates related to a particular body are described in the corresponding body coordinate systems, e.g. the result reference coordinate system."(Det Norske Veritas 2009)

From this we find that responses will be given in the body coordinate system, which according to the HydroD user manual is identical to the input coordinate systems. According to the user manuals we will hence find the responses for both structures in a coordinate system as shown in Figure 32 and on the previous page to the left. When analysing the result output from the Wadam run according to this coordinate system, none of the results made sense, and the results for single body runs with a tandem arrangement with a large spacing (800 m) gave results far from the single body runs in all the three evaluated modes of motion. The pitch results should be similar for WindFlip singlebody and WindFlip multibody with large spacing even though the coordinate systems are different. This was not the case for our analyses, and the reason for the deviation was not understood by anyone.

After spending several days without finding any solutions to the problems DNV Software Support was contacted. I sent a clean Java script containing information about the runs ran, and the panel and mass models for Hywind and WindFlip. Jan Henrik Berg-Jensen in DNV ran the same analyses that were run by me, and it became clear that the results were not correct. The set-up was, according to Berg-Jensen, right and hence the errors had to be within the analysis.

Due to the modelling of the two structures a trim angle of about 5 degrees had to be specified in the pre-processor HydroD. I pointed out to DNV that the COG changed in both z- and x-direction from the singlebody to the multibody runs, and this did not make sense when comparing to the user manuals. This deviation in z-direction indicates that the results were not given in the input system, and the deviance in x-direction made me suspect that something else was wrong as well.

What the DNV Support team found out is that the trim angle defined in HydroD is lost when the analyses are run in Wadam. So due to shortcomings in the HydroD/Wadam connection trim angles are not taken into account in Wadam analyses, which for our case gave large miscalculations in the results. In addition to this malfunction, it was also made clear by DNV that the results are not given in the input coordinate system, but in a system with the same x-axis but moved to the mean free surface, as in a single body run.

In order to be able to carry out the planned analyses the models were rotated in GeniE before taken into HydroD. Now no trim angle had to be specified in HydroD, and the trim angle problem in Wadam was avoided. The input coordinate system was also changed as shown in Figure 33 and above to the right. This coordinate system is the same that will be defined by Wadam in the single body runs, and all the response amplitudes from both multibody and singlebody analyses will now be represented in the same coordinate system and hence be directly comparable. The phase angles are given according to the global coordinate system, which corresponds to the input system of Hywind when we only move WindFlip in the multibody runs.

An e-mail from Berg-Jensen confirming the limitations and errors mentioned above are given on the next page.

Hei Susanne

Takk for praten tidligere i dag.
Vi har funnet ut et par ting om multibodyanalyse i Wadam ved hjelp av din modell.

- Som nevnt, ser det ut til at Wadam ikke tillater at en multibodyanalyse inneholder modeller som er roterte i HydroD, dvs. vha. trim og/eller heel. Etter alt å dømme, blir denne informasjonen neglisjert i selve Wadam-analysen. Noe som kan ha stor påvirkning på resultatene.

- Resultatene fra multibodyanalysen i Wadam, som er gitt for det som heter body-systemet (for hvert enkelt legeme), refererer til et punkt i vannflaten, over origo til input-systemet. Body-systemet er dermed ikke, som det dessverre står i brukermanualen, identisk med input-systemet. Etter å ha inspisert kjøringen nærmere, ser jeg at dette blir definert av HydroD, ved at origo i input-systemet blir satt til å være f.eks. (0, 0, -121.36) i body-systemet. Dette blir definert i inputfilen til Wadam, Wadam1.fem, som HydroD lager. Det gjelder dermed også ved postprosessering av resultatene i Postresp.
Vi har dessverre ikke oppdaget dette tidligere.
Den horisontale posisjonen blir bestemt av X/Y posisjonen som defineres i oppsettet av multibodymodellen i HydroD.

Vi har ennå ikke bekreftet dette fullstendig, men er rimelig sikre på at konklusjonene er riktige.
Begge disse problemene bør imidlertid kunne løses ved å lage modellene i den ønskede posisjonen i GeniE, dvs. med origo i vannlinjen og ferdig rotert (trimmet). Dette vil også alltid være en fornuftig test dersom det er mistanke til resultatene, for å elliminere feilmuligheter.

Jeg kan bare beklage at det har tatt tid å finne ut av dette. Som nevnt, har det sammenheng med stor pågang til vårt supportarbeid, i tillegg til at en multibodyanalyse i seg selv ikke er triviell.

Med vennlig hilsen - Best regards,
for Det Norske Veritas AS

Jan Henrik Berg-Jensen

Principal Support Engineer
DNV Software

Phone: +47 95 92 11 76
E-mail: Jan.Henrik.Berg.Jensen@dnv.com

Appendix I Heave and Pitch reference response

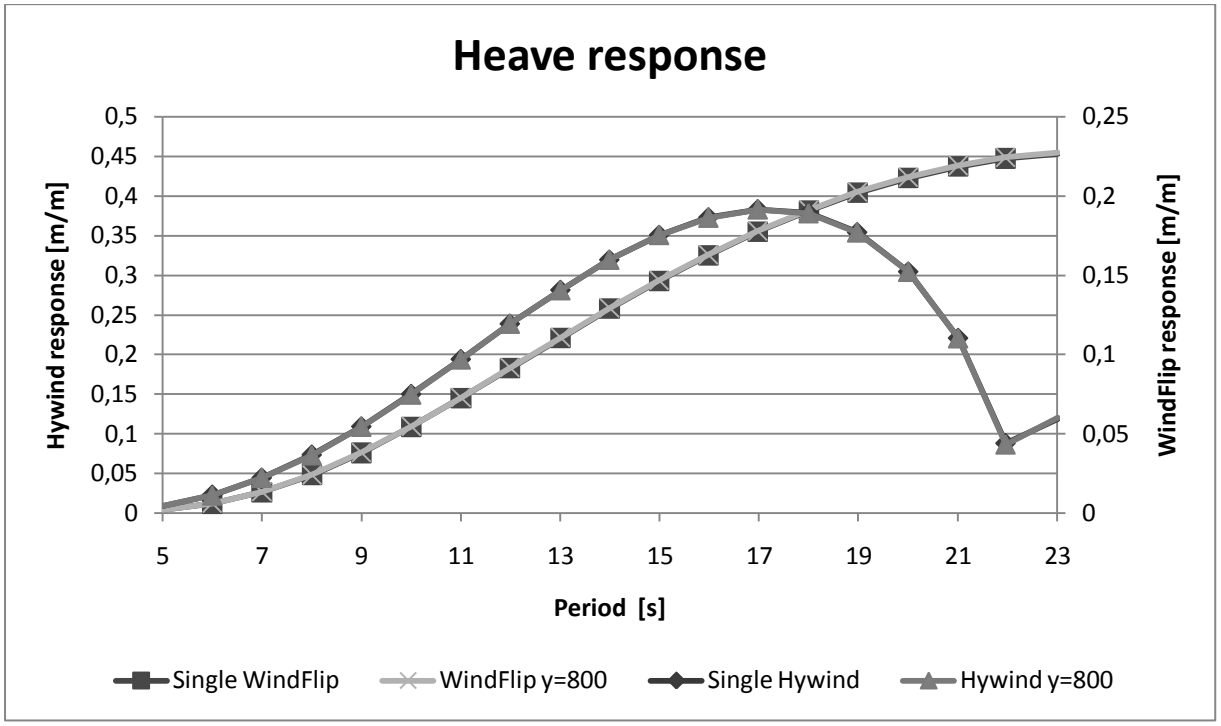

Graph 34 Heave reference runs

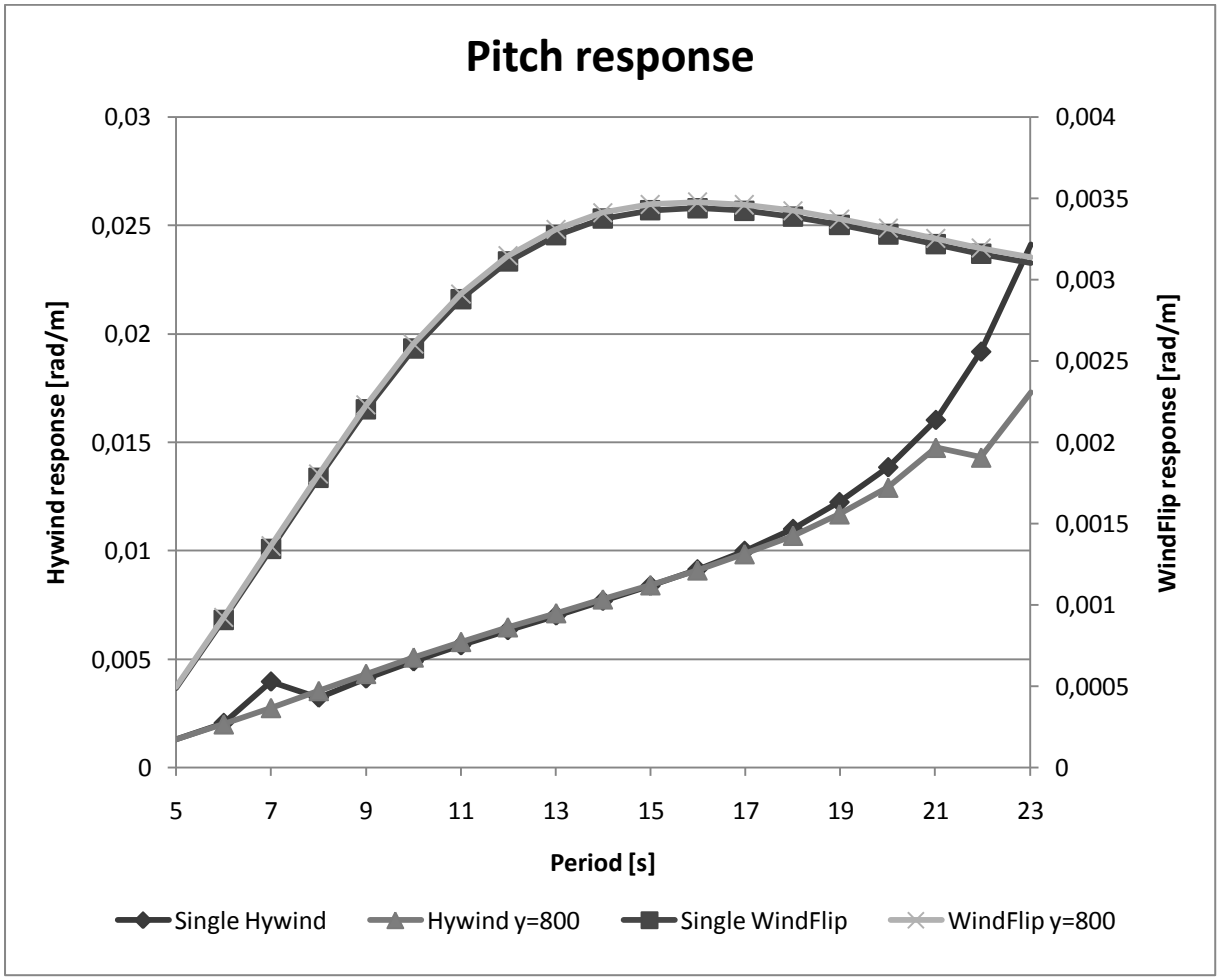

Graph 35 Pitch reference runs

Appendix J Hywind and WindFlip resonance run

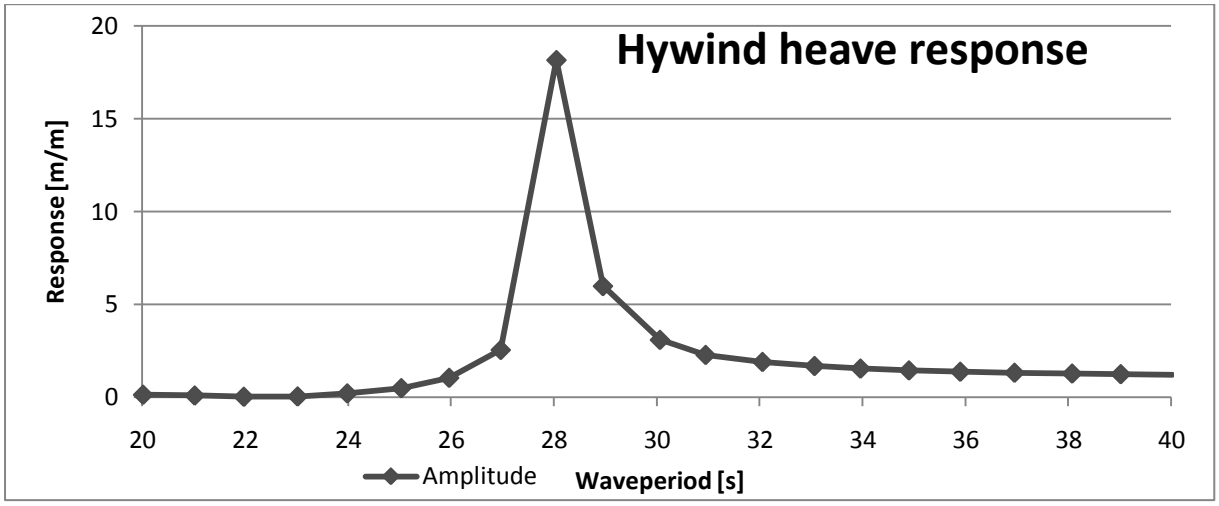

Graph 36 Hywind at heave resonance

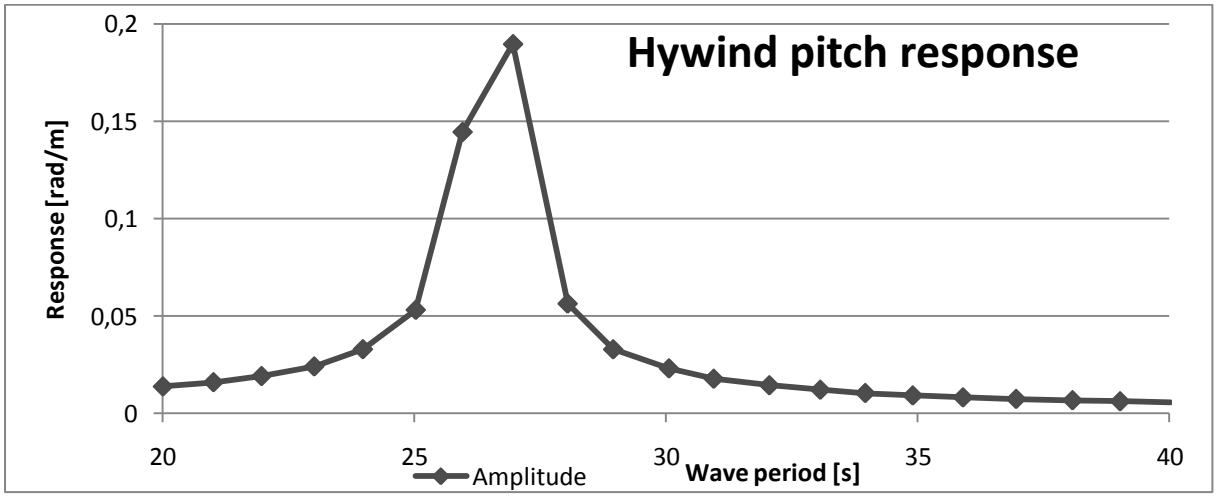

Graph 37 Hywind at pitch resonance

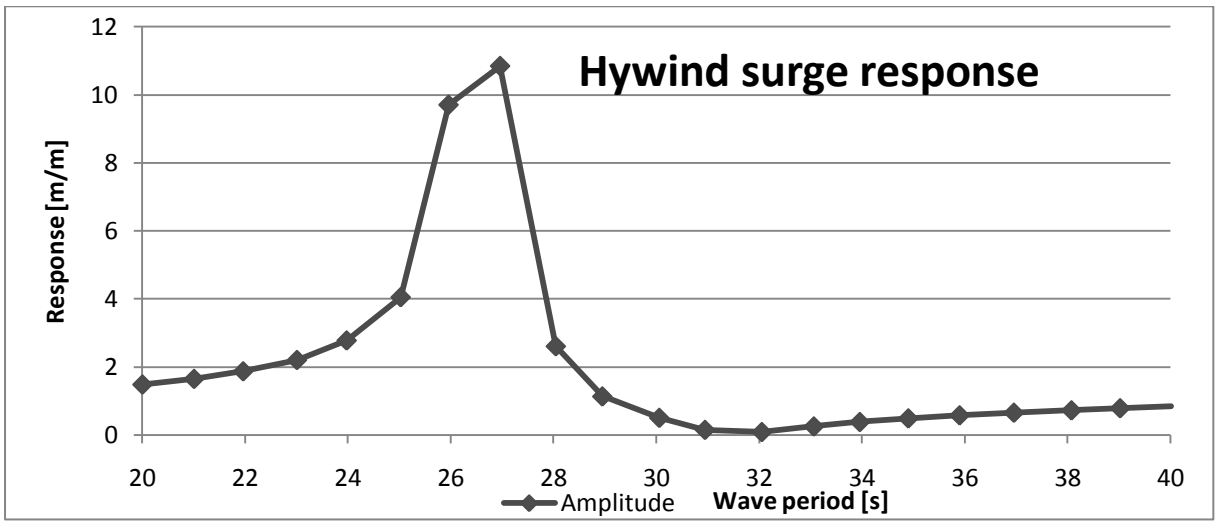

Graph 38 Hywind surge at resonance

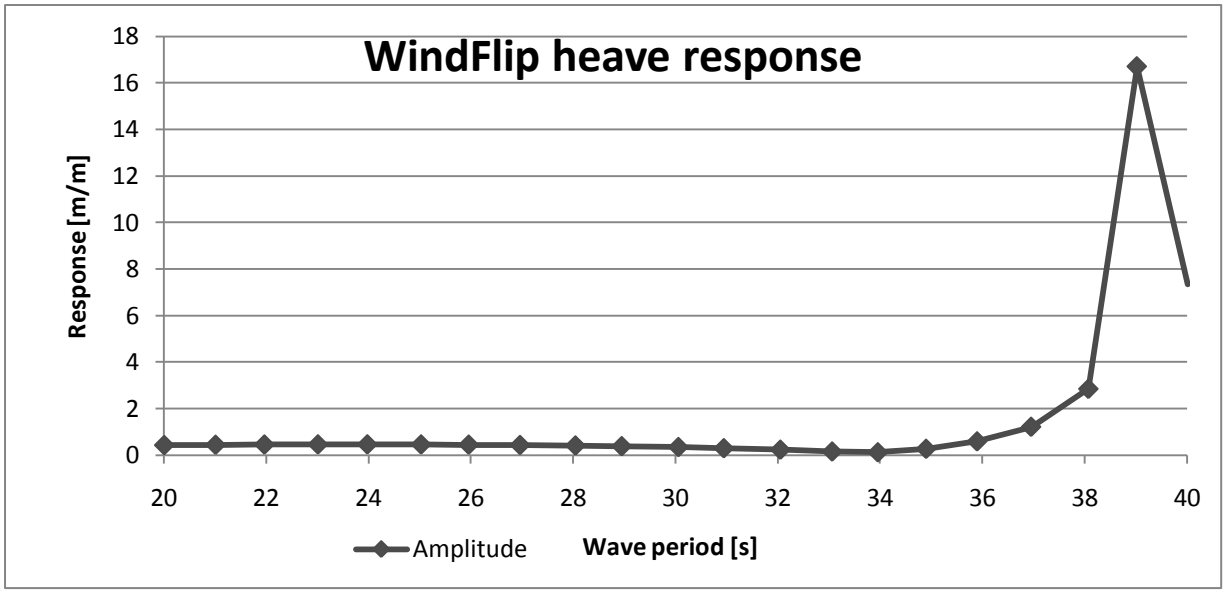

Graph 39 Hywind at heave resonance

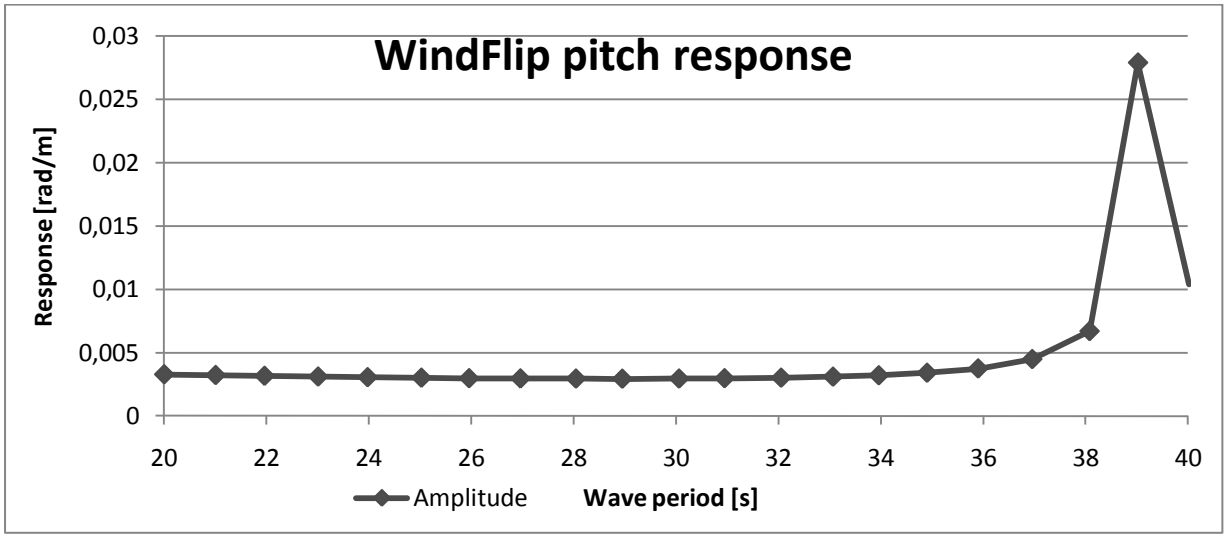

Graph 40 Hywind at pitch resonance

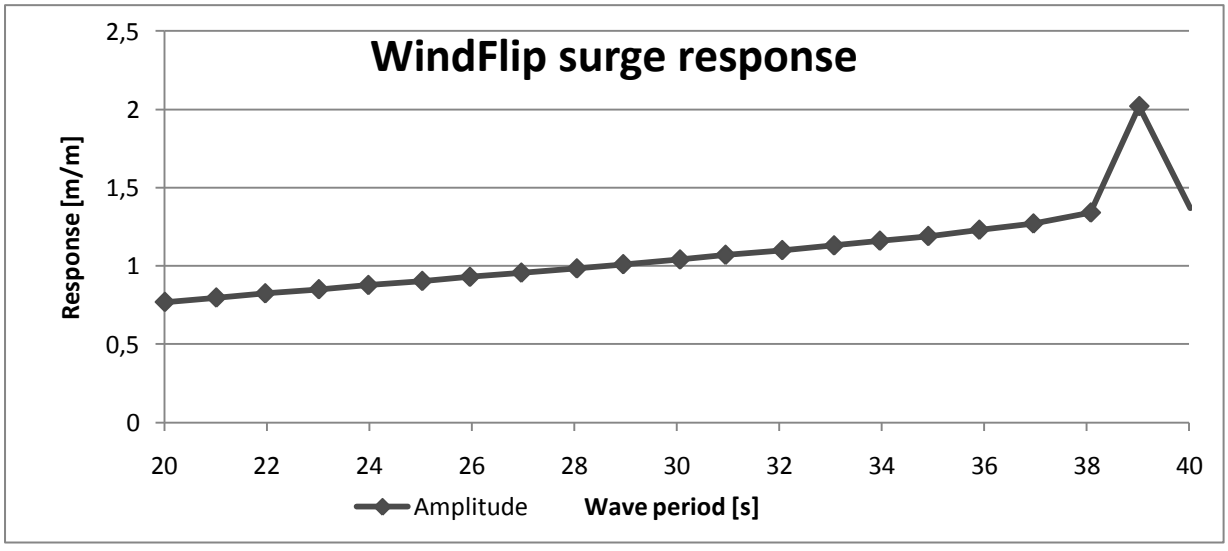

Graph 41 Hywind at surge resonance

Appendix K Spreadsheet for Hywind and WindFlip multibody analyses

	Hywind (body 1) Amplitude												
	Frequency	Period	Single	y 800	30	20	15	10	5	3	2	1	0
Heave	1.257	5	4.50E-03	4.42E-03	4.36E-03	4.91E-03	4.80E-03	4.26E-03	3.72E-02	4.47E-03	4.61E-03	4.78E-03	4.96E-03
	1.047	6	1.15E-02	1.13E-02	1.23E-02	1.19E-02	1.21E-02	1.26E-02	1.31E-02	1.31E-02	1.31E-02	1.31E-02	1.31E-02
	0.898	7	2.23E-02	2.24E-02	2.33E-02	2.39E-02	2.43E-02	2.45E-02	2.28E-02	2.45E-02	2.44E-02	2.44E-02	2.44E-02
	0.785	8	3.68E-02	3.66E-02	3.85E-02	3.91E-02	3.93E-02	3.95E-02	3.95E-02	3.95E-02	3.95E-02	3.95E-02	3.95E-02
	0.698	9	5.46E-02	5.46E-02	5.68E-02	5.73E-02	5.75E-02	5.76E-02	5.78E-02	5.78E-02	5.79E-02	5.79E-02	5.80E-02
	0.628	10	7.51E-02	7.48E-02	7.75E-02	7.80E-02	7.82E-02	7.84E-02	7.86E-02	7.88E-02	7.88E-02	7.89E-02	7.90E-02
	0.571	11	9.71E-02	9.70E-02	9.96E-02	1.00E-01	1.00E-01	1.01E-01	1.01E-01	1.01E-01	1.01E-01	1.01E-01	1.02E-01
	0.524	12	1.19E-01	1.20E-01	1.22E-01	1.23E-01	1.23E-01	1.23E-01	1.24E-01	1.24E-01	1.24E-01	1.24E-01	1.24E-01
	0.483	13	1.41E-01	1.41E-01	1.43E-01	1.44E-01	1.44E-01	1.45E-01	1.45E-01	1.45E-01	1.46E-01	1.46E-01	1.46E-01
	0.449	14	1.60E-01	1.60E-01	1.62E-01	1.63E-01	1.63E-01	1.64E-01	1.64E-01	1.65E-01	1.65E-01	1.65E-01	1.65E-01
	0.419	15	1.75E-01	1.75E-01	1.78E-01	1.78E-01	1.79E-01	1.79E-01	1.80E-01	1.80E-01	1.81E-01	1.81E-01	1.81E-01
	0.393	16	1.87E-01	1.86E-01	1.89E-01	1.89E-01	1.90E-01	1.90E-01	1.91E-01	1.92E-01	1.92E-01	1.92E-01	1.93E-01
	0.37	17	1.92E-01	1.92E-01	1.94E-01	1.95E-01	1.95E-01	1.96E-01	1.97E-01	1.97E-01	1.98E-01	1.98E-01	1.99E-01
	0.349	18	1.89E-01	1.89E-01	1.91E-01	1.92E-01	1.93E-01	1.93E-01	1.95E-01	1.95E-01	1.96E-01	1.96E-01	1.97E-01
	0.331	19	1.77E-01	1.77E-01	1.79E-01	1.80E-01	1.81E-01	1.82E-01	1.83E-01	1.84E-01	1.84E-01	1.85E-01	1.86E-01
	0.314	20	1.52E-01	1.52E-01	1.55E-01	1.56E-01	1.56E-01	1.57E-01	1.59E-01	1.60E-01	1.61E-01	1.61E-01	1.62E-01
	0.299	21	1.10E-01	1.10E-01	1.13E-01	1.14E-01	1.15E-01	1.16E-01	1.18E-01	1.19E-01	1.20E-01	1.21E-01	1.23E-01
	0.286	22	4.40E-02	4.34E-02	4.68E-02	4.82E-02	4.92E-02	5.08E-02	5.35E-02	5.52E-02	5.60E-02	5.63E-02	5.34E-02
	0.273	23	5.95E-02	6.01E-02	5.63E-02	5.49E-02	5.40E-02	5.29E-02	5.15E-02	5.03E-02	4.95E-02	4.96E-02	4.79E-02
Pitch	1.257	5	1.30E-03	1.31E-03	1.24E-03	1.39E-03	1.32E-03	1.09E-03	6.43E-04	9.74E-04	9.82E-04	9.90E-04	9.88E-04
	1.047	6	2.05E-03	2.00E-03	2.11E-03	1.97E-03	1.92E-03	1.91E-03	1.88E-03	1.84E-03	1.81E-03	1.77E-03	1.70E-03
	0.898	7	3.96E-03	2.75E-03	2.80E-03	2.78E-03	2.75E-03	2.70E-03	2.78E-03	2.49E-03	2.44E-03	2.38E-03	2.30E-03
	0.785	8	3.22E-03	3.54E-03	3.60E-03	3.55E-03	3.50E-03	3.41E-03	3.25E-03	3.15E-03	3.09E-03	3.01E-03	2.91E-03
	0.698	9	4.10E-03	4.32E-03	4.36E-03	4.30E-03	4.23E-03	4.12E-03	3.92E-03	3.80E-03	3.73E-03	3.64E-03	3.53E-03
	0.628	10	4.89E-03	5.08E-03	5.09E-03	5.01E-03	4.93E-03	4.80E-03	4.57E-03	4.43E-03	4.35E-03	4.25E-03	4.12E-03
	0.571	11	5.63E-03	5.80E-03	5.77E-03	5.69E-03	5.60E-03	5.45E-03	5.19E-03	5.04E-03	4.94E-03	4.83E-03	4.69E-03
	0.524	12	6.33E-03	6.48E-03	6.43E-03	6.33E-03	6.23E-03	6.07E-03	5.79E-03	5.62E-03	5.52E-03	5.40E-03	5.25E-03
	0.483	13	7.01E-03	7.13E-03	7.06E-03	6.95E-03	6.85E-03	6.67E-03	6.37E-03	6.19E-03	6.08E-03	5.95E-03	5.78E-03
	0.449	14	7.68E-03	7.77E-03	7.68E-03	7.57E-03	7.46E-03	7.27E-03	6.95E-03	6.76E-03	6.65E-03	6.51E-03	6.33E-03
	0.419	15	8.38E-03	8.42E-03	8.32E-03	8.20E-03	8.09E-03	7.89E-03	7.56E-03	7.36E-03	7.23E-03	7.08E-03	6.88E-03
	0.393	16	9.14E-03	9.10E-03	9.00E-03	8.87E-03	8.76E-03	8.55E-03	8.20E-03	7.99E-03	7.86E-03	7.70E-03	7.47E-03
	0.37	17	9.99E-03	9.85E-03	9.74E-03	9.61E-03	9.49E-03	9.28E-03	8.91E-03	8.68E-03	8.54E-03	8.36E-03	8.11E-03
	0.349	18	1.10E-02	1.07E-02	1.06E-02	1.05E-02	1.03E-02	1.01E-02	9.70E-03	9.45E-03	9.30E-03	9.10E-03	8.82E-03
	0.331	19	1.22E-02	1.17E-02	1.16E-02	1.14E-02	1.13E-02	1.10E-02	1.06E-02	1.03E-02	1.02E-02	9.94E-03	9.62E-03
	0.314	20	1.39E-02	1.29E-02	1.28E-02	1.26E-02	1.24E-02	1.22E-02	1.16E-02	1.13E-02	1.11E-02	1.09E-02	1.05E-02
	0.299	21	1.60E-02	1.48E-02	1.45E-02	1.43E-02	1.40E-02	1.35E-02	1.28E-02	1.24E-02	1.21E-02	1.18E-02	1.14E-02
	0.286	22	1.92E-02	1.43E-02	1.22E-02	1.17E-02	1.16E-02	1.14E-02	1.13E-02	1.10E-02	1.06E-02	1.03E-02	1.02E-02
	0.273	23	2.41E-02	1.73E-02	1.83E-02	1.86E-02	1.85E-02	1.72E-02	2.15E-02	2.07E-02	2.68E-02	1.64E-02	1.64E-02
Surge	1.257	5	1.24E-01	1.24E-01	1.19E-01	1.33E-01	1.25E-01	1.01E-01	7.18E-02	8.55E-02	8.58E-02	8.62E-02	8.56E-02
	1.047	6	1.92E-01	1.93E-01	2.04E-01	1.88E-01	1.81E-01	1.77E-01	1.74E-01	1.71E-01	1.69E-01	1.66E-01	1.60E-01
	0.898	7	2.74E-01	2.70E-01	2.73E-01	2.68E-01	2.65E-01	2.60E-01	2.63E-01	2.45E-01	2.41E-01	2.37E-01	2.29E-01
	0.785	8	3.52E-01	3.55E-01	3.57E-01	3.53E-01	3.48E-01	3.42E-01	3.31E-01	3.24E-01	3.19E-01	3.13E-01	3.05E-01
	0.698	9	4.42E-01	4.45E-01	4.45E-01	4.40E-01	4.35E-01	4.28E-01	4.14E-01	4.06E-01	4.00E-01	3.93E-01	3.84E-01
	0.628	10	5.33E-01	5.36E-01	5.35E-01	5.29E-01	5.24E-01	5.15E-01	5.00E-01	4.90E-01	4.84E-01	4.76E-01	4.65E-01
	0.571	11	6.24E-01	6.28E-01	6.24E-01	6.18E-01	6.13E-01	6.03E-01	5.85E-01	5.74E-01	5.67E-01	5.59E-01	5.47E-01
	0.524	12	7.14E-01	7.17E-01	7.13E-01	7.06E-01	7.00E-01	6.89E-01	6.70E-01	6.58E-01	6.51E-01	6.41E-01	6.29E-01
	0.483	13	8.02E-01	8.05E-01	8.00E-01	7.93E-01	7.86E-01	7.74E-01	7.53E-01	7.41E-01	7.33E-01	7.23E-01	7.10E-01
	0.449	14	8.88E-01	8.91E-01	8.85E-01	8.77E-01	8.70E-01	8.58E-01	8.36E-01	8.22E-01	8.14E-01	8.04E-01	7.89E-01
	0.419	15	9.73E-01	9.76E-01	9.69E-01	9.61E-01	9.53E-01	9.40E-01	9.17E-01	9.03E-01	8.94E-01	8.83E-01	8.68E-01
	0.393	16	1.06E+00	1.06E+00	1.05E+00	1.05E+00	1.04E+00	1.02E+00	9.99E-01	9.84E-01	9.75E-01	9.63E-01	9.47E-01
	0.37	17	1.15E+00	1.15E+00	1.14E+00	1.13E+00	1.12E+00	1.11E+00	1.08E+00	1.07E+00	1.06E+00	1.04E+00	1.03E+00
	0.349	18	1.25E+00	1.24E+00	1.23E+00	1.22E+00	1.21E+00	1.20E+00	1.17E+00	1.15E+00	1.14E+00	1.13E+00	1.11E+00
	0.331	19	1.36E+00	1.33E+00	1.33E+00	1.32E+00	1.31E+00	1.29E+00	1.26E+00	1.24E+00	1.23E+00	1.21E+00	1.19E+00
	0.314	20	1.49E+00	1.45E+00	1.44E+00	1.42E+00	1.41E+00	1.39E+00	1.36E+00	1.33E+00	1.32E+00	1.30E+00	1.28E+00
	0.299	21	1.65E+00	1.60E+00	1.58E+00	1.56E+00	1.54E+00	1.51E+00	1.46E+00	1.43E+00	1.41E+00	1.39E+00	1.36E+00
	0.286	22	1.88E+00	1.56E+00	1.59E+00	1.62E+00	1.63E+00	1.63E+00	1.64E+00	1.77E+00	1.99E+00	2.38E+00	2.88E+00
	0.273	23	2.21E+00	1.80E+00	1.87E+00	1.90E+00	1.89E+00	1.80E+00	2.13E+00	2.07E+00	2.53E+00	1.75E+00	1.76E+00

			WindFlip (body 2) Amplitude										
	Frequency	Period	Single	y 800 m	x 30 m	x 20 m	x 15 m	x 10 m	x 5 m	x 3 m	x 2 m	x 1 m	x 0 m
Heave	1.257	5	4.31E-03	4.42E-03	3.27E-03	5.88E-03	4.74E-03	2.85E-03	2.71E-02	4.86E-03	5.35E-03	5.83E-03	6.31E-03
	1.047	6	1.22E-02	1.24E-02	1.39E-02	1.07E-02	1.07E-02	1.26E-02	1.48E-02	1.53E-02	1.54E-02	1.54E-02	1.54E-02
	0.898	7	2.67E-02	2.70E-02	2.54E-02	2.62E-02	2.78E-02	2.92E-02	2.93E-02	2.97E-02	2.95E-02	2.94E-02	2.93E-02
	0.785	8	4.82E-02	4.84E-02	4.77E-02	4.97E-02	5.05E-02	5.09E-02	5.08E-02	5.06E-02	5.04E-02	5.03E-02	5.03E-02
	0.698	9	7.61E-02	7.66E-02	7.71E-02	7.82E-02	7.85E-02	7.84E-02	7.81E-02	7.80E-02	7.79E-02	7.78E-02	7.79E-02
	0.628	10	1.09E-01	1.10E-01	1.11E-01	1.11E-01	1.11E-01	1.11E-01	1.11E-01	1.11E-01	1.11E-01	1.11E-01	1.11E-01
	0.571	11	1.45E-01	1.46E-01	1.47E-01	1.47E-01	1.47E-01	1.47E-01	1.47E-01	1.47E-01	1.47E-01	1.47E-01	1.47E-01
	0.524	12	1.83E-01	1.84E-01	1.84E-01	1.84E-01	1.84E-01	1.84E-01	1.84E-01	1.84E-01	1.84E-01	1.84E-01	1.85E-01
	0.483	13	2.21E-01	2.22E-01	2.22E-01	2.22E-01	2.22E-01	2.22E-01	2.22E-01	2.22E-01	2.22E-01	2.22E-01	2.23E-01
	0.449	14	2.58E-01	2.59E-01	2.59E-01	2.59E-01	2.59E-01	2.59E-01	2.59E-01	2.59E-01	2.59E-01	2.59E-01	2.60E-01
	0.419	15	2.93E-01	2.94E-01	2.94E-01	2.94E-01	2.94E-01	2.94E-01	2.94E-01	2.94E-01	2.94E-01	2.95E-01	2.95E-01
	0.393	16	3.25E-01	3.26E-01	3.26E-01	3.26E-01	3.26E-01	3.27E-01	3.27E-01	3.27E-01	3.27E-01	3.27E-01	3.28E-01
	0.37	17	3.55E-01	3.56E-01	3.56E-01	3.56E-01	3.56E-01	3.56E-01	3.57E-01	3.57E-01	3.57E-01	3.57E-01	3.58E-01
	0.349	18	3.81E-01	3.82E-01	3.82E-01	3.82E-01	3.83E-01	3.83E-01	3.83E-01	3.83E-01	3.84E-01	3.84E-01	3.84E-01
	0.331	19	4.04E-01	4.05E-01	4.05E-01	4.05E-01	4.05E-01	4.06E-01	4.06E-01	4.06E-01	4.07E-01	4.07E-01	4.07E-01
	0.314	20	4.23E-01	4.24E-01	4.24E-01	4.24E-01	4.24E-01	4.25E-01	4.25E-01	4.26E-01	4.26E-01	4.26E-01	4.26E-01
	0.299	21	4.37E-01	4.39E-01	4.39E-01	4.39E-01	4.39E-01	4.40E-01	4.40E-01	4.41E-01	4.41E-01	4.41E-01	4.42E-01
	0.286	22	4.47E-01	4.49E-01	4.49E-01	4.49E-01	4.49E-01	4.50E-01	4.50E-01	4.50E-01	4.49E-01	4.45E-01	4.35E-01
	0.273	23	4.53E-01	4.55E-01	4.55E-01	4.56E-01	4.56E-01	4.56E-01	4.58E-01	4.59E-01	4.63E-01	4.57E-01	4.59E-01
Pitch	1.257	5	4.88E-04	4.97E-04	4.51E-04	5.70E-04	4.45E-04	4.09E-04	3.88E-03	5.40E-04	5.56E-04	5.69E-04	5.76E-04
	1.047	6	9.08E-04	9.22E-04	9.02E-04	8.60E-04	9.36E-04	9.98E-04	9.86E-04	9.56E-04	9.37E-04	9.17E-04	8.95E-04
	0.898	7	1.34E-03	1.36E-03	1.34E-03	1.42E-03	1.42E-03	1.38E-03	1.11E-03	1.30E-03	1.29E-03	1.29E-03	1.28E-03
	0.785	8	1.78E-03	1.80E-03	1.85E-03	1.83E-03	1.80E-03	1.77E-03	1.75E-03	1.74E-03	1.74E-03	1.74E-03	1.74E-03
	0.698	9	2.20E-03	2.23E-03	2.25E-03	2.22E-03	2.20E-03	2.19E-03	2.18E-03	2.18E-03	2.18E-03	2.19E-03	2.19E-03
	0.628	10	2.58E-03	2.60E-03	2.60E-03	2.58E-03	2.58E-03	2.57E-03	2.58E-03	2.58E-03	2.58E-03	2.59E-03	2.59E-03
	0.571	11	2.88E-03	2.91E-03	2.90E-03	2.89E-03	2.89E-03	2.90E-03	2.90E-03	2.91E-03	2.91E-03	2.91E-03	2.92E-03
	0.524	12	3.11E-03	3.15E-03	3.14E-03	3.13E-03	3.14E-03	3.14E-03	3.15E-03	3.16E-03	3.17E-03	3.17E-03	3.18E-03
	0.483	13	3.27E-03	3.31E-03	3.30E-03	3.31E-03	3.31E-03	3.32E-03	3.33E-03	3.34E-03	3.35E-03	3.36E-03	3.36E-03
	0.449	14	3.37E-03	3.41E-03	3.41E-03	3.41E-03	3.42E-03	3.43E-03	3.45E-03	3.47E-03	3.47E-03	3.48E-03	3.49E-03
	0.419	15	3.43E-03	3.46E-03	3.47E-03	3.47E-03	3.48E-03	3.50E-03	3.53E-03	3.54E-03	3.55E-03	3.56E-03	3.58E-03
	0.393	16	3.44E-03	3.48E-03	3.48E-03	3.50E-03	3.51E-03	3.53E-03	3.56E-03	3.58E-03	3.59E-03	3.61E-03	3.62E-03
	0.37	17	3.42E-03	3.46E-03	3.47E-03	3.49E-03	3.50E-03	3.53E-03	3.57E-03	3.60E-03	3.61E-03	3.63E-03	3.64E-03
	0.349	18	3.39E-03	3.42E-03	3.44E-03	3.46E-03	3.48E-03	3.51E-03	3.57E-03	3.59E-03	3.61E-03	3.63E-03	3.65E-03
	0.331	19	3.34E-03	3.37E-03	3.40E-03	3.42E-03	3.45E-03	3.49E-03	3.55E-03	3.58E-03	3.60E-03	3.62E-03	3.65E-03
	0.314	20	3.28E-03	3.32E-03	3.35E-03	3.38E-03	3.41E-03	3.45E-03	3.53E-03	3.57E-03	3.59E-03	3.61E-03	3.64E-03
	0.299	21	3.22E-03	3.25E-03	3.30E-03	3.34E-03	3.37E-03	3.43E-03	3.51E-03	3.55E-03	3.57E-03	3.60E-03	3.63E-03
	0.286	22	3.16E-03	3.19E-03	3.24E-03	3.28E-03	3.33E-03	3.40E-03	3.52E-03	3.65E-03	3.81E-03	4.09E-03	4.43E-03
	0.273	23	3.10E-03	3.14E-03	3.21E-03	3.28E-03	3.34E-03	3.41E-03	3.67E-03	3.76E-03	4.08E-03	3.70E-03	3.80E-03
Surge	1.257	5	4.63E-02	4.72E-02	4.33E-02	5.43E-02	4.20E-02	3.81E-02	4.02E-01	4.97E-02	5.11E-02	5.23E-02	5.29E-02
	1.047	6	8.93E-02	9.06E-02	8.85E-02	8.40E-02	9.10E-02	9.63E-02	9.49E-02	9.23E-02	9.07E-02	8.90E-02	8.73E-02
	0.898	7	1.38E-01	1.40E-01	1.38E-01	1.45E-01	1.45E-01	1.41E-01	1.65E-01	1.34E-01	1.34E-01	1.33E-01	1.33E-01
	0.785	8	1.94E-01	1.96E-01	2.00E-01	1.97E-01	1.94E-01	1.92E-01	1.90E-01	1.91E-01	1.91E-01	1.91E-01	1.91E-01
	0.698	9	2.54E-01	2.57E-01	2.58E-01	2.55E-01	2.53E-01	2.53E-01	2.54E-01	2.54E-01	2.55E-01	2.55E-01	2.55E-01
	0.628	10	3.16E-01	3.20E-01	3.19E-01	3.17E-01	3.17E-01	3.18E-01	3.19E-01	3.20E-01	3.20E-01	3.21E-01	3.21E-01
	0.571	11	3.78E-01	3.82E-01	3.80E-01	3.80E-01	3.81E-01	3.82E-01	3.84E-01	3.85E-01	3.85E-01	3.86E-01	3.86E-01
	0.524	12	4.38E-01	4.42E-01	4.41E-01	4.41E-01	4.42E-01	4.43E-01	4.45E-01	4.46E-01	4.47E-01	4.48E-01	4.48E-01
	0.483	13	4.94E-01	4.98E-01	4.97E-01	4.98E-01	4.99E-01	5.01E-01	5.03E-01	5.04E-01	5.05E-01	5.06E-01	5.06E-01
	0.449	14	5.45E-01	5.50E-01	5.50E-01	5.51E-01	5.52E-01	5.53E-01	5.56E-01	5.58E-01	5.58E-01	5.59E-01	5.60E-01
	0.419	15	5.92E-01	5.97E-01	5.97E-01	5.98E-01	6.00E-01	6.02E-01	6.05E-01	6.07E-01	6.07E-01	6.08E-01	6.09E-01
	0.393	16	6.34E-01	6.39E-01	6.40E-01	6.42E-01	6.43E-01	6.46E-01	6.49E-01	6.51E-01	6.52E-01	6.53E-01	6.55E-01
	0.37	17	6.72E-01	6.78E-01	6.79E-01	6.81E-01	6.83E-01	6.85E-01	6.90E-01	6.92E-01	6.93E-01	6.94E-01	6.96E-01
	0.349	18	7.07E-01	7.13E-01	7.15E-01	7.17E-01	7.19E-01	7.22E-01	7.27E-01	7.29E-01	7.31E-01	7.32E-01	7.34E-01
	0.331	19	7.39E-01	7.45E-01	7.48E-01	7.50E-01	7.52E-01	7.56E-01	7.61E-01	7.64E-01	7.66E-01	7.67E-01	7.69E-01
	0.314	20	7.69E-01	7.75E-01	7.78E-01	7.81E-01	7.84E-01	7.88E-01	7.94E-01	7.97E-01	7.98E-01	8.00E-01	8.02E-01
	0.299	21	7.97E-01	8.04E-01	8.07E-01	8.11E-01	8.14E-01	8.18E-01	8.25E-01	8.28E-01	8.30E-01	8.31E-01	8.34E-01
	0.286	22	8.24E-01	8.31E-01	8.34E-01	8.38E-01	8.42E-01	8.47E-01	8.58E-01	8.69E-01	8.84E-01	9.10E-01	9.36E-01
	0.273	23	8.50E-01	8.57E-01	8.63E-01	8.68E-01	8.73E-01	8.79E-01	9.02E-01	9.09E-01	9.38E-01	9.01E-01	9.09E-01

	Hywind (body 1) Phase angle											
	Frequency	Period	Single	y 800 m	x 30 m	x 20 m	x 15 m	x 10 m	x 5 m	x 3 m	x 2 m	x 1 m	x 0 m
Heave	1.257	5	9.118	11.646	-6.939	-11.962	-8.115	-15.109	-124.212	-35.979	-38.061	-39.504	-40.165
	1.047	6	4.43	4.614	-4.962	-7.031	-10.624	-14.168	-16.254	-16.647	-16.797	-16.946	-17.117
	0.898	7	2.358	3.021	-3.284	-5.141	-6.203	-7.382	2.64	-9.727	-10.177	-10.662	-11.179
	0.785	8	1.174	0.986	-2.075	-3.098	-3.901	-5.013	-6.568	-7.349	-7.777	-8.23	-8.702
	0.698	9	0.646	0.959	-1.373	-2.292	-3.016	-4.004	-5.365	-6.046	-6.419	-6.814	-7.223
	0.628	10	0.362	0.471	-1.081	-1.902	-2.53	-3.385	-4.575	-5.182	-5.515	-5.869	-6.237
	0.571	11	0.201	0.342	-0.93	-1.649	-2.197	-2.949	-4.018	-4.568	-4.874	-5.199	-5.539
	0.524	12	0.105	0.139	-0.832	-1.468	-1.955	-2.631	-3.61	-4.121	-4.405	-4.711	-5.03
	0.483	13	0.044	0.09	-0.765	-1.336	-1.778	-2.399	-3.313	-3.794	-4.064	-4.355	-4.659
	0.449	14	0.002	0.019	-0.719	-1.243	-1.652	-2.234	-3.102	-3.565	-3.825	-4.104	-4.398
	0.419	15	-0.028	0.036	-0.691	-1.182	-1.57	-2.127	-2.967	-3.418	-3.673	-3.948	-4.236
	0.393	16	-0.053	-0.01	-0.68	-1.152	-1.528	-2.074	-2.904	-3.354	-3.609	-3.883	-4.17
	0.37	17	-0.077	-0.051	-0.688	-1.154	-1.53	-2.08	-2.924	-3.384	-3.646	-3.926	-4.219
	0.349	18	-0.103	-0.068	-0.72	-1.199	-1.589	-2.163	-3.053	-3.541	-3.817	-4.114	-4.421
	0.331	19	-0.14	-0.085	-0.794	-1.313	-1.738	-2.371	-3.359	-3.901	-4.21	-4.539	-4.875
	0.314	20	-0.203	-0.127	-0.955	-1.567	-2.073	-2.83	-4.02	-4.673	-5.043	-5.434	-5.827
	0.299	21	-0.352	-0.269	-1.396	-2.244	-2.947	-4.004	-5.664	-6.567	-7.072	-7.594	-8.103
	0.286	22	-1.141	-0.197	-3.076	-5.266	-7.052	-9.663	-13.765	-16.744	-19.485	-24.074	-30.269
	0.273	23	-178.846	-179.544	-176.946	-174.671	-172.693	-169.743	-162.453	-158.626	-152.224	-156.499	-152.971
Pitch	1.257	5	82.058	81.669	66.406	58.813	62.419	57.657	-161.731	40.806	39.118	38.06	37.893
	1.047	6	87.373	86.206	75.786	73.19	69.981	67.359	66.924	67.443	67.827	68.318	69.048
	0.898	7	108.832	88.273	81.349	79.443	78.785	78.455	80.86	78.305	78.308	78.374	78.647
	0.785	8	87.671	89.264	84.667	83.867	83.464	83.044	82.593	82.419	82.359	82.362	82.56
	0.698	9	88.877	89.695	86.651	86.009	85.615	85.162	84.699	84.526	84.468	84.467	84.636
	0.628	10	89.364	89.93	87.723	87.157	86.798	86.391	85.956	85.801	85.747	85.741	85.88
	0.571	11	89.617	90.024	88.354	87.86	87.541	87.177	86.787	86.641	86.586	86.572	86.678
	0.524	12	89.769	90.066	88.758	88.325	88.044	87.719	87.362	87.222	87.167	87.14	87.215
	0.483	13	89.873	90.1	89.031	88.648	88.397	88.105	87.776	87.638	87.577	87.541	87.59
	0.449	14	89.956	90.101	89.222	88.88	88.653	88.386	88.076	87.941	87.876	87.831	87.857
	0.419	15	90.031	90.108	89.362	89.051	88.842	88.595	88.299	88.162	88.096	88.043	88.054
	0.393	16	90.103	90.122	89.468	89.18	88.984	88.751	88.464	88.327	88.258	88.2	88.199
	0.37	17	90.177	90.143	89.558	89.284	89.096	88.871	88.587	88.448	88.377	88.316	88.307
	0.349	18	90.255	90.191	89.649	89.381	89.195	88.97	88.681	88.538	88.464	88.4	88.387
	0.331	19	90.336	90.311	89.779	89.503	89.308	89.073	88.764	88.612	88.533	88.464	88.446
	0.314	20	90.421	90.622	90.061	89.752	89.527	89.249	88.881	88.705	88.61	88.527	88.499
	0.299	21	90.511	92.176	91.373	90.925	90.561	90.021	89.315	89.004	88.845	88.698	88.61
	0.284	22	90.606	85.109	86.137	86.703	86.925	86.822	85.031	82.163	78.39	70.833	54.935
	0.273	23	90.704	88.217	89.486	89.432	89.125	87.351	90.301	92.254	99.175	82.8	86.622
Surge	1.257	5	81.586	81.639	66.602	58.126	61.354	56.763	75.524	42.342	41.242	40.821	41.382
	1.047	6	86.191	86.195	75.249	72.701	70	68.456	69.719	70.982	71.722	72.561	73.666
	0.898	7	89.758	88.256	81.102	79.83	79.831	80.464	81.99	81.969	82.182	82.449	82.936
	0.785	8	89.095	89.248	84.85	84.733	84.891	85.218	85.646	85.806	85.901	86.053	86.407
	0.698	9	89.584	89.678	87.079	87.032	87.094	87.226	87.474	87.576	87.648	87.775	88.079
	0.628	10	89.814	89.91	88.248	88.182	88.199	88.283	88.44	88.524	88.587	88.7	88.965
	0.571	11	89.924	90.003	88.894	88.822	88.821	88.874	88.996	89.066	89.121	89.219	89.447
	0.524	12	89.977	90.044	89.274	89.203	89.193	89.229	89.325	89.383	89.429	89.511	89.705
	0.483	13	90.003	90.078	89.507	89.437	89.423	89.448	89.521	89.566	89.602	89.669	89.833
	0.449	14	90.018	90.08	89.654	89.586	89.567	89.581	89.634	89.666	89.692	89.745	89.883
	0.419	15	90.029	90.087	89.751	89.681	89.658	89.662	89.694	89.712	89.73	89.771	89.885
	0.393	16	90.041	90.101	89.818	89.744	89.715	89.708	89.719	89.725	89.735	89.764	89.86
	0.37	17	90.057	90.122	89.871	89.79	89.753	89.734	89.723	89.716	89.718	89.737	89.816
	0.349	18	90.078	90.162	89.927	89.834	89.786	89.751	89.714	89.694	89.687	89.697	89.762
	0.331	19	90.108	90.258	90.012	89.899	89.834	89.776	89.706	89.669	89.653	89.651	89.702
	0.314	20	90.147	90.496	90.212	90.061	89.964	89.861	89.729	89.666	89.633	89.615	89.65
	0.299	21	90.199	91.682	91.19	90.916	90.702	90.389	89.99	89.821	89.739	89.67	89.654
	0.286	22	90.268	86.465	87.312	87.775	87.989	87.997	86.785	84.558	81.4	74.768	60.482
	0.273	23	90.36	88.712	89.72	89.723	89.542	88.351	90.511	92.007	97.579	85.299	88.008

	WindFlip (body 2) Phase angle in global coordiante system												
	Frequency	Period	Single	y 800 m	x 30 m	x 20 m	x 15 m	x 10 m	x 5 m	x 3 m	x 2 m	x 1 m	x 0 m
Heave	1.257	5	-80.514	22.145	-59.141	-154.453	-179.226	120.011	54.219	27.217	19.908	13.644	8.327
	1.047	6	-52.031	19.557	-144.79	151.782	109.123	72.283	45.373	36.401	32.071	27.753	23.373
	0.898	7	-34.038	18.205	160.988	108.348	84.512	63.044	38.644	34.958	30.92	26.835	22.693
	0.785	8	-23.8	16.448	122.788	86.565	69.437	52.727	36.1	29.385	26.001	22.595	19.17
	0.698	9	-17.675	14.038	98.475	70.641	56.964	43.339	29.664	24.155	21.389	18.615	15.837
	0.628	10	-13.761	11.995	80.825	58.224	46.974	35.721	24.43	19.894	17.621	15.346	13.074
	0.571	11	-11.129	10.13	67.295	48.488	39.093	29.692	20.269	16.491	14.601	12.71	10.824
	0.524	12	-9.294	8.504	56.689	40.797	32.853	24.904	16.943	13.755	12.16	10.565	8.977
	0.483	13	-7.98	7.229	48.244	34.652	27.855	21.054	14.247	11.521	10.158	8.796	7.439
	0.449	14	-7.019	6.052	41.428	29.675	23.796	17.914	12.026	9.669	8.49	7.313	6.14
	0.419	15	-6.308	5.091	35.85	25.588	20.453	15.314	10.169	8.109	7.079	6.049	5.025
	0.393	16	-5.777	4.23	31.227	22.188	17.661	13.129	8.591	6.773	5.864	4.955	4.051
	0.37	17	-5.384	3.465	27.349	19.32	15.296	11.265	7.226	5.609	4.799	3.99	3.185
	0.349	18	-5.1	2.79	24.057	16.87	13.264	9.649	6.026	4.573	3.846	3.119	2.396
	0.331	19	-4.906	2.177	21.23	14.747	11.491	8.224	4.946	3.632	2.973	2.314	1.66
	0.314	20	-4.792	1.603	18.77	12.879	9.916	6.938	3.951	2.753	2.152	1.551	0.953
	0.299	21	-4.753	1.057	16.587	11.192	8.476	5.747	3.012	1.916	1.367	0.817	0.27
	0.286	22	-4.788	0.496	14.71	9.723	7.191	4.631	2.01	0.776	-0.063	-1.171	-2.226
	0.273	23	-4.902	-0.047	12.868	8.197	5.824	3.499	0.593	-0.386	-1.575	-0.975	-1.552
Pitch	1.257	5	75.86	179.069	91.087	9.024	-32.041	-93.66	48.985	-161.934	-169.546	-176.729	176.429
	1.047	6	82.429	154.333	-8.724	-81.523	-114.987	-144.013	-171.251	177.355	171.361	165.097	158.493
	0.898	7	86.68	139.473	-81.849	-127.364	-148.936	-171.077	-171.305	155.065	149.904	144.663	139.317
	0.785	8	88.698	129.129	-123.013	-157.543	-175.326	166.238	147.115	139.306	135.37	131.406	127.39
	0.698	9	89.684	121.655	-152.244	179.408	164.891	150.111	135.077	128.995	125.934	122.852	119.727
	0.628	10	90.218	116.115	-174.205	162.501	150.702	138.779	126.706	121.823	119.364	116.885	114.368
	0.571	11	90.524	111.931	169.313	150.025	140.3	130.49	120.558	116.538	114.511	112.466	110.388
	0.524	12	90.688	108.669	156.751	140.559	132.404	124.18	115.849	112.474	110.772	109.054	107.306
	0.483	13	90.753	106.06	146.949	133.164	126.222	119.219	112.122	109.246	107.796	106.332	104.842
	0.449	14	90.738	103.916	139.121	127.237	121.251	115.212	109.092	106.613	105.362	104.1	102.815
	0.419	15	90.656	102.105	132.734	122.38	117.164	111.901	106.569	104.411	103.324	102.225	101.107
	0.393	16	90.515	100.527	127.425	118.32	113.733	109.106	104.423	102.531	101.576	100.615	99.634
	0.37	17	90.318	99.124	122.936	114.865	110.801	106.701	102.56	100.891	100.048	99.201	98.338
	0.349	18	90.067	97.845	119.077	111.876	108.247	104.595	100.913	99.432	98.689	97.937	97.172
	0.331	19	89.76	96.648	115.715	109.244	105.99	102.719	99.434	98.115	97.455	96.789	96.111
	0.314	20	89.397	95.496	112.738	106.898	103.966	101.026	98.088	96.917	96.33	95.741	95.142
	0.299	21	88.967	94.364	110.082	104.8	102.159	99.521	96.897	95.855	95.328	94.802	94.268
	0.286	22	88.47	93.231	107.568	102.697	100.254	97.797	95.112	93.441	91.746	88.212	80.147
	0.273	23	87.892	92.133	105.375	100.953	98.766	96.554	94.616	94.301	95.758	91.805	92.119
Surge	1.257	5	75.152	178.366	90.12	9.006	-31.768	-93.728	-129.571	-163.055	-170.857	-178.256	174.654
	1.047	6	81.284	153.196	-9.593	-82.466	-116.057	-145.492	-173.566	174.614	168.414	161.968	155.228
	0.898	7	85.201	138.001	-83.235	-128.911	-150.789	-173.443	151.872	151.943	146.743	141.495	136.186
	0.785	8	87.016	127.452	-124.71	-159.553	-177.608	163.635	144.262	136.429	132.506	128.576	124.62
	0.698	9	87.891	119.866	-154.182	177.221	162.539	147.595	132.453	126.381	123.343	120.296	117.226
	0.628	10	88.372	114.273	-176.234	160.313	148.417	136.4	124.282	119.419	116.981	114.535	112.066
	0.571	11	88.666	110.082	167.296	147.908	138.123	128.258	118.31	114.31	112.303	110.287	108.252
	0.524	12	88.858	106.858	154.807	138.55	130.358	122.101	113.769	110.415	108.731	107.039	105.329
	0.483	13	88.988	104.33	145.121	131.294	124.329	117.308	110.219	107.364	105.93	104.489	103.032
	0.449	14	89.076	102.311	137.451	125.541	119.542	113.494	107.387	104.926	103.689	102.447	101.191
	0.419	15	89.136	100.673	131.264	120.895	115.672	110.406	105.088	102.945	101.869	100.787	99.694
	0.393	16	89.175	99.318	126.2	117.088	112.498	107.871	103.198	101.316	100.37	99.419	98.458
	0.37	17	89.199	98.19	122.002	113.929	109.863	105.764	101.625	99.958	99.12	98.279	97.429
	0.349	18	89.211	97.241	118.486	111.282	107.653	103.996	100.303	98.816	98.07	97.319	96.561
	0.331	19	89.213	96.432	115.519	109.045	105.785	102.499	99.184	97.849	97.18	96.506	95.825
	0.314	20	89.206	95.735	112.996	107.143	104.196	101.227	98.232	97.027	96.422	95.814	95.2
	0.299	21	89.188	95.129	110.846	105.528	102.853	100.158	97.437	96.342	95.789	95.235	94.675
	0.286	22	89.162	94.599	108.953	104.061	101.592	99.092	96.457	95.129	94.071	92.139	88.004
	0.273	23	89.125	94.142	107.365	102.872	100.61	98.308	96.067	95.34	95.62	93.773	93.575

Appendix L Heave and pitch RAOs with and without interaction

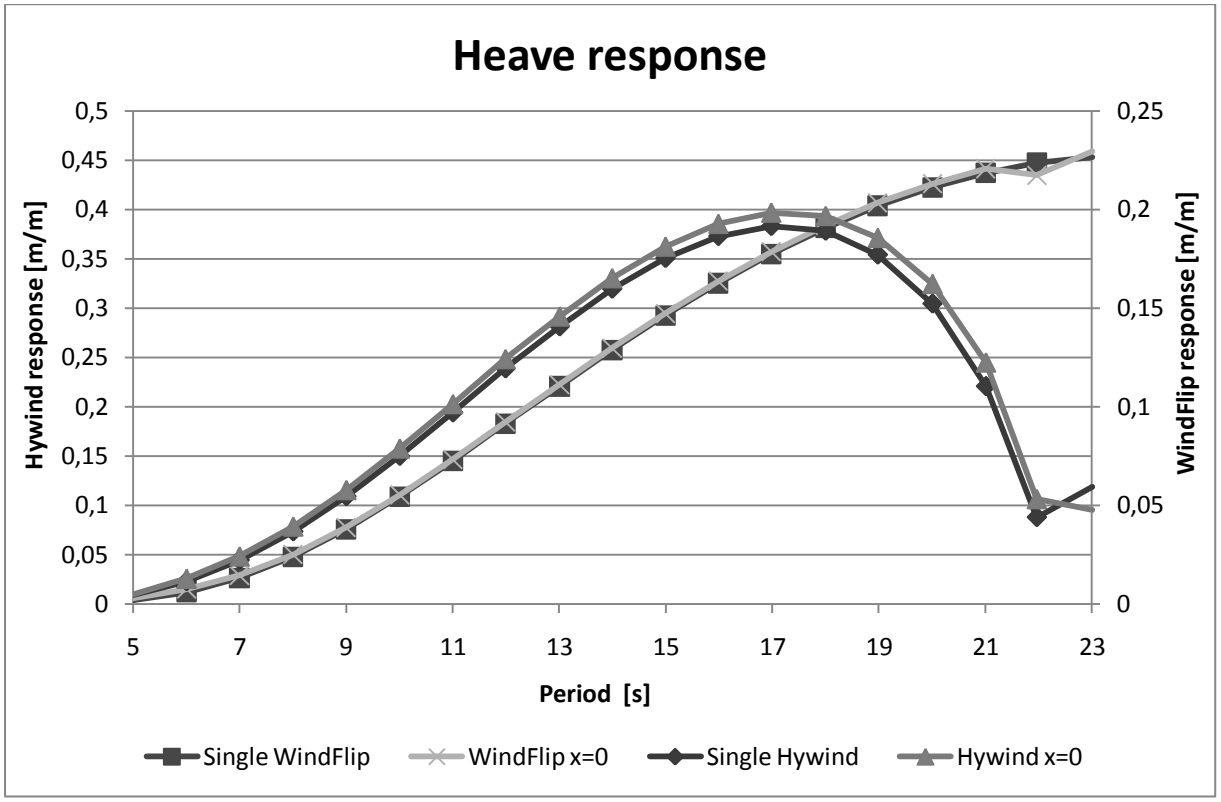

Graph 42 Heave RAOs with and without interaction effects

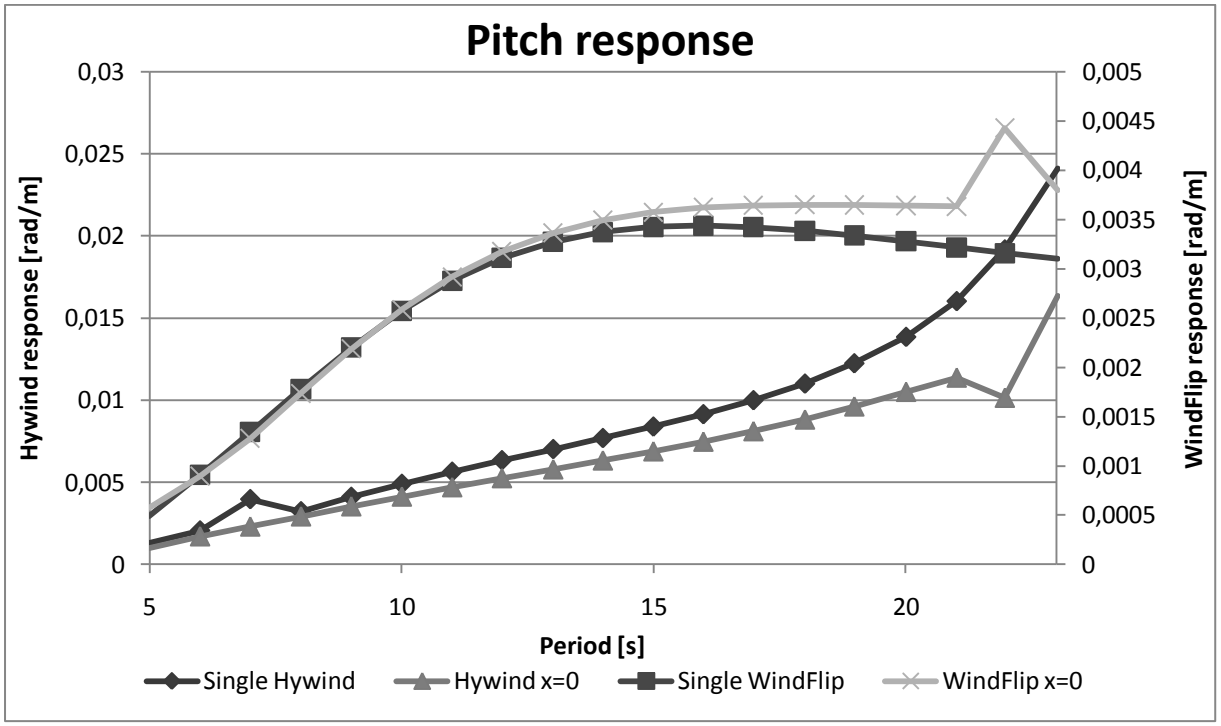

Graph 43 Pitch RAOs with and without interaction effects

Appendix M Interaction effects at 19 seconds period

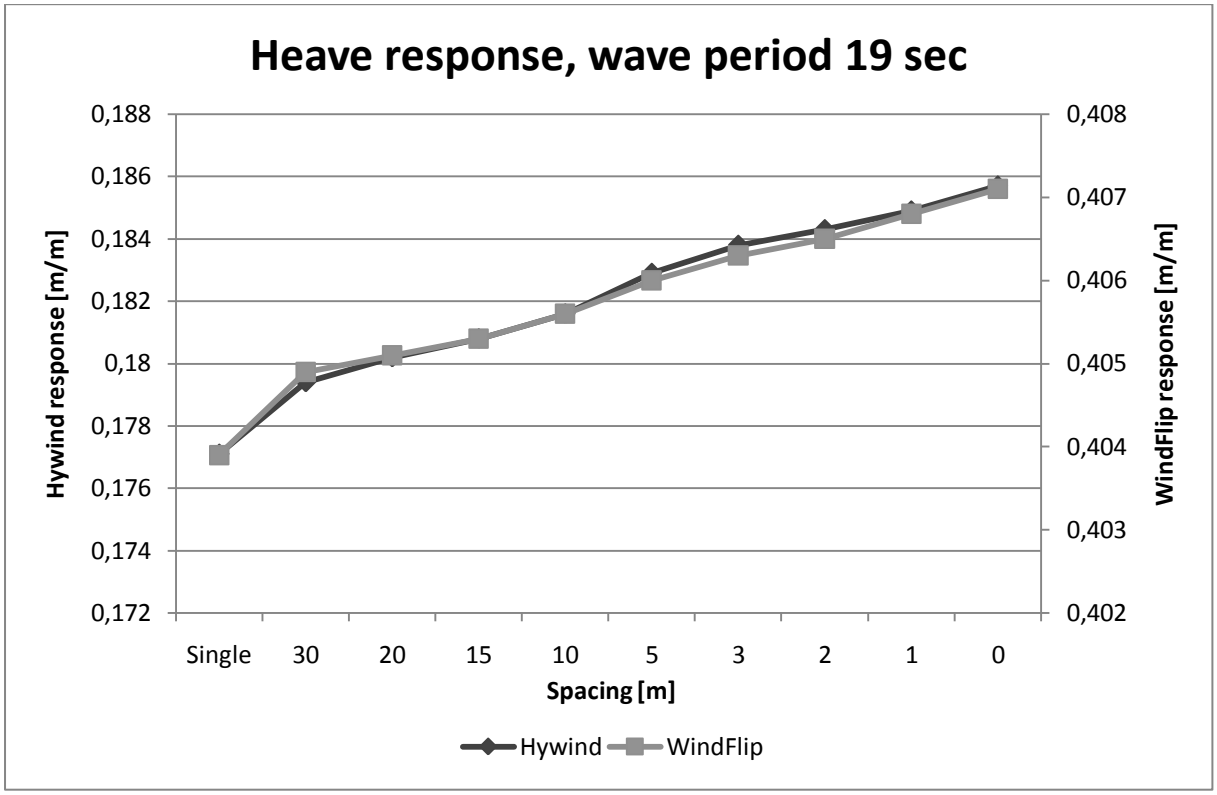

Graph 44 Heave response 19 sec period

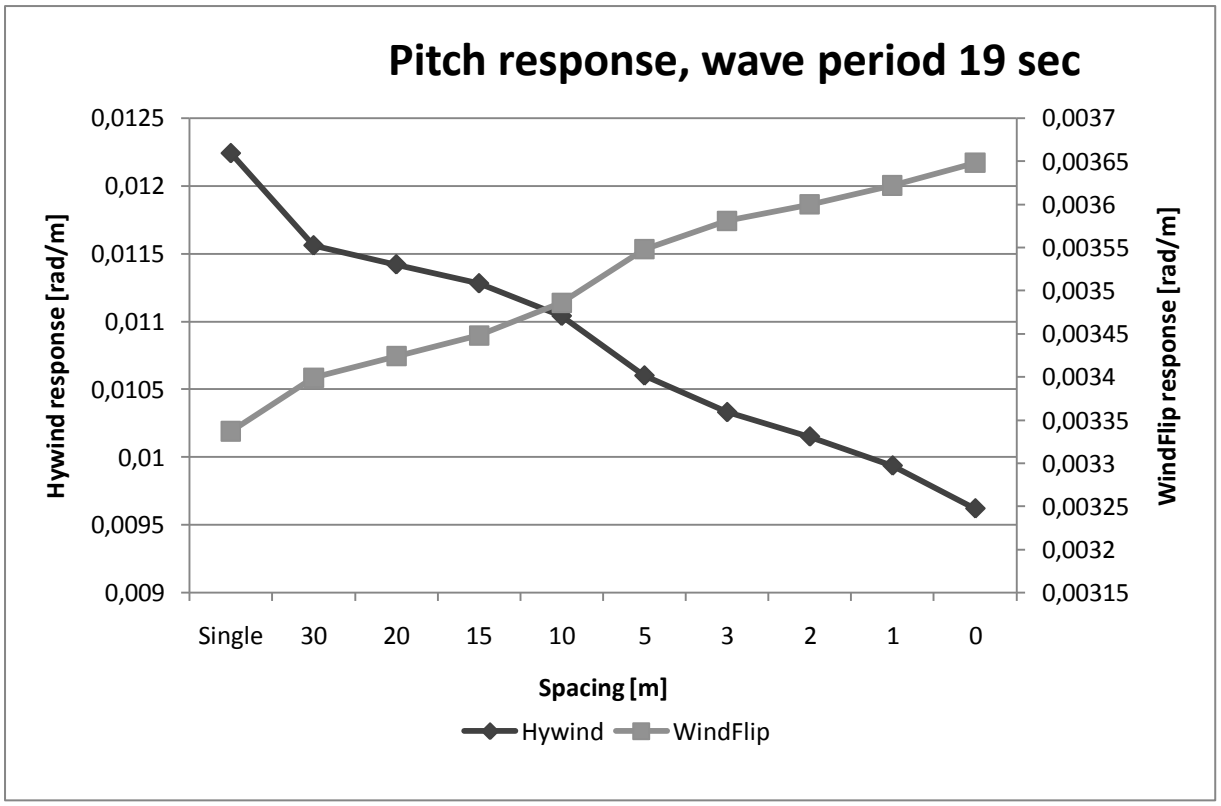

Graph 45 Pitch response at 19 sec period

Appendix N Interaction effects at 22 seconds period

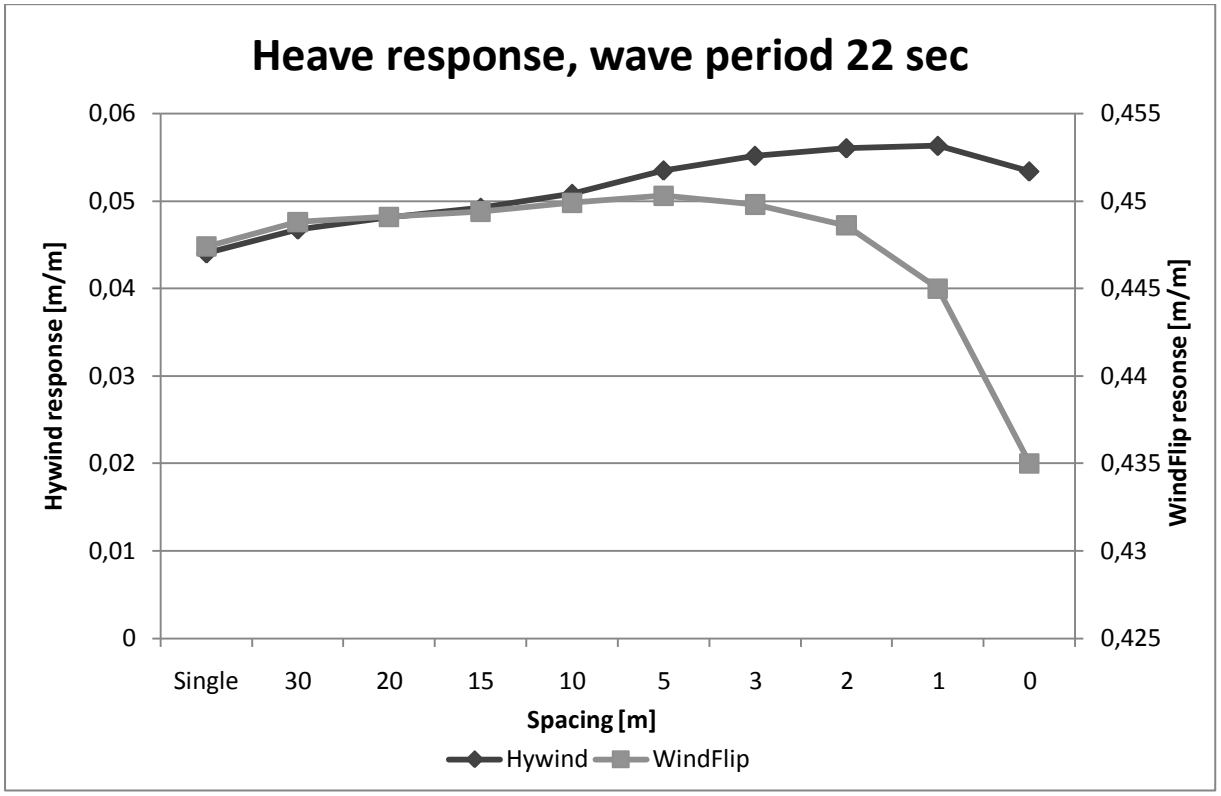

Graph 46 Heave response at 22 sec period

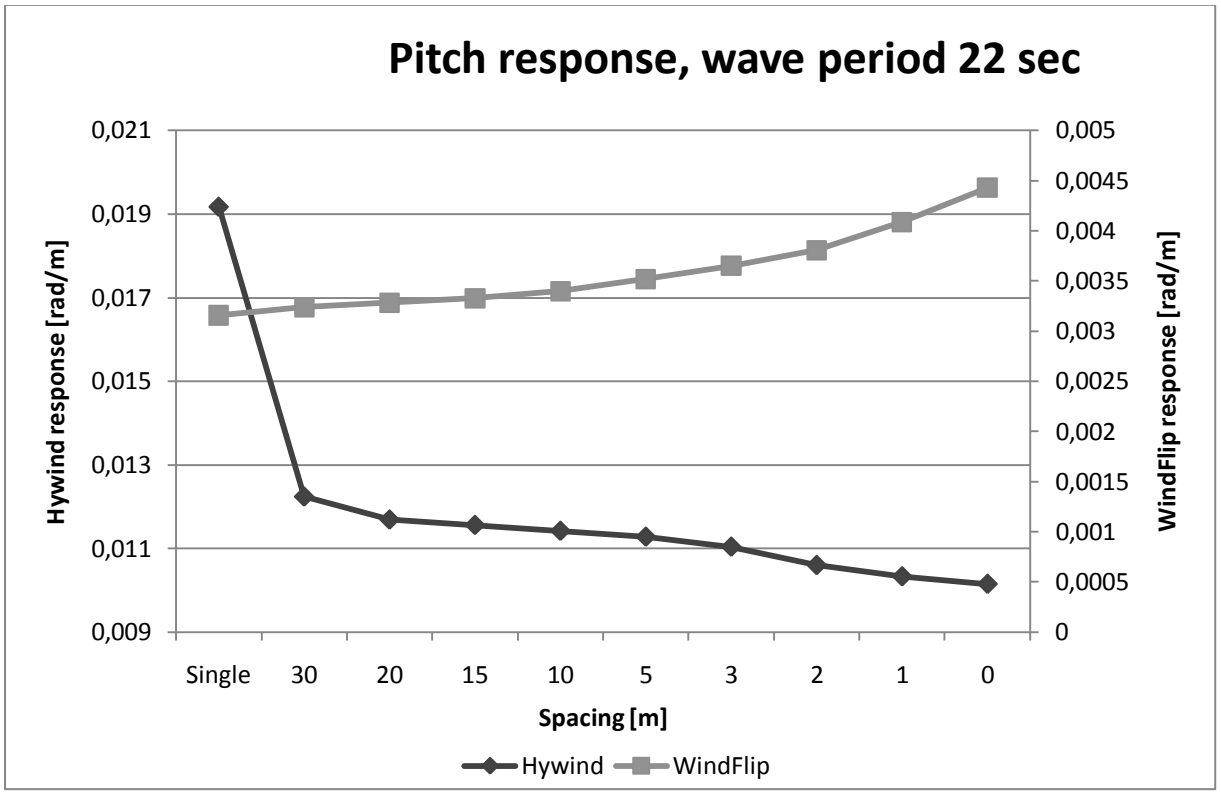

Graph 47 Pitch response at 22 sec period

Appendix O Comparing Hywind for waves of 19 and 22 second period

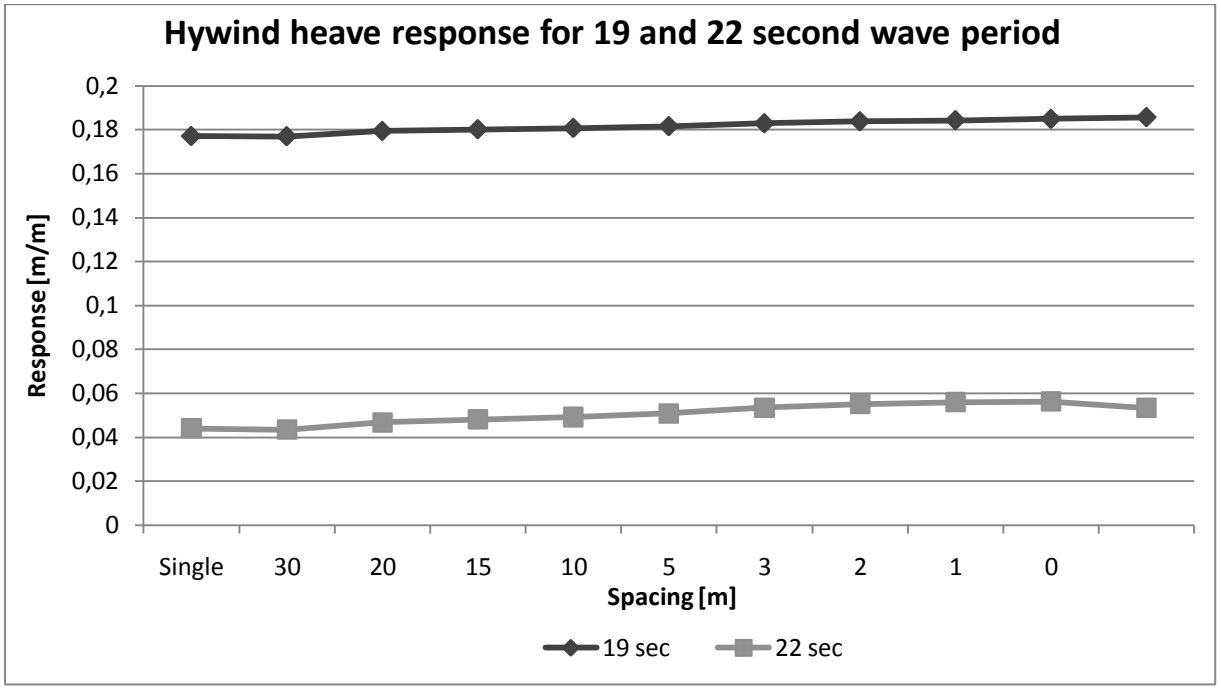

Graph 48 Hywind heave response for 19 and 22 sec

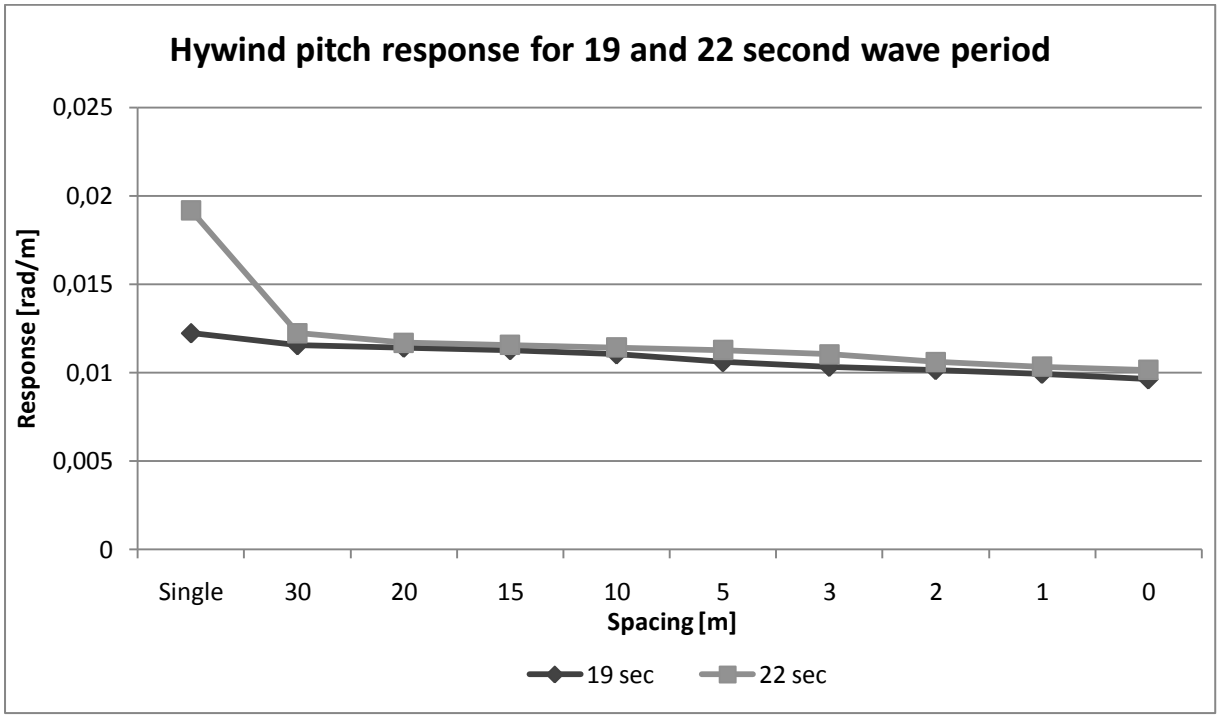

Graph 49 Hywind pitch response for 19 and 22 sec